Biorefinery Strategies for Co–generation of Cellulose Nanocrystals and Value–added Products from Wood Pulp

by

Dawit Beyene

A thesis submitted in partial fulfillment of the requirements for the degree of

Doctor of Philosophy

in

Bioresource and Food Engineering

Department of Agricultural, Food and Nutritional Science

University of Alberta

Abstract

Cellulose nanocrystals (CNCs) are sustainable and renewable nanoparticles derived from cellulose with desirable properties for various applications. CNCs can be isolated from purified cellulose such as wood pulp by concentrated sulfuric acid hydrolysis. The acid degrades non–crystalline cellulose and hemicelluloses, while CNC precursors representing the bulk highly crystalline celluloses are converted to CNC by fragmentation. This process has limitations due to low CNC yield (10 wt % initial feedstock) and loss of valuable sugars in the acid stream that decreases acid recovery efficiency. In this thesis, biorefinery strategies were developed to integrate cellulase and hydrothermal treatments with acid hydrolysis to (a) transform non–crystalline constituents of wood pulp to value–added co–products and (b) generate a crystalline feedstock to improve CNC yield from acid hydrolysis (wt % feedstock for acid hydrolysis, CNC $yield_1$) and the CNC yield from the initial feedstock, accounting for the mass loss due to the treatments (wt % original feedstock, CNC $yield_2$).

In the first strategy, cellulase treatment (using a Novozymes enzyme preparation supplemented with xylanase) was introduced prior to acid hydrolysis of Whatman™ No. 1 filter paper (model feedstock) and wood pulp. The objectives were to: (a) identify a treatment period for efficient saccharification for ethanol production without compromising CNC $yield_2$, and (b) improve CNC $yield_1$. The hypothesis was that cellulase treatment period is a determining factor for preferential degradation of non–crystalline cellulose and xylan with linear hydrolysis rate and minimal loss to CNC precursors. Preferential hydrolysis will generate a feedstock with concentrated CNC precursors that improves acid hydrolysis efficiency. During 10 h cellulase treatment, glucose yield plateaued at 6 h (36.5 ± 0.3 wt % original feedstock) for filter paper with a significant increase in

the crystallinity of the residual solid. Therefore, 2–6 h cellulase treatment of filter paper lead to an efficient saccharification. Steady hydrolysis rate was maintained even at 10 h for an efficient saccharification of wood pulp to glucose and xylose (44.2 ± 1.4 and 12.1 ± 0.3 wt % original feedstock, respectively), with surprisingly no changes in crystallinity. CNC $yield_1$ significantly improved from cellulase–treated filter paper (up to 1.2 fold) and wood pulp (almost doubled). CNC precursors were likely accumulated due to hydrolysis of non–crystalline chains. Hence, cellulase treatment can reduce acid and water consumption upstream and operation costs downstream from improved throughput. Less sugars in the acid stream will also ease acid recovery processes. CNC $yield_2$ significantly decreased for filter paper even at 2 h. This implies simultaneous degradation of CNC precursors, which was more abundant in filter paper. CNC $yields_2$ were constant for wood pulp from 2–8 h. Hence a biorefinery strategy with efficient saccharification and CNC isolation was achieved from 8 h cellulase treatment mediated acid hydrolysis. CNCs of comparable quality were isolated from cellulase–treated feedstock based on particle size, zeta potential, thermal stability and crystallinity analysis.

The second strategy was to integrate hydrothermal treatment and acid hydrolysis to (a) generate furfural as a value–added co–product, and (b) form new CNC precursors in wood pulp and improve CNC yields from acid hydrolysis. The hypotheses were that hydrothermal treatment can substantially degrade xylan to furfural and also re–orient para–crystalline chains to form new CNC precursors. Xylan degradation ranged from 19–90 (wt % original feedstock) at 175–225 °C treatment while significant cellulose hydrolysis was only apparent at 225 °C (7.0 ± 1.5 wt % original feedstock). Substantial furfural yields were generated at 200 °C and 225 °C (19 and 21% xylan conversion, respectively). Hydrothermal treatment significantly improved the crystallinity

index of wood pulp and consequently CNC $yield_1$ and $yield_2$ improved by up to 4 and 2 fold, respectively, relative to the untreated pulp. These improvements can be translated to reduced cost of CNC production and increased capacity. The particle size, zeta potential and crystallinity of CNC generated from hydrothermally treated pulp were not affected due to the treatment. However, a dark brown colored CNC was generated from hydrothermally treated pulp at 225 °C possibly due to caramelization.

These studies demonstrated that cellulase and hydrothermal treatment mediated acid hydrolysis biorefinery strategies can efficiently generate fermentable sugar and furfural co–products, respectively and improve CNC yields.

Preface

All of the research on the cellulase mediated CNC isolation biorefinery strategy presented in this thesis has been published in 2 papers. The findings pertaining to the proof of–concept of this pathway was published as Beyene, D.; Chae, M.; Dai, J.; Danumah, C.; Tosto, F.; Demesa, A. G.; Bressler, D. C. Enzymatically–Mediated Co–Production of Cellulose Nanocrystals and Fermentable Sugars. *Catalysts*. **2017**, *7*, 322. David C. Bressler, Michael Chae, and Frank Tosto conceived the idea for the study; Dawit Beyene, David C. Bressler, Michael Chae, and Christophe Danumah designed the experiments; Dawit Beyene, Jing Dai, and Abayneh Getachew Demesa performed the experiments; Dawit Beyene analyzed the data and is the primary author. Michael Chae contributed substantially to the drafts. All authors read, contributed to, and approved the final manuscript. The characterization studies on the components of this strategy were published as Beyene, D.; Chae, M.; Dai, J.; Danumah, C.; Tosto, F.; Demesa, A. G.; Bressler, D. C. Characterization of Cellulase–Treated Fibers and Resulting Cellulose Nanocrystals Generated through Acid Hydrolysis. *Materials.* **2018**, *11*, 1272. David C. Bressler, Michael Chae, and Frank Tosto conceptualized the idea for the study; Dawit Beyene, David C. Bressler, Michael Chae, and Christophe Danumah designed the experiments; Dawit Beyene executed the formal analysis; Dawit Beyene, Jing Dai, and Abayneh Getachew Demesa performed the experiments; David C. Bressler, Frank Tosto, and Christophe Danumah provided resources; Dawit Beyene prepared the draft manuscript; all authors contributed to writing–review and editing; David C. Bressler and Michael Chae acquired funding, administered, and supervised the research study. The contents from the 2 publications were modified, reformatted and merged to maintain a good logical and continuous flow of discussion in the thesis.

Part of a study on endoglucanase mediated CNC isolation that was discussed in the thesis was published as Dai, J.; Chae, M.; Beyene, D.; Danumah, C.; Tosto, F.; Bressler, D. C. Co-Production of Cellulose Nanocrystals and Fermentable Sugars Assisted by Endoglucanase Treatment of Wood Pulp. *Materials.* **2018**, *11*, 1645. David C. Bressler, Michael Chae, and Frank Tosto conceptualized the idea for the study; Jing Dai, David C. Bressler, Michael Chae, Dawit Beyene, and Christophe Danumah designed the experiments; Jing Dai, and Dawit Beyene performed the experiments;

David C. Bressler, Frank Tosto, and Christophe Danumah provided resources; Jing Dai and Michael Chae prepared the draft manuscript; All authors contributed to writing–review and editing; Jing Dai, Michael Chae, and Dawit Beyene did the visualization; David C. Bressler and Michael Chae acquired funding, administer, and supervised the research study.

Acknowledgments

I want to sincerely express my heart–felt gratitude to Dr. David Bressler for giving me the opportunity and support to carry out my PhD program and freedom with trust to independently execute the research project in his laboratory. Dave has been an excellent mentor through his great vision, exemplary dedication, top level professionalism, direct and practical approach, strong opinion and incredible critical thinking abilities. I may have disliked the scientific arguments we had in some of our meetings in the heat of the moment, but at the end of the day, you always had a lesson for me to learn. I also want to thank Dave for showing compassion to help me and my colleagues to face and deal with challenges in research and life in general. I appreciate the time and effort you take to also make sure that your students are successful in their future career development. Overall, Dave has been instrumental in shaping my perspective and character to become a better research scientist, communicator and a good person in general.

I would like to thank my supervisory committee, Dr. Thava Vasanthan and Dr. Fred West, for forwarding excellent suggestions and comments that helped me visualize certain aspects of my project from a different perspective. Thank you for opening your doors and making time for consultation outside of the regular committee meetings. A special thank you goes to Dr. Michael Chae, Dr. Bressler's lab program manager. Your invaluable and brilliant recommendations that helped shape the objectives of my project, expert guidance in troubleshooting, great vision in providing edits and comments on the numerous writings over the years are truly appreciated. You have done all this with admirable enthusiasm, patience and dedication with those unforgettable close to midnight emails. I have said this before and I will say it again, you are a great mentor and deserve to be a professor.

During my study program I was grateful to have had the privilege to collaborate with Alberta Pacific (Al–Pac) Forest Industries Inc, the Biorefining Conversions Network (BCN), BioFuelNet Canada, Future Energy Systems (FES), InnoTech Alberta, the Natural Sciences and Engineering Research Council of Canada (NSERC), Novozymes and various centers and facilities at the University of Alberta. Thank you for your generosity in providing financial and material support that made this project and my PhD program a reality. I would like to acknowledge Frank Tosto

(InnoTech Alberta) and Dr. Christophe Danumah (InnoTech Alberta) for facilitating materials and equipments access, elaborate guidance, practical suggestions, and valuable comments on my writings. I am very thankful to Geoff Clarke (Al-Pac Forest Industries Inc.) and Kasper Bay Tingsted for material and chemical support, and making time and effort to provide consultations in meetings.

I want to express my appreciation to all my past and present lab mates Andres, Biren, Chengyong, Damaris, Emily, Emma, Hector, Jesse, Jie, Lin, Michael, Olga, Pooran, Rita, Samuel, Susan, Tao, Vadim, Victor, Vinay, Yeling, Yeye and Yuko. I want to particularly thank Justice Asomaning, Research Associate in Dr. Bressler's lab, for his honest and direct opinions, advice, mentorship and, those debates (rational and sometimes pointless) that added lots of fun to our lunch time. A special thanks to Jingui Lan, Laboratory Technician in Dr. Bressler's lab, for his invaluable practical suggestions and technical support in troubleshooting from his vast know–how in instrumentation and analysis. His humble and kind personality to unconditionally provide help made life in the lab much easier. I also want to appreciate the great help and companionship I had with all the industrious summer students I got to work with throughout the program.

Many thanks to all the friends I have made in Edmonton for helping me settle as a newcomer, providing love, generosity, guidance and just making time to have some fun together. I want to particularly acknowledge the Saint Virgin Mary Ethiopian Orthodox Tewahedo Church Community for their unconditional love and support over the years.

I want to sincerely thank my immediate and extended family for the overwhelming encouragement and love that kept me going. My kind and beautiful wife Tsion, I can't thank you enough for the unconditional love and respect you gave me. Your support has been incredible in understanding my late working schedules especially at a time when we are blessed with a newborn baby to love and attend 24/7 at home. Baby Nati, you don't do or say much, but that cute face and smile just makes my day. I love you all.

None of this would have been possible without the grace and blessing from Almighty God and His guidance and protection through the intercessions of the Virgin Mary, all the angels and saints who are with us all the way, whatsoever. Amen!

Table of Contents

List of Tables

List of Figures

List of abbreviations

ANOVA– analysis of variance

Al–Pac– Alberta Pacific forest industries

ASA– allmennaksjeselskap (Norwegian term for public limited company)

A/S– aktieselskab (Danish term for stock based company)

CBM– carbohydrate binding module

DP– degree of polymerisation

CBH– cellobiohydrolase

CNC– cellulose nanocrystals

DNS– dinitrosalicylic acid

EC– enzyme commission number

EG– endoglucanase

FPU– filter paper unit

gt– gauche–trans

HPLC– high performance liquid chromatography

MFC–microfibrillated cellulose

MPa– mega pascal

PQM– pulp quality monitoring

SEM– scanning electron microscopy

SHF– separate hydrolysis and fermentation

SSF– simultaneous saccharification and fermentation

TEM– transmission electron microscopy

tg– trans–gauche

UV– ultraviolet

XRD– X–ray diffraction

1. Introduction and objectives

The pulp and paper industry plays an integral role in the economy of countries that have abundant forestry resources in North America, Northern Europe, East Asia and South America [1]. The industry is currently facing multiple challenges, particularly a shrinking global market for newsprint products [2]. In response, the forestry sector is making efforts to generate fuels, biochemical, and biomaterial co–products. Cellulose nanocrystals (CNCs) are one of the value–added purified cellulose materials that are gaining a lot of attention. They are a highly crystalline cellulose isolated in nanoscale dimensions (3–5 nm width and 50–500 nm length) from cellulosic feedstock such as wood [3]. CNCs are highly reactive due their large surface area as nanoparticles and show superior strength resulting from their high crystallinity [4]. These materials are light–weight with mechanical strength properties comparable with carbon fiber and steel [3]. Therefore, CNCs have potential application as biodegradable and renewable reinforcement fillers for composite materials used in automotive, construction and food packaging industries [5]–[8]. In addition, their shear thinning, optical iridescence, high absorbance, oxygen and water barrier properties are also attractive for application in products used in aviation, pharmaceutical, food, cosmetics, paint, and film industries [9]–[18].

Cellulose, which makes up the major structural component in lignocellulosic biomass, is composed of tightly packed crystalline regions, poorly ordered amorphous chains, and relatively less ordered para–crystalline domains [19][20]. CNCs can be isolated by hydrolysis of the non–crystalline cellulose and hemicellulose chains, and fragmentation of crystalline cellulose to nanoscale size with mineral acids, organic acids, oxidants, enzymes and hydrothermal treatments [21]–[26]. Acid hydrolysis using concentrated sulfuric acid (64 wt %) is the most common method for isolating CNCs [21]. High production process cost is one of the limiting factors that is hindering commercial applications [27]. Some of the major challenges of the process are: (a) the loss of reusable sugars from hydrolysis of non–crystalline cellulose in the acid stream, (b) reaction of the acid with sugars that reduces acid hydrolysis efficiency, and (c) low CNC yield (10 wt % original feedstock) [28]. These issues arise because of the high composition of non–crystalline cellulose and hemicellulose in a feedstock such as wood pulp, which do not contribute to CNC production.

These limitations can be addressed by generating value–added products from degradation and/or modification of these non–crystalline domains. This can be achieved by integrating cellulase and hydrothermal treatment with CNC isolation to develop a biorefinery strategy.

Cellulases are extracellular enzymes produced by fungi and bacteria that catalyze the degradation of celluloses. There are three classes of cellulases that work synergistically to hydrolyze cellulose by first opening up the chain with endoglucanases, followed by the more aggressive cellobiohydrolase degradation of the polysaccharide to cellobiose units, which are hydrolyzed to glucose with β–glucosidase [29]. Currently, cellulases are used for saccharification of cellulose to generate ethanol as an alternative renewable and sustainable biofuel to reduce greenhouse gas emission and reliance on petroleum oil [30][31]. Generally, cellulases rapidly degrade amorphous cellulose due to the ease in accessibility that allows the crystalline cellulose to accumulate over time as the latter is recalcitrant due to tight packing [32]–[36]. Pretreatment and cellulose hydrolysis processes that reduce the crystallinity of cellulose to achieve maximum saccharification incur cost to the ethanol industry. Alternatively, a biorefinery strategy can be developed through preferential cellulase hydrolysis that (a) efficiently saccharifies non–crystalline cellulose and hemicelluloses to fermentable sugars, and (b) leads to the preservation and accumulation of CNC precursors (large crystalline cellulose fragmented to CNC by the acid) for efficient acid hydrolysis that improves the yield (wt % feedstock for acid hydrolysis, CNC yield$_1$) (Figure 1).

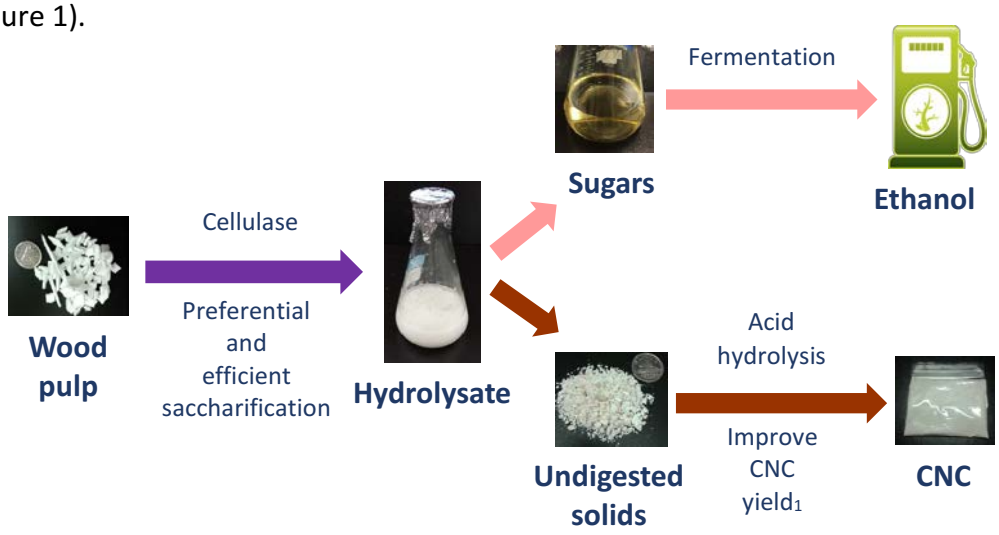

Figure 1 Flow chart of a biorefinery pathway that integrates cellulase treatment and acid hydrolysis for co–generation of sugars efficiently and CNC with improvement in yield.

An alternative biorefinery pathway is the integration of hydrothermal treatment with acid hydrolysis. Hydrothermal treatment involves modification and partial degradation of lignocellulose biomass components (in a slurry) with water heated at 150–230 °C [37][38]. During this treatment, moist heat facilitates the rotation of some bond angles in glucose to promote cellulose chains in para–crystalline cellulose to re–orient and crystallize. Hydrothermal treatment of raw wood has improved the CNC yield from the initial feedstock (wt % original feedstock, CNC $yield_2$) due to the formation of new CNC precursors [39]. It will be interesting to explore the effect of hydrothermal treatment on a purified feedstock such as wood pulp with lower hemicelluloses and only trace amount of lignin compositions. Studies show that the kraft pulping process increases crystallinity of wood pulp due to: (a) partial degradation of some amorphous celluloses and hemicelluloses, and (b) an increase in reaction temperature from 105 to 160 °C [40][41]. Yet, it is probable that further heating through hydrothermal treatment can increase the crystallinity of cellulose beyond what could be achieved from kraft pulping process and improve CNC $yield_2$.

In addition, hydrothermal treatment attacks hemicellulose that generates sugar degradation products such as furfural and organic acids [38][42]. Furfural is a valuable platform chemical and solvent with applications in agriculture, cosmetics and pharmaceutical industries [43][44]. A biorefinery strategy that integrates hydrothermal treatment with acid hydrolysis to co–produce furfural from hemicellulose degradation is yet to be explored (Figure 2).

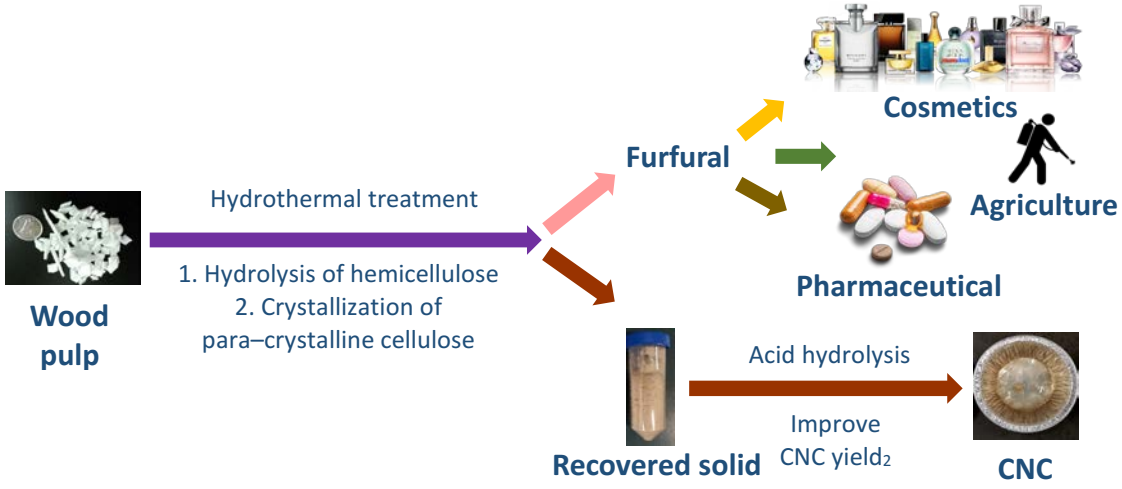

Figure 2 Flow chart of a biorefinery pathway that integrates hydrothermal treatment and acid hydrolysis for co–generation of furfural and CNC with improvement in yield.

Overall, the global objective of this study was to develop 2 novel biorefinery strategies that integrate CNC production from wood pulp with cellulase and hydrothermal treatments to co–generate ethanol and furfural, respectively, as value–added products. The specific objectives were to integrate CNC isolation with:

(a) cellulase treatment (2–10 h) using a Novozymes enzyme preparation supplemented with xylanase to:
    i. identify an efficient cellulase saccharification period that preferentially degrades non–crystalline cellulose and xylan to fermentable sugars with minimum loss to CNC precursors,
    ii. recover fermentable sugars from the saccharification process for co–production of ethanol, and
    iii. improve CNC $yield_1$ from acid hydrolysis of a cellulase–treated feedstock that has high CNC precursor concentration.

(b) hydrothermal treatment (150–225 °C) to:
    i. identify processing conditions (temperature range) that form new CNC precursors with minimal thermal degradation of cellulose,
    ii. improve CNC $yield_1$ and $yield_2$ from acid hydrolysis of a hydrothermally treated feedstock, and
    iii. co–generate furfural from degradation of xylan.

2. Literature review

2.1. Cellulose nanocrystals

In recent years, the demand for print media products has been declining due to the ever–growing use and popularity of electronic media [2]. Accordingly, the pulp and paper industry is aiming to diversify its purified cellulose product line through the isolation of cellulose nanocrystals (CNCs) as a high value–added product.

CNCs are nanoscale particles with characteristic high crystallinity that are isolated from cellulosic feedstock [45]. Different authors have designated multiple names to CNCs including cellulose nanowhiskers (due to the resemblance of the tapered ends), nanocrystalline cellulose (now a registered brand name by CelluForce, NCC™), nanoparticles, nanocrystals and nanofibers [3][45]. In recent literature, CNC seems to be the most frequently used term. Generally, the crystals have nanoscale dimensions of 3–5 nm width and 50–500 nm length with crystallinity in the range of 54–88% [3]. There is variability in the dimensions of CNCs isolated depending on the cellulosic feedstocks (Table 1).

Table 1 Length and width of cellulose nanocrystals (CNCs) from different sources.

Feedstock	Length (nm)	Width (nm)	Aspect Ratio	Reference
Wood	105–147	4.5–5	23–31	[46]
Cotton	130–180	10–14	NR	[47]
Coconut fiber	177–218	5–7	35–44	[48]
Rice straw	117–270	11–30	9–11	[49]
Bagasse	250–480	20–60	NR	[50]
Bacteria	1103	14	94	[51]
Tunicate	1187	9	148	[51]

NR—not reported.

2.1.1. Properties

Just like any other nanoparticle, CNCs exhibit high reactivity due to the high surface area to volume ratio and multiple hydroxyl groups for introducing functional groups [4]. The surface charge with or without modification can be exploited for electrostatic absorption of important chemical groups [52]. CNCs have superior mechanical strength due to their high crystallinity [4][53]. The tensile strength and axial elastic modulus (7.5–7.7 GPa and 110–220 GPa, respectively) of the light weight (1.6 g/cm^3 density) CNC are greater than or comparable with carbon fiber (1.5–5.5 GPa and 150–500 GPa, respectively) and steel (4.1 GPa and 210 GPa, respectively at 7.8 g/cm^3 density) [3].

Another unique feature of CNC is the formation of an iridescent colloid or film at a critical concentration. An anisotropic phase forms at high CNC concentration whereby CNC particles self assemble to a chiral nematic liquid crystalline ordering (twisted in helical structure) that reflect varying colors of light at different angles (as in soap) [54][55]. Addition of salt prior to drying allows the films to exhibit iridescence of visible light and strong magnetic or electric field can be used to manipulate the orientation of the crystals [12]. In addition, CNC films have gas and water barrier properties due to the strong hydrogen bonding network [56].

CNC colloids also exhibit shear thinning rheological behavior over time (as thixotropic non–Newtonian fluids) because the liquid crystals can align in the direction of shear flow [12]. This characteristic is desirable for maintaining low viscosity at high shear conditions in certain applications. CNCs can also form gels at 8–10 wt % concentration by sonic dispersion to form a 3-dimensional hydrogen bonded network [57].

As CNCs are produced from cellulose (mostly sourced from plant), these nanoparticles are abundant, biodegradable, sustainable and renewable. In addition, reports suggest no dermal or oral toxicity and low cytotoxicity, which makes CNCs applicable for reinforcing biomedical composite structures [58][59]. Hence, CNCs can serve as alternative substitutes to inorganic nanoparticles that exhibit high cytotoxicity [60]. Furthermore, ecotoxicological tests on 9 marker aquatic animals show that CNCs pose low toxicity to the environment [61].

2.1.2. Application and commercial production

CNCs can be used as reinforcement fillers to improve the performance of composite materials in various industries. The surface hydroxyl groups can be functionalized with charged or hydrophobic groups by chemical grafting (covalently linked) to ensure stable dispersion and allow the CNC to mix and react with nonpolar matrices, respectively [45][62]. CNC reinforced nanocomposites of cement, polylactic acid films, polyurethane foams and adhesives have shown improved mechanical properties [5]–[8]. CNC has also been studied as a bio–compatible filler to reinforce nanostructured biomedical materials such as hydrogels for tissue engineering and controlled transdermal drug delivery systems [63][64].

CNCs can confer shear thinning characteristics to fluids used for oil drilling, aviation (aircraft anti–icing), pharmaceutical, food, cosmetics, and paint industries [9]–[11]. The iridescent optical feature of CNCs can be exploited to develop colored films, security papers (such as bank notes and passports) and sensors [12]–[14]. The addition of CNC in food packaging films improves oxygen barrier property and water vapor permeability [15][16]. CNC exhibits high adsorbant properties due to electrostatic attraction with surface functional groups to remove cationic or anionic dye from waste waters or spill sites [17][18].

There are multiple scientific studies in the literature with promising findings that support these viable applications. Some of these potentials have been realized and CNCs are making way into commercial products. CNC is used as an absorbant in a high–performance anti–fog solution (FogKicker®) developed by Treaty Biotech LLC (MA, USA) for mirror, dive masks, goggles and visors [65]. Shlumberger Ltd (TX, USA) is using CNCs in its deep sea oil–drilling fluids to avoid sand contamination and reduce the carbon footprint of the process [66].

With growing research interest for bio–based renewable composite materials and the exciting potential applications in various industries, multiple companies and institutes in North America are currently producing CNCs at different scales to meet the demand. These include InnoTech Alberta (AB, Canada), CelluForce (QC, Canada), FPInnovations (QC, Canada), Bluegoose Biorefineries Inc (SK, Canada), Forest Product Laboratories (WI, USA) and InnoTech Materials LLC (WI, USA) [67]–[71]. CelluForce has a demonstration plant while other facilities operate at pilot

scale. Melodea Ltd (Sweden), Guilin Qihong Technology Co. Ltd (Gui, China) and Caspian Nanocellulose Polymer Development Co. (Iran) are companies producing CNC in Europe, Asia and the Middle East, respectively [72]–[74].

2.2. Structure and composition of lignocellulose: overview

Lignocellulose is composed of cellulose as a major reinforcement constituent embedded in a matrix of hemicellulose, lignin and minor components such as pectin, starch, protein, extractives and inorganics [75]. The following sections discuss the chemistry and organization of the major structural constituent celluloses as well as hemicelluloses and lignin to provide an insight on the transformations that occur during feedstock preparation and CNC isolation.

2.2.1. Cellulose

Cellulose is the most abundant natural homopolymer and major structural component of the plant cell wall (40–55% in hardwood and 45–50% in softwood) [76]. The homopolysaccharide is a linear chain of β–D–glucopyranose units held together by β1→4 glycosidic ether linkages (Figure 3) [77]. Cellulose in wood has an average degree of polymerization (DP, number of glucose units per chain) from 9000 to 15000 [75]. It is possible to completely hydrolyze celluloses with strong inorganic acids (H_2SO_4, HCl, H_3PO_3) while some Lewis acids (LiCl, $ZnCl_2$ and $Be(ClO_4)$), strong bases (NaOH) and metal complexes ($C_2H_6CuN_2$) can reduce the size of cellulose to low DP [78].

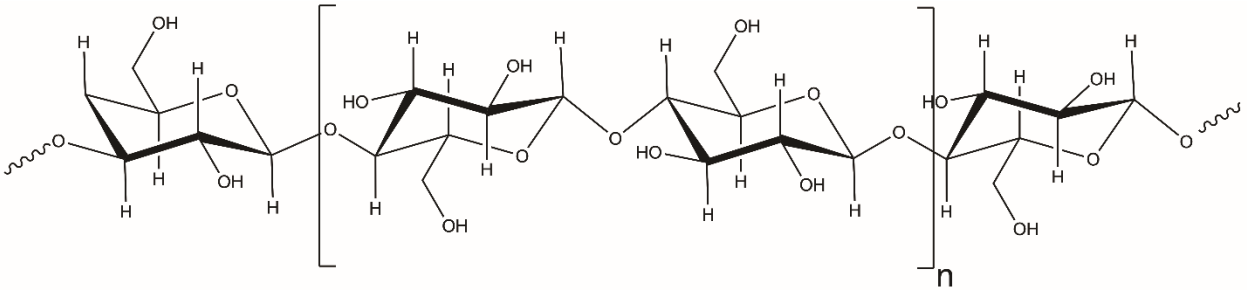

Figure 3 Linear chain structure of cellulose.

2.2.1.1. Structural organization

The surface of adjacent glucose units on a cellulose chain allows intrachain O_2–O_6 and O_3–ring O hydrogen bonds (Figure 4) [77]. Chains are then organized in parallel to form sheets through lateral interchain O_3–O_6 hydrogen bonds [79]. The sheets are then stacked in layers through multiple van der Waals forces as hydrogen bonds can no longer be formed [75][77][80]. This highly ordered organization with a hydrophobic core makes cellulose a rigid, crystalline and recalcitrant structure impermeable to acid, water and enzymes [79][81]. This native crystalline cellulose structure is referred to as cellulose I to differentiate it from other forms that are generated by chemical modifications (that will be discussed later). The lattice crystal structure of cellulose I can have 2 types of unit cells, I_α and I_β (Figure 5). Cellulose I_α has a triclinic unit cell whereby all sides (a, b and C) and angles (α, β and ϒ) are unequal while Cellulose I_β has a monoclinic unit cell comprised of 2 chains with all sides also unequal while angles α and ϒ are 90° [82][83]. Bacterial and algal cellulose have Cellulose I_α crystals while plants have both lattices [45].

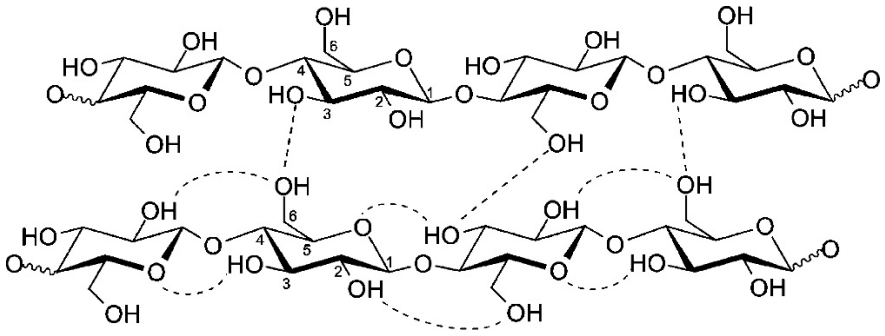

Figure 4 Intrachain (O_2–O_6 and O_3–ring O) and interchain (O_3–O_6) hydrogen bond within and between cellulose chains, respectively. The figure was republished with permission from Ionic Liquids and Their Interaction with Cellulose, Pinkert, A., Marsh, K.N., Pang, S., Staiger, M.P., Chem Rev, 109, 2009; permission conveyed through Copyright Clearance Center, Inc.

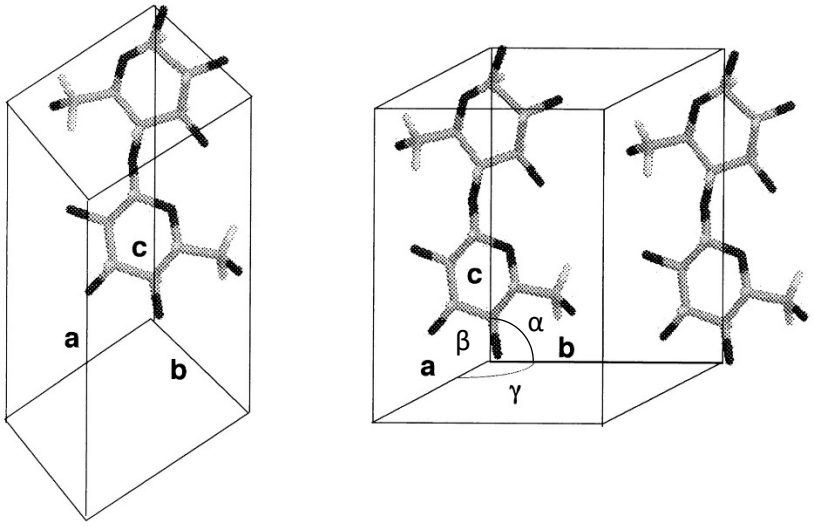

(a) (b)

Figure 5 A triclinic unit cell of cellulose I_α (a) and a monoclinic unit cell of cellulose I_β with 2 chains (b). The figure was adopted from National Academy of Sciences Copyright (1997) from Koyama, M., Helbert, W., Imai, T., Sugiyama, J., Henrissat, B. PNAS, 94, 1997.

The organization of the lignocellulose structure in the plant cell wall begins at the level of cellulose synthesis. The assembly is dictated by the rosette structure of cellulose synthase, an enzyme on the plant cell membrane that synthesizes cellulose [78]. Cellulase synthase is made up of 6 polypeptide units that bundle to form a globular subunit (Figure 6) [84]. The globular subunits are assembled in a group of 6 to form a rosette enzyme complex structure [85]. Each polypeptide unit polymerizes a single cellulose chain; hence, 36 parallel chains are simultaneously synthesized from the rosette structure, and the growing cellulose chains associate to form the elementary microfibril (3.5–7 nm wide) [84][86]. Multiple elementary microfibrils are bundled in a hemicellulose matrix to form a microfibril (10–25 nm wide) [77][87][88]. Lignin forms a gluing sheath around the outer surface of the microfibril or embeds in the interspaces between polysaccharides [89]. These microfibrils then further aggregate to macrofibrils (500 nm) that make up the fiber cell wall layer (1.7–3.7 µm wide) [87]. This cable like fiber network that is wrapped around plant cells gets further support from the internal turgor pressure to keep the plant structure erect and bear the heavy load [85].

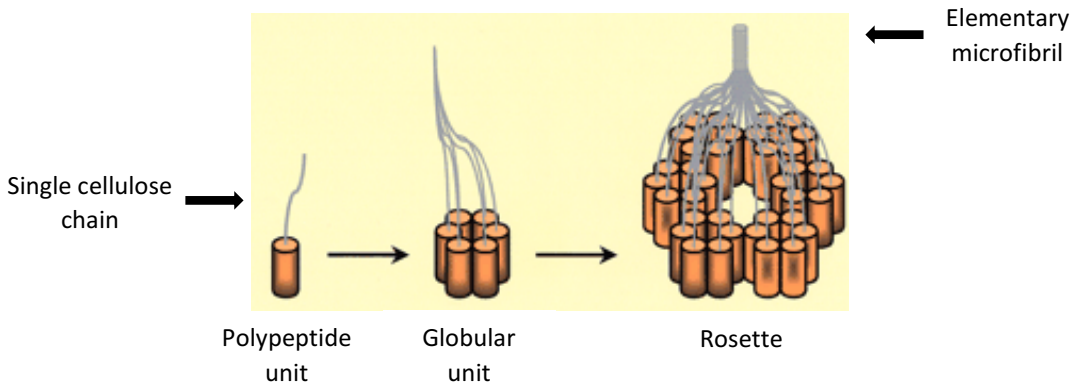

Figure 6 Structural components of cellulose synthase showing a polypeptide unit (left), a globular unit with bundles of 6 polypeptides (middle) and an assembly of 6 globular units forming a rosette structure (right). The figure was republished with permission of Oxford University Press, from Cellulose Biosynthesis in Plant: from Genes to Rosettes, Doblin, M.S., Kurek, I., Jacob–Wilk, D. and Delmer, D.P., Plant Cell Physiol., 43, 2002; permission conveyed through Copyright Clearance Center, Inc.

The process of wood cell wall formation follows sequential synthesis of layers to allow flexibility during cell growth and development. Accordingly, the cell wall is structured into 3 layers: middle lamella, primary and secondary cell wall (Figure 7) [90]. Middle lamella is the first layer formed during cell division, which is composed of highly lignified pectin [77]. Then, cellulose microfibrils, lignin, hemicelluloses, pectin and proteins are assembled to form the primary wall [90]. Proteins such as expansins in the primary wall may serve as cell wall loosening agent to promote cell wall expansion [91]. Once the cell completes its development, cellulose mirofibrils are organized in a highly ordered parallel orientation to form the highly rigid and thick secondary wall [90]. This inner most cell wall has 3 layers named S1, S2 and S3 with varying composition of lignin, hemicellulose and cellulose [75].

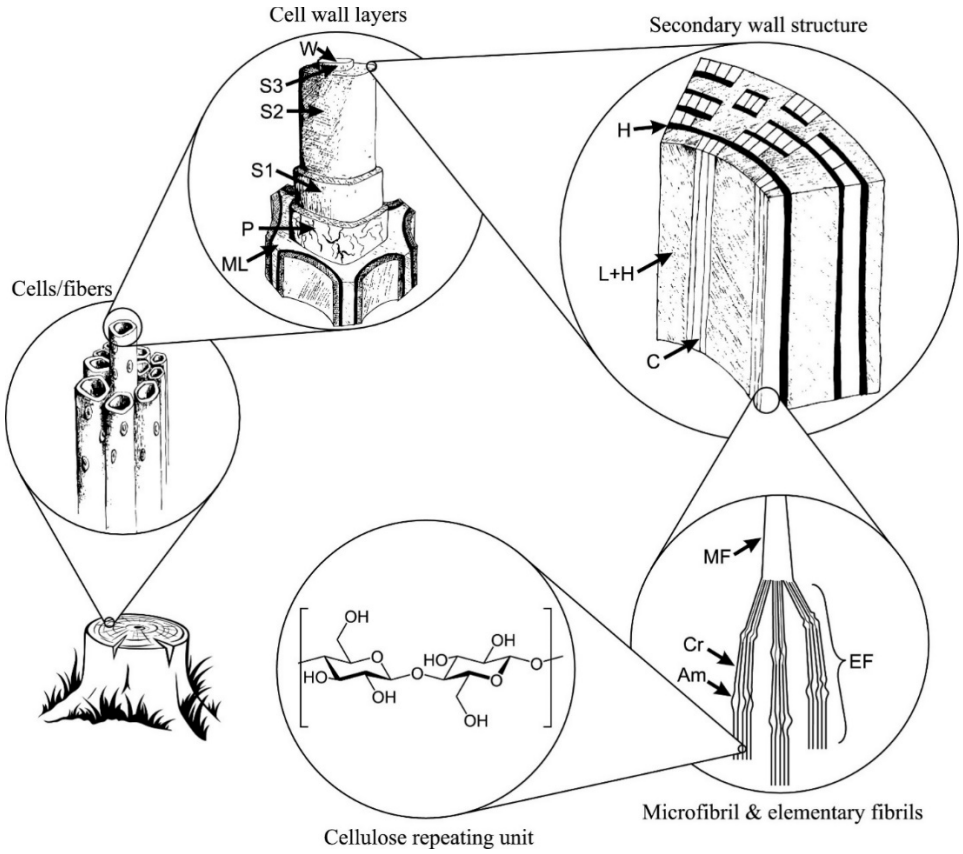

Figure 7 Organization of the cell wall structure at different levels showing the middle lamella (ML), primary wall (P), outer (S1), middle (S2) and inner (S3) secondary walls, warty layer (W), cellulose (C), hemicellulose (H), lignin (L), microfibril (MF), elementary fibril (EF), crystalline domain (Cr) and amorphous domain (Am). The figure was republished with permission of Elsevier BV, from Production of Cellulose Nanofibrils: A Review of Recent Advances, Nechyporchuk, O., Belgacem, M. N. and Bras, J., Ind. Crops Prod., 93, 2016; permission conveyed through Copyright Clearance Center, Inc.

Chemical treatment of cellulose can change the native structure (referred to as cellulose I) to different forms [86]. Cellulose II is formed when cellulose I is dissolved in strong alkali solution and regenerated with carbon disulfide [75]. Dissolution allows the chains to reorient in an antiparallel direction, which permits a thermostable structure with 2 new hydrogen bonds formed between layers that is not permitted in cellulose I (Figure 8) [77]. The antiparallel configuration cannot be achieved in nature because the chains in the elementary fibrils are synthesized at the same time from the rosette enzyme complex with the simultaneous formation of hydrogen and van der Waals bonds [85]. Regenerated cellulose is used to make textile products such as rayon and viscose through different chemical processing [78]. Modification of

cellulose I or II with amines generates cellulose III, which has a hexagonal unit cell [83][86]. Cellulose IV is formed by heating cellulose III in glycerol at high temperatures (260 °C)[75].

(a) (b)

Figure 8 Parallel and antiparallel arrangements of chains in (a) cellulose I and (b) cellulose II, respectively, showing 2 extra hydrogen bonds in cellulose II. The figure was republished with permission of Elsevier Ltd, from Mercerization of Cellulose: 1. Determination of the Structure of Mercerized Cotton, Kolpak, F.J., Weih, M. and Blackwell, J., Polymer, 19, 1978; permission conveyed through Copyright Clearance Center, Inc.

2.2.1.2. Crystallinity

The cellulose fiber is not entirely crystalline due to imperfections in the extent of chain ordering. Hence, the structure of cellulose has been divided into crystalline, poorly ordered or amorphous and relatively less ordered or para–crystalline domains [19][20]. Amorphous and para–crystalline celluloses will be collectively referred to as non–crystalline celluloses in the rest of the body of this thesis unless required to state and specify the level of the ordering. The disorders have been identified at different organization levels in the cellulose structure. There are some irregularities in the intramolecular O_2–O_6 hydrogen bonds within each cellulose chain [92]. Elementary fibrils have deformities along the length (Figure 7) and the order of crystallinity weakens from the core to the outer layer [36][93]. Some level of disorder is also apparent in the microfibril due to the change in angle along the longitudinal axis [94]. This implies that amorphous celluloses could be found interspersed with or buried within crystalline cellulose in the fiber structure at a different structural level of organization [95]. Amorphous celluloses are much more susceptible to enzymatic or acid hydrolysis due to accessibility of the glycosidic bonds. However, amorphous cellulose domains located in the core of crystalline layers are not accessible to hydrolysis [96].

The crystallinity of purified cellulose, which can be measured by X–ray diffraction (XRD) intensity analysis, varies depending on the source (Table 2). Tunicate cellulose has high crystallinity while

low levels of crystalline ordering are reported from herbaceous plants. However, these values may not accurately represent the crystallinity of the native cellulose as the physico–chemical processes to purify cellulose may have altered the original structure.

Table 2 Crystallinity of cellulose from different sources.

Cellulose source	Crystallinity index*	Reference
Hemp pulp	52	[97]
Corn pulp	63	[98]
Softwood pulp	71	[99]
Hardwood pulp	73	[99]
Cotton pulp	83	[99]
Tunicate pulp	95	[100]
Microcrystalline cellulose**	92	[101]
Bacterial microcrystalline cellulose	95	[101]

*Crystallinity index was calculated by the peak height method from X–ray diffraction analysis

**Microcrystalline cellulose is a model crystalline cellulose generated by acid hydrolysis of amorphous cellulose from purified cellulose (kraft pulp).

2.2.2. Hemicellulose

Hemicellulose is the second most abundant polymer (24–40% in hardwood and 25–35% in softwood) and is composed of pentose and hexose sugars [76]. The sugars are linked together by β1→4 glycosidic bonds, but unlike cellulose, the polymer has lower DP (100–200) and it is branched at β(1→2, 1→3 and 1→6) with acetylated and methylated side groups (Figure 9) [75][102]. The side chains hinder intra– and inter–molecular hydrogen bonding, making hemicelluloses amorphous [103]. The different hexose and pentose sugar constituents determine the nomenclature of the heteropolymer (glucuronoxylan, galactoglucomannan, arabinogalactan, etc) [75]. If the hemicellulose in either hardwood or softwood has xylose composition, it is simply referred to as xylan [77]. Xylan and galactoglucomannan constitute the major hemicelluloses found in hardwood and softwood, respectively [75]. Hemicellulose forms covalent bonds with lignin while it is linked to cellulose through non–covalent interactions due to the similarity in surface functional groups [78][79]. The physiological role of hemicellulose is depicted to be mainly in maintaining the cell wall architecture and cell growth regulation [78].

The polysaccharide can be dissolved in highly alkaline solutions and it can be degraded with acids [104].

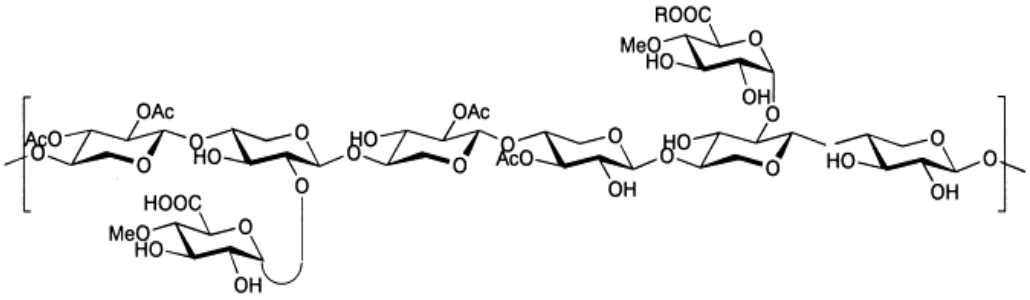

Figure 9 Linear chain structure of xylan with acetylated and methylated side groups. The figure was republished with permission of Elsevier, from Structure of Neutral Branched Xylooligosaccharides Produced by Xylanase from In Situ Reduced Hardwood Xylan, Nishimura, T., Ishihara, M., Ishii, T., Kato A. Carbohydr. Res., 308, 1998; permission conveyed through Copyright Clearance Center, Inc.

2.2.3. Lignin

Lignin is an amorphous polypropane polymer, which makes up another important component of the plant cell wall (18–25% in hardwood and 25–35% in softwood) [76][78]. The major building blocks for lignin synthesis are p–coumaryl, coniferyl and sinapyl alcohols [79]. These alcohols polymerize to form syringyl, guaiacyl and p–hydroxyphenyl units that are linked with ether and C–C bonds to form complex structures (Figure 10) [104][105]. Hardwood lignin is mostly composed of syringyl and guaiacyl lignin (predominantly comprised of synapyl and coniferyl alcohols) while guaiacyl lignin (mostly from coniferyl alcohol polymerisation) is mainly prevalent in softwood [75]. Lignin can be dissolved in alkali–salt solutions (lignosulfonate) and organic solvents such as dimethyl sulfoxide, methanol, ethanol and acetone (organosolv lignin) [78]. Inorganic acid digestion (72% H_2SO_4) generates Klason lignin and an acid insoluble residue [104][106].

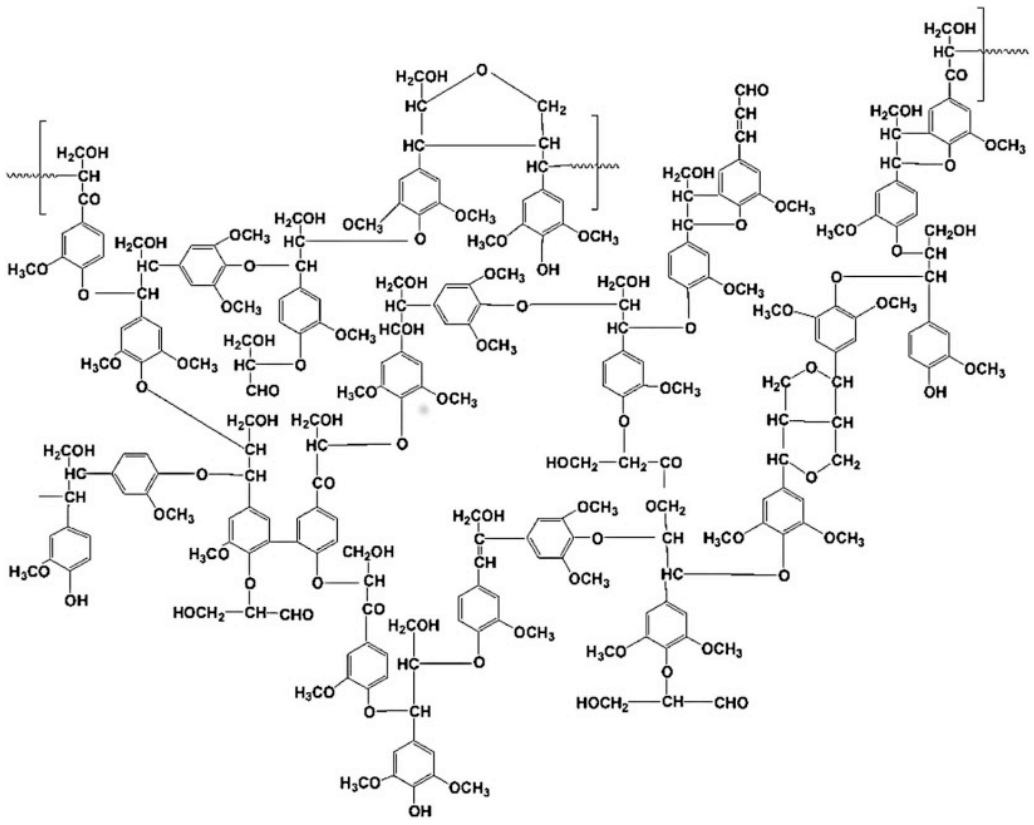

Figure 10 Model structure of lignin. The figure was republished with permission of Elsevier, from Polysaccharides and Lignin from Oak wood Used in Cooperage: Composition, Interest, Assays: A Review, Floch, A. Le, Jourdes, M., Teissedre, P–L., Carbohydr. Res., 417, 2015; permission conveyed through Copyright Clearance Center, Inc.

2.3. Wood pulp: an ideal feedstock for cellulose nanocrystal isolation

CNC can be isolated from cellulose mostly derived from plants as well as bacteria and animals (tunicate) (Table 1). For commercial CNC isolation, wood pulp is the most feasible feedstock as it is a highly purified form of cellulose produced on large scale in pulp mills. It is also currently used as a feedstock in facilities such as InnoTech Alberta and CelluForce [67][68]. The kraft pulp process for production of wood pulp and its effect on the composition and structure of fiber will be discussed in the following sections.

2.3.1. Kraft pulp overview

Pulping is the chemical and/or physical process of redistributing components of wood or other lignocellulosic biomass to isolate and disperse cellulose fibers in order to reform a web structure [107]. Wood or waste paper feedstock are subjected to mechanical, chemical, semi–chemical and

recycling processes in pulp mills [108]. Mechanical processes (grinding) give high yields with lower pulp strength while chemical pulping processes lower the yields but produce long fibers that form strong hydrogen bonds [107]. Semi–chemical pulping involves chemical pre–treatment so that the mechanical refining process can be moderated to generate long fibers [108]. As the yield and properties of pulp from each process is variable, the paper industry makes techno–economical considerations to produce specific products from each pulp. Mechanical pulps are used to make low grade print materials; chemical pulps are suited for high quality printing papers and tissue and semi–chemical pulps can be processed to produce corrugated boards and food packaging papers [108]. Most pulp mills commonly transform virgin wood by a chemical process referred to as kraft pulping [108]. The word 'kraft' in Swedish and German translates to strength as the process preserves longer fibers that confer high strength properties to the pulp [109].

Kraft pulping involves cooking the fiber material in an alkaline solution composed of NaOH and Na_2S (white liquor) at elevated temperature (160–170 °C) to remove lignin in a pressurized reactor (digester) [108][110]. Hydroxide and hydrosulfide ions degrade and solubilize lignin to small fragments due to the introduction of hydrophilic groups [109]. After alkaline lignin solubilization, the digester is de–pressurized suddenly to physically separate the fiber particles [110]. The pulp is separated from the spent alkaline solution (black liquor) for washing to remove residual alkaline solution and soluble lignin [108]. The black liquor is concentrated and burnt to combust organic wood degradation products and to recover the chemicals used in the white liquor [110]. Chemical recovery and energy captured from combustion (steam generation) makes the pulping process economically feasible [108]. Even though most of the lignin is dissolved in the cooking process, raw kraft pulp appears brown due to some residual lignin that can be removed by subsequent bleaching [111]. Oxygen delignification is the first step in bleaching whereby, phenolic groups in lignin are ionized by highly alkaline solutions followed by degradation with molecular oxygen bubbled into the tank [110]. The pulp is subsequently brightened with bleaching agents such as chlorine gas, chlorine dioxide and hydrogen peroxide [111]. Due to environmental pollution concerns with elemental chlorine, modern pulp mills (such as the Alberta Pacific Forest Industries Inc plant) use elemental chlorine–free bleaching chemicals [108][112].

2.3.2. Effect of kraft pulping on fiber composition and structure

Kraft pulping changes the composition of lignin and structural carbohydrates of virgin wood (Table 3) [113]. Substantial degradation of lignin allows cellulose to accumulate while hemicellulose is partially hydrolyzed. It has been suggested that alkaline pulping can lead to degradation of cellulose and hemicellulose chains from the reducing ends (peeling) [109]. Bleaching may also result in the breakdown of hemicelluloses [111]. Gumuskaya *et al.* observed that the crystallinity index of cotton cellulose improved due to alkaline pulping and increase in reactor temperature from 105 to 160 °C [40]. Kraft pulping also leads to degradation of amorphous cellulose that increases the crystallinity of wood pulp [41]. The partial degradation of hemicelluloses could facilitate cellulose chains to form a more compact structure evident from an increase in the aggregate size [114][115]. The residual hemicelluloses (such as xylan) initially solubilizes during pulping with the loss of side groups; but as alkalinity decreases in subsequent cooking, it precipitates to a more crystalline structure and gets interspersed with crystalline cellulose [116].

Table 3 Lignocellulose composition of raw and bleached kraft pulp

Constituent	**Composition (wt %)**			
	Birch		**Poplar**	
	Raw	**Bleached Kraft pulp**	**Raw**	**Bleached Kraft Pulp**
Lignin	22.0	NR (2.9)*	20.8	NR (2.2)*
Cellulose	41.0	66.6	49.2	74.3
Xylan	27.5	22.1	21.1	15.0
Glucomannan	2.3	0.2	3.1	0.2

*Lignin composition in kraft pulp prior to bleaching as determined from Kappa number, NR–not reported. Table recreated and republished with permission of Springer Nature, from European Hardwoods Versus *Eucalyptus globulus* as a raw material for pulping, Patt, R., Kordsachia, O. and Fehr, J., Wood Sci. Technol., 40, 2005; permission conveyed through Copyright Clearance Center, Inc.

2.4. Cellulose nanocrystal isolation processes

CNCs represent nanoscale highly crystalline elementary fibril isolated by severe degradation of amorphous cellulose using chemical, enzymatic and thermochemical processes [45]. The following sections discuss established methods and different approaches under development that can be integrated into CNC isolation processes.

2.4.1. Mineral acid hydrolysis

Acid hydrolysis experiments on cellulose towards the end of 1940s led to the discovery of CNCs. Nickerson and Harble noticed that mild acid hydrolysis (with 2.5 N HCl) starts rapidly during initial stages from degradation of amorphous and para–crystalline cellulose, which stabilizes over time when the crystalline cellulose remains [20]. Ranby later on generated stable CNC colloids (sols) by washing the undigested crystalline cellulose from controlled acid hydrolysis as free acid was removed and the pH was raised above 3 [117]. Acid hydrolysis still remains to be the most common method for isolating CNCs [21]. Strong inorganic mineral acids such as sulfuric (H_2SO_4) or hydrochloric (HCl) acid are mainly used for hydrolysis [117]–[121]. The strong acid degrades the readily accessible glycosidic bonds in the non–crystalline cellulose chains, whereas the tightly packed highly crystalline region remains recalcitrant as it limits the penetration of acid and water [3][45][81][122]. In this process, the acid protonates either the glycosidic or cyclic oxygen to promote nucleophilic attack on the glycosidic bonds (and therefore cellulose chains) with water [123]. Under controlled conditions, acid hydrolysis stabilizes over time and releases homogenous size fragments (also referred to a level–off DP), which are thought to correspond with the native size of the crystals with the highest level of ordering [20][45].

A CNC isolation process using sulfuric acid involves (a) hydrolysis with strong acid concentrations (typically 64–65 wt%), (b) termination of the reaction with cold water, (c) multiple washing steps and dialysis to remove excess acid or sodium sulfate salt (if neutralized with NaOH), (d) sonication to ensure dispersion of aggregates in the colloid, and (e) filtration to separate the over–size particles [12][46][118][120][124]. Optimization studies show that the critical acid concentration is between 58–62% as ≤ 55% acid lead to incomplete hydrolysis while ≥ 65% significantly solubilizes crystals [21][125][126].

The type of acid used for extracting CNCs can affect the characteristics of the final CNC product. When sulfuric acid is used, sulfate groups from the acid esterify the free hydroxyl groups on the CNC surface [123]. Negative charges on the surface create an electrostatic repulsion force that maintains a stably dispersed CNC colloid in non–acidic aqueous solutions [127]. In contrast, CNCs generated from HCl hydrolysis do not have surface charge that allow the crystals to aggregate and flocculate due to van der Waals attraction in aqueous solutions [120]. This is relevant for reinforcement applications because when particles self–aggregate, the high surface area that allows CNCs to bond with the matrix and impart strong mechanical properties is compromised [4]. However, these esterified sulfates could be dissociated in mild alkaline solutions and chemical functionalization with a charged group may be necessary [45]. Furthermore, it has been demonstrated that the CNC generated from HCl hydrolysis are not thixotropic (shear thinning not achieved over finite time) at concentrations below 0.5% due to the poor surface charge density [12]. On the other hand, CNC from H_2SO_4 hydrolysis are less stable at elevated temperature due to de–sulfation and subsequent release of H_3O^+ that can catalyze cellulose degradation [128]. Hence, H^+ is exchanged with Na^+ by neutralizing the colloid with NaOH to improve the thermal stability, which is very important as most composites are processed at high temperatures [22][121].

The CNC isolation process requires large volumes of concentrated and highly corrosive acid that also generates significant effluent to be treated prior to disposal. Domtar (which has ownership in CelluForce) developed a patented process for recovering the acid used for hydrolysis [28]. Undisclosed water–insoluble solvents were used to separate the acid from the aqueous streams by simple liquid–liquid extraction. The acid could then be recovered from the water–insoluble solvent via conventional distillation techniques. Implementation of an acid recovery system has been indicated by CelluForce in its production process [129].

2.4.2. Hydrolysis with organic acids and oxidants

Efforts have also been made to isolate CNCs using organic acids and oxidants. Chen *et al*. used oxalic acid at high concentrations (30–80%) and temperature (80–120 °C) to generate CNC with surface carboxyl functional groups [22]. The acid has relatively lower toxicity and can be recycled

via crystallization. However, the reactions need to be carried out at very high temperatures and CNC yields were relatively lower due to the poor acid strength.

Strong oxidants such as ammonium persulfate have been explored for CNC isolation from flax and hemp fibers with promising results [23]. Ammonium persulfate can dissolve lignin, hemicellulose and pectin. Hence, the process does not require a purified cellulose feedstock, which can significantly reduce the process cost. The reaction is carried out with 0.5–1.0 M ammonium persulfate at 45–60 °C for 5–16 h. The CNC generated yields uniform size distribution, with high aspect ratio and surface carboxyl groups (acid or sodium salt form), which can be functionalized. Relative to acid hydrolysis, ammonium persulfate is advantageous in terms of lower cost and long–term toxicity [130].

2.4.3. Cellulase hydrolysis

Cellulases can be employed for preferential degradation of amorphous cellulose to isolate CNCs. In the subsections below, the mechanism of cellulase catalysis will first be discussed to establish a general understanding on cellulose hydrolysis followed by different approaches to regulate and integrate cellulase catalysis to CNC isolation process.

2.4.3.1. Introduction to cellulase catalysis

A. Class, structure and mechanism of cellulase hydrolysis

Microbes that utilize dead or living plant materials as a carbon source produce cellulase enzymes to degrade the insoluble, recalcitrant and large cellulose substrate to release and metabolize simple sugars. Cellulases are produced as extracellular sets of hydrolytic enzymes supplemented by accessory oxidative enzymes such lytic polysaccharide monooxygenase and other proteins such as swollenin and expansin, that loosen the tightly packed domains [131]. Hydrolytic cellulases are divided into three major groups namely (a) endoglucanases (EG, enzyme commission number {EC 3.2.1.4}), (b) exoglucanases that are further divided in to cellobiohydrolases (CBH, EC 3.2.1.91) and glucanohydrolase (EC 3.2.1.74) and (c) β–glucosidases or cellobiases (EC 3.2.1.21) (Figure 11) [132]. Endoglucanases have an open groove conformation that limits the enzymes to non-processive and random fragmentation of internal amorphous

cellulose chains to create accessible open ends and release oligosaccharides (Figure 11, 12a) [29][133]. In contrast, the tunnel configuration of cellobiohydrolases allows the processive channelling of chains (Figure 12) [29]. Hence, cellobiohydrolases can bind to reducing or non–reducing ends (CBHI and CBHII, respectively) of crystalline or amorphous cellulose and thread through the chains to cleave off cellobiose units (Figure 11) [134]. Glucanohydrolase, which is the other type of exoglucanase, can directly release glucose units from chain ends [132]. Cellobiose and glucans with low DP are degraded to glucose with β–glucosidases [29].

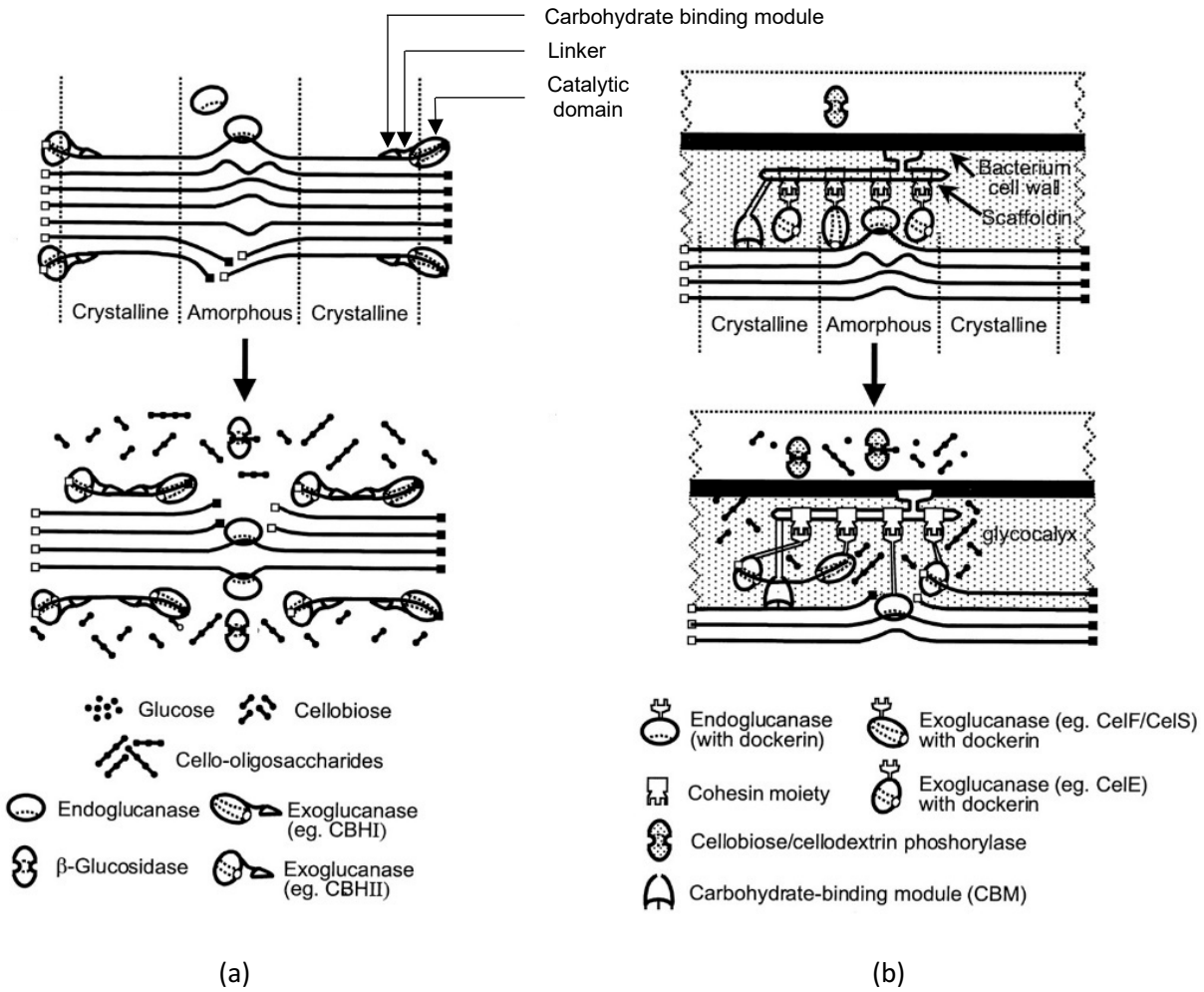

(a) (b)

Figure 11 Illustrations of the mechanism of cellulose hydrolysis through the synergistic action of (c) cell free extracellular and (d) cell bound cellulases showing multiple components. The figure was adopted from Microbial Cellulose Utilization: Fundamentals and Biotechnology, Lynd, L.R., Weimer, P.J., van Zyl, W.H. and Pretorius, I.S., Microbiol. and Mol. Biol. Rev., 66, 2002.

(a) (b)

Figure 12 Open cleft and tunnel structures of (a) endoglucanase and (b) exoglucanase enzymes, respectively. The figure was republished with permission of Cell Press, from Structures and Mechanisms of Glycosyl Hydrolases, Davies, G. and Henrissat, B., Structure, 3, 1995; permission conveyed through Copyright Clearance Center, Inc.

Hydrolytic cellulases are glycosylated proteins with two main components: the catalytic domain and the carbohydrate binding module (CBM) attached with a glycosylated linker (Figure 11a) [135][136]. Amino acid residues in the catalytic domain participate in protonation, deprotonation and nucleophilic substitution reactions that activate water to attack the glycosidic oxygen and cleave the glycosidic bond [137][138]. The role of the CBM is to bring the enzyme in close proximity to the cellulose surface, thereby increasing the concentration and improving processivity [139]. There are also suggestions that CBMs can open up the cellulose structure [135]. In anaerobic bacteria and fungi, the hydrolytic cellulases form multi–enzyme complexes called cellulosomes [133]. Cellulosomes contain a scaffold protein, which bears the catalytic enzyme domain and a cohesion unit with a receptor for the dockerin domain that is attached to and locks the catalytic domain on the scaffold (Figure 11b) [140]. These complexes can bind to the cell surface through a hydrophilic domain and form elongated filamentous extensions that connect the cell to the substrate; alternatively, the enzyme complex can also function detached from the cell [140][141]. Cellulosomes promote efficient synergism as all the catalytic cellulases are localized [29]. However, relative to the free enzyme counterparts, due to the large molecular weight of the cellulosome structures, penetration into cellulose is limited [134]. Interestingly, most aerobic filamentous wood decaying fungi that efficiently degrade cellulose (such as *Trichoderma* sp.) do not produce cellulosomes and secrete free extracellular cellulase sets that bear CBM and catalyze celluloses synergistically [133]. In addition to hydrolytic catalysis, accessory enzymes such as lytic polysaccharide monooxygenase (specifically AA9 family,

previously referred to a glycoside hydrolase) greatly enhance the activity of hydrolytic cellulases [142]. These proteins induce oxidative cleavage of cellulose by insertion of oxygen on C–H bonds adjacent to glycosidic linkages (C1 and C4) and increase the accessibility of crystalline cellulose domains [143][144].

Various reports show that cellulases rapidly hydrolyze amorphous cellulose [32]–[34]. During the course of hydrolysis, the reaction rate slows down due to the increase in concentration of the crystalline substrate [35]. Crystalline cellulose degradation is relatively delayed because cellulases cannot enter the tightly packed core until the enzymes gradually loosen the structure [36]. However, as amorphous cellulose has non–uniform distribution in the microfibril (as discussed in section 2.2.1.2), some chains are likely to be buried between layers of crystalline structures that limits exposure. Studies show that during enzymatic digestion, the total amorphous celluloses are not simultaneously accessible as the cell wall is only gradually peeled off layer by layer [36][145]. Zhao *et al*. observed no change in the crystallinity of cotton cellulose, even after controlled acid hydrolysis to degrade amorphous cellulose, which further supports the suggestion that amorphous cellulose in the core is not accessible to enzymes [96].

B. Xylanase as an accessory enzyme

Xylanase is an important accessory enzyme for efficient saccharification of cellulosic biomass. Hu *et al*. showed that cellulase supplemented with xylanase improved cellulose hydrolysis by 10–100% [146]. It has been suggested that xylan could have limited the processive activity of cellulases by steric hinderance. Furthermore, the competitive binding of xylanases with the substrate also induces the displacement of cellulases that are non–productively adsorbed. Commercial cellulase preparations such as Novozyme's Cellic CTec 3 contain hemicellulases that are extracted either from the producer or another organism source [147]. Novozymes also suggests additional hemicellulase supplementation if the substrate has significant hemicellulose composition.

Complete hydrolysis is achieved through random cleavage of xylan to short chain xylo–oligosaccharides by endoxylanase (EC 3.2.1.8) followed by removal of xylose units from non–reducing xylo–oligosaccharide ends by xylohydrolase (EC 3.2.1.37) [148]. Xylanases have been

well studied for various applications in various industries such as: (a) pulp and paper to enhance bleaching by removal of xylan to free lignin, (b) bakeries to increase dough viscosity and bread volume, (c) beverage industries to improve the clarity of fruit juice; and (d) textile industries to facilitate de–sizing to remove coating on thread and scouring to remove non–cellulosic contents in cotton [149]–[152].

C. Commercial cellulase production

Cellulases are produced by various fungi and bacteria. However, commercial cellulase solutions are primarily produced from the filamentous fungus *Trichoderma reesei*. This fungus expresses 8 endoglucanases, 2 cellobiohydrolases, 7 β–glucosidases and swollenin [133]. CBHI (60%), CBH II (20%) and EG I (10 %) account for 90 % of the total protein secretion while β–glucosidases are only produced in low titers [153][154]. Hence, cellulase preparations (Celluclast 1.5L) have been supplemented with β–glucosidases to improve cellulose hydrolysis by up to 38% [155]. However, it is speculated that the latest commercial cellulase solutions (Cellic®CTec series by Novozymes and Accelerase® by Genencor) are prepared from genetically engineered *T. reesei* strains that produce β–glucosidases in high titers [134]. Further strain development on *T. reesei* have been made to improve the activity of commercial cellulase preparations through genetic manipulations such as expression of native or exogenous thermostable CBHs, xylanases and glucose hydrolase proteins as well as overexpression of EG [156]. Currently, the three major commercial producers of cellulases are Novozymes® A/S, DuPont® (now a subsidiary of Dow Chemical Company) and Royal DSM NV Ltd (Dutch State Mining) [157].

2.4.3.2. Endoglucanase mediated cellulose nanocrystal isolation

Endoglucanases can selectively cleave amorphous cellulose chains (as discussed in section 2.4.3.1.) to generate a residue of crystalline fragments with CNC dimensions. Filson *et al.* isolated CNC from endoglucanase hydrolysis (84 Endoglucanase Units, 2 h) of recycled pulp [25]. However, endoglucanase degradation had to be carried out in multiple cycles to get substantial yield and the isolated CNC had a very broad particle size distribution (100–3500 nm). Anderson *et al*. also hydrolyzed pulp with endoglucanase (7.85 U/mg activity, 10 wt % pulp) for 24 h to get a maximum 10% CNC yield after 62 h [158]. Teixeira *et al*. hydrolyzed microfibrillated cellulose

(MFC) prepared from various substrates with endoglucanases (supplemented with β–glucosidase) for 72 h to isolate glucose (17–67 % cellulose conversion) and CNC (500–750 nm long and 4–12 nm in diameter) [159]. Some of the MFC were still apparent and CNC yield from some of the substrates was very poor.

Mechanical combined with/ without chemical treatment prior to endoglucanase hydrolysis has been introduced to increase the surface area and hence improve enzyme activity. Siqueira *et al.* and Xu *et al*. studied the effect of shearing and chemical–sonication–microwave treatments of pulp, respectively; but the CNC generated still had broad size distribution with lengths spanning to micrometer dimension [160][161]. George *et al*. hydrolyzed mechanically sheared (5000 to 6000 rpm, 30 min) bacterial cellulose with endoglucanase to successfully isolate CNCs with length and diameter in the range of 100–300 nm and 10–15 nm, respectively [162]. Endoglucanase treatments have also been employed to supplement standard CNC isolation processes. Siqueira *et al*. and Campos *et al*. isolated CNC with homogenous size distribution from acid hydrolysis and sonication of endoglucanase–treated cellulose [160][163].

2.4.3.3. Integrated bioethanol and cellulose nanocrystal co–production

Even though endoglucanases are selective, (a) hydrolysis is generally very slow as the enzyme is not processive, (b) sugar co–products that could be fermented to fuels or other chemicals cannot be generated as saccharification is incomplete without cellobiohydrolases and β–glucosidase activities, and (c) the CNC yield is very low. An alternative strategy is to adopt a biorefinery approach and integrate CNC isolation with a cellulose saccharification process that is already established from the cellulosic ethanol industry. In the sections below, cellulosic ethanol production process will be briefly introduced and a biorefinery pathway that integrates CNC isolation with ethanol production will be discussed.

A. An overview on cellulosic ethanol production

Ethanol is an alternative liquid fuel that can mitigate concerns over dependence on petroleum oil and greenhouse gas emission from combustion [30][31]. Corn and sugarcane are the major feedstocks used for fermentation of what is referred to as the first generation bioethanol from simple sugars [164]. However, the utilization of these crops for biofuel production can influence

food supply and pricing for the continually growing world population, which in turn aggravates the “food vs fuel” conflict [30]. This issue can be resolved by producing second generation or cellulosic bioethanol from lignocellulosic biomass feedstock, which is a highly abundant, renewable and low cost feedstock [165]. These feedstocks include wood, energy crops (miscanthus and switch grass), agricultural residues (wheat straw and corn stover) and municipal residue biomass [166].

Lignocellulosic biomass requires pretreatment to make cellulose, the major sugar reservoir, accessible for hydrolysis [76][103][167]. Pretreated biomass is subsequently subjected to either acid or cellulase hydrolysis to saccharify cellulose to fermentable sugars. Dilute acid (1.5%) at elevated temperatures can completely hydrolyze cellulose; but the process co–generates sugar degradation products such as hydroxymethyl furfural and furfural that inhibit yeast fermentation [76]. Weyland AS (a cellulosic ethanol pilot plant in Norway) developed a concentrated acid hydrolysis technology to release sugars at higher yields with a patented acid recycling process to ensure economic feasibility [166]. On the other hand, cellulase hydrolysis is an environmentally friendly biological degradation process [31]. Cellulase preparations composed of all the three classes (discussed in section 2.4.4.1.) are required for complete saccharification to simple sugars. The major limitations in utilizing cellulase are the relatively higher cost of the enzyme and slower hydrolysis rates mainly due to cellulose crystallinity (as discussed in section 2.4.4.1.) compared with other enzymatic processes (for example, starch hydrolysis rate with amylase is 100 fold faster) [103][167]. Yet, cellulases are currently employed in the saccharification process for the production of cellulosic ethanol on a commercial scale by companies such as POET–DSM (Project Liberty, US, corn crop residue feedstock) and Iogen Energy Corporation (Raizen, Brazil, bagasse feedstock) [168][169]. Ethanol fermentation can be carried out at the same time during hydrolysis (simultaneous saccharification and fermentation, SSF) or sequentially after collecting the hydrolysate (separate hydrolysis and fermentation, SHF). SSF eliminates feedback inhibition and the use of a single reactor decreases process time and reactor volume [76]. SHF on the other hand allows optimal conditions for both hydrolysis and fermentation with high substrate loading [167]. *Saccharomyces cerevisiae* is the most common yeast used to ferment glucose while

companies like Iogen use genetically modified yeasts that can ferment both hexose and pentose sugars [169].

Even though cellulosic ethanol is an advanced biofuel alternative, the sustainability of the industry is under threat due to inefficiency and high cost of the production process and inability to compete with low price of gasoline [170]. Major industry players such as DuPont and Abengoa have recently sold their established commercial plants to other companies with alternative interests, which indicate lack of future business interest in cellulosic ethanol [171]. Biorefinery strategies that can integrate cellulosic ethanol production with other processes that transform the lignocellulosic feedstock to value–added chemicals could potentially give the industry diverse market opportunities to ensure sustainability.

B. A biorefinery approach

There is increasing interest in a lignocellulose biorefinery approach to sustainably generate renewable and marketable chemicals, fuels and materials by integrating physical, chemical, biological and thermochemical biomass conversion processes in a single facility [172][173]. This strategy allows maximum utilization of biomass due to production of a spectrum of high-value products [174].

Pulp mills can adopt such biorefinery pathways by expanding process technologies to add cellulosic ethanol and CNC into their traditional product streams. In this approach, the wood pulp cellulose can be partially saccharified and CNC can be co–produced from the recalcitrant crystalline cellulose. This strategy eliminates the need for costly pretreatment and saccharification processes adopted in biofuel industries to reduce cellulose crystallinity. Very limited studies have shown insights into this pathway (Table 4). Novo *et al*. lowered the reaction temperature from 50 to 35 °C and extended the cellulase hydrolysis time to 120 h to switch the hydrolysis reaction outcome from saccharification to CNC isolation [26]. Other studies have evaluated the integration of cellulase hydrolysis with conventional CNC isolation processes. Camargo *et al*. used acid hydrolysis to isolate CNCs from solid residue left over from a saccharification process (55–60% conversion) of an ethanol plant [175]. In these studies, the CNC yields were not determined to assess the efficiency of the process. Beltramino *et al*. reported

improvement in CNC yield by acid hydrolysis due to cellulase treatment; but the prospect of sugar recovery from cellulase hydrolysis was not explored [176]. Oksman *et al*. isolated CNC with very high yield from cellulose residue of an ethanol plant using mechanical homogenization that requires high energy and is difficult to scale–up [177]. CNC isolation from recalcitrant cellulose residue generated from an ethanol plant may have low efficiency as there would be substantial loss in CNC precursors (large crystalline cellulose that are converted to CNC by fragmentation) from pretreatment and saccharification processes. The compromise in CNC yield is also not cost–effective as the price of CNC is much higher than sugars.

Table 4 Integrated cellulase treatment and CNC isolation processes

Feedstock	Cellulase*	Cellulose conversion (wt %)	CNC isolation process	CNC yield (wt %)	CNC dimension Length X diameter (nm)	Reference
Eucalyptus Pulp	Cellic CTec3	63	Cellic CTec3, 120 h, 35 °C	NR	200 X 15	[26]
Pretreated bagasse	Cellic CTec2	55–60	Acid hydrolysis 60 v %	NR	193–246 X 14–18	[175]
Cotton linter	Fungal Bioproducts®	NR	Acid hydrolysis 62 wt % 64 wt %	68–71 28	147–158** 90–93**	[176]
Purified cellulose from bio–residue of an ethanol plant	NR	NR	Mechanical homogenization (50 MPa)	96%	in hundreds X 10–20	[177]

*cellulase treatments were carried out for 24 h at 50–55 °C, ** hydrodynamic diameter was analyzed from dynamic light scattering analysis, NR–not reported.

Alternatively, Piriani *et al*. adopted a unique approach whereby Whatman filter paper was acid hydrolyzed (65% H_2SO_4, 2 h, 25 °C followed by dilution with 50% H_2SO_4) to generate solid and liquid fractions [178]. CNC was isolated from the undigested solids (61–71% yield) while amorphous cellulose was recovered from the liquid fraction by ethanol precipitation. The recovered cellulose (21% yield) was subsequently subjected to cellulase hydrolysis to release sugars for ethanol fermentation. However, the CNC particles isolated had longer lengths (670 nm) and wider diameters (40 nm) due to incomplete hydrolysis at room temperature.

2.4.4. Hydrothermal treatment

The following sections briefly introduce hydrothermal process in general and discuss how this treatment can employed for CNC isolation and co-generation of furfural as a value–added coproduct.

2.4.4.1. Hydrothermal process overview

Hydrothermal processing is the thermal transformation of biomass in aqueous slurries by heating water at high temperatures to solubilize and/or modify some components of lignocelluloses to generate liquid, gaseous or solid products [179]. The process is advantageous over pyrolysis and gasification in transforming wet feedstock such as slurry waste that are abundantly generated in most industries including paper mills, food processing and wastewater treatment plants. Hence, hydrothermal conversions conserve energy and cost from drying; however, the process requires large reactors, biomass size reduction and high pressure pumps [179][180].

At high temperatures, water can exist in steam or liquid phase as a function of vapor pressure (Figure 13). Water becomes subcritical in liquid phase when heated at a temperature range above the boiling point (100 °C) and below the critical point (374 °C) and above the saturation vapor pressure [181]. Subcritical water acts as an effective polar solvent with increased [H^+] and [OH^-] concentrations that promotes acid–base catalyzed reactions [182]. When water is heated above the critical temperature and critical pressure (22.1 MPa), it becomes supercritical and exhibits different properties [181]. The dielectric constant of water drops substantially, which reduces the ionic properties and solubility of salts [179]. Water now behaves like an organic solvent and permanent gases like nitrogen and hydrogen become soluble [179]. Consequently, reactions shift from ionic to free radical formation, but reaction rates remain unchanged [179].

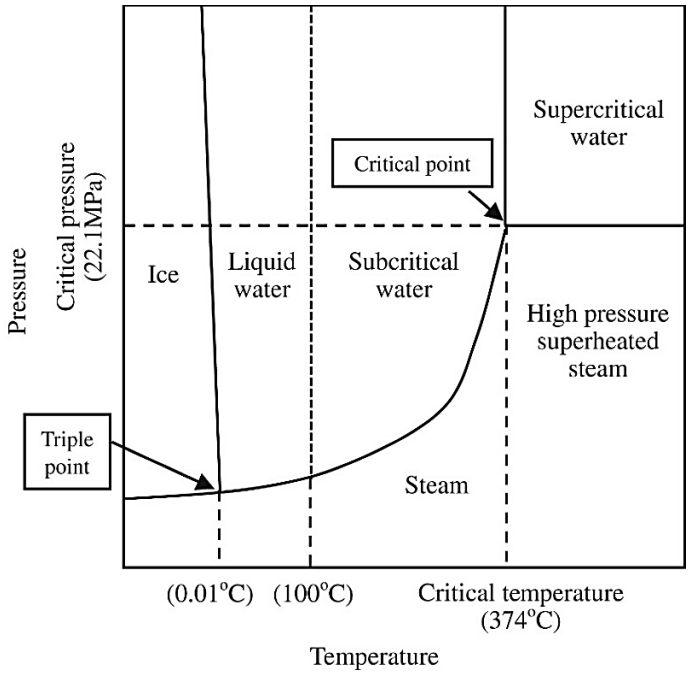

Figure 13 Phase diagram of water. This figure was republished with permission of Elsevier, from Energy Conversion of Biomass with Supercritical and Subcritical water using large scale plants, Okajima, I. and Sako, T., J. Biosci. Bioeng., 117, 2014; permission conveyed through Copyright Clearance Center, Inc.

Hydrothermal processes have be carried out using (a) subcritical temperatures (250–350 °C and 4–16.5 MPa) to generate bio–oil, and (b) supercritical water at 300–400 °C to mainly produce CH_4 or at elevated temperatures in the range of 600–700 °C to generate H_2 as the primary gas [182]. Alternatively, hydrothermal treatment employs moderated process conditions to partially degrade and modify the lignocellulose structure with the objective of improving the properties of the biomass material. A wide array of temperatures can be found in literature as the conditions for hydrothermal treatment are not well defined with varying pressure. But generally, the temperature is between 150–230 °C with the liquid to solid ratio ranging from 1–40 (w/w) [37][38].

Heat treatment of wood has been practiced by early civilizations (Egyptians and Vikings) for the purpose of increasing flexibility to craft bent structures [75]. Currently, thermal modifications are applied on indoor and outdoor materials that require high dimensional stability and durability [183][184]. Hydrothermally treated wood is characterized by low hygroscopicity, improved resistance to microbial degradation, and brown coloration but with some loss in strength

[75][184]. Hydrothermal treatments are carried out at 160–260 °C with varying operating conditions such as moisture, aeration/ inert atmosphere, heating medium (dry air, steam, oil), process steps/ cycles depending on the technology, which have been well developed to industrial scale processes [184]. Generally, the modifications involve partial depolymerization via a hydrothermal process followed by a curing whereby re–condensation reactions complete the modification [183].

2.4.4.2. Cellulose nanocrystal isolation

Novo *et al*. employed sub–critical water (120 °C, 20.3 MPa for 30 min) to isolate CNC from microcrystalline cellulose. Substantial CNC yield (21.9 %) was reported with characteristics comparable to acid hydrolysis [24]. Compared with chemical processes, this method is advantageous as it does not require any corrosive chemicals, large volumes of water for washing or generate effluents. This is the only report in the literature on CNC isolation via hydrothermal treatment.

Alternatively, it is also possible to integrate hydrothermal treatment with acid hydrolysis to improve CNC yields. Agarwal *et al*. isolated lignin containing CNC by acid hydrolysis of raw wood (composed of lignin, cellulose and hemicellulose) to only achieve 2% CNC yield with 46.6% crystallinity (based on Raman spectroscopy analysis) [39]. Hydrothermal treatment (167–225 °C) of raw wood improved the CNC yield and crystallinity by up to 19 and 65%, respectively. Interestingly, this is the only account of an attempt to isolate CNC from a hydrothermally treated feedstock by acid hydrolysis. Beyond improving CNC yield, hydrothermal treatment also presents an opportunity to generate valuable sugar degradation products such as furfural. The following sections discuss how hydrothermal treatment improves crystallinity of cellulose and allows the generation of furfural as an important value-added product to justify integration with CNC isolation.

A. Cellulose crystallization

Hydrothermal treatment at temperatures below 230 °C only confers minor degradation of cellulose [38]. Cellulose is more stable to degradation than hemicelluloses due to the inaccessibility of glycosidic bonds [75][183]. However, hydrothermal treatment causes structural

changes in cellulose as studies have shown improvement in crystallinity from crystallization of para–crystalline or even amorphous cellulose [185]–[187]. Even though the mechanism is not well understood, it has been suggested that heat transforms the bond angles of the functional groups in glucose to a conformation that promotes crystalline ordering [39]. High temperature can change the torsion angle (ω) of O_6–C_6–C_5–O_5 from gauche–trans (gt, ω=60°) to trans–gauche (tg, ω=180°) orientation in glucose subunits, which favors more interplanar hydrogen bonding between chains (Figure 14) [39][188]. Heat treatment under dry conditions does not have the same effect and even reduces crystallinity relative to hydrothermal treatment whereby steam promotes restructuring by reducing internal stress [186][187][189]. Hence, it is likely that the formation of new crystals in the cellulose feedstock via hydrothermal treatment can improve CNC yield from acid hydrolysis.

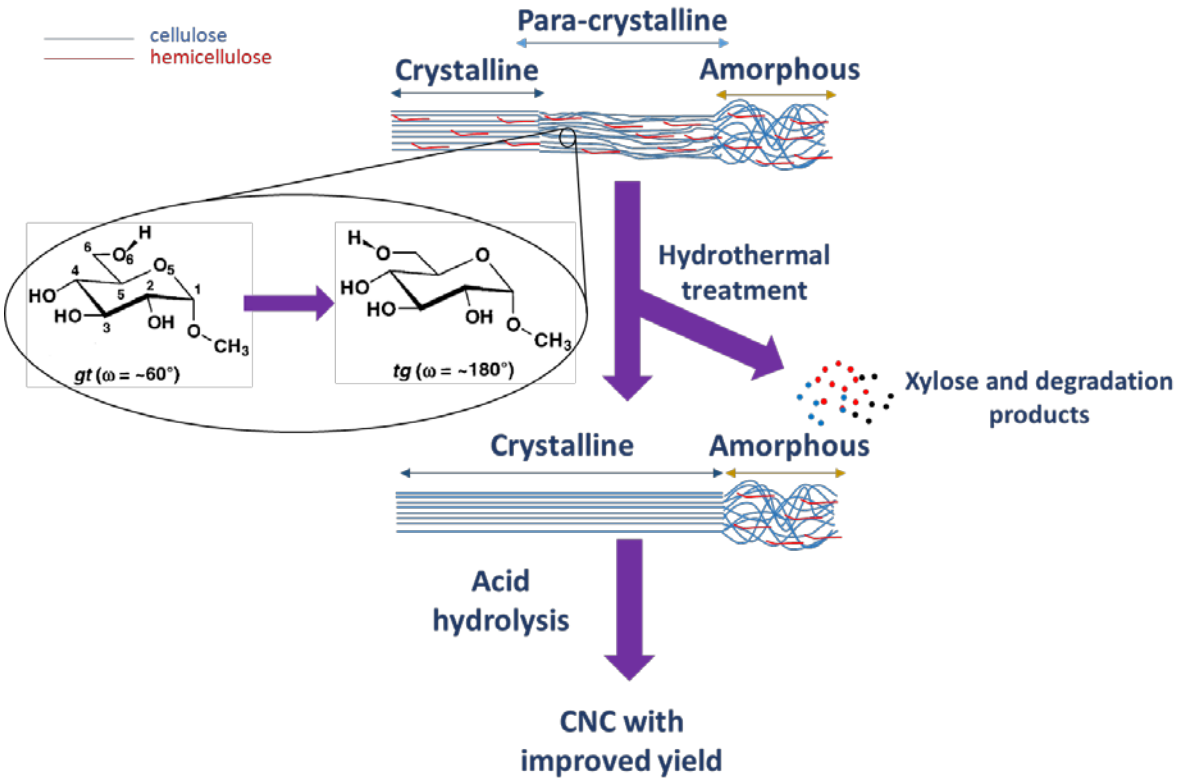

Figure 14 Mechanism of crystallization of para–crystalline cellulose through hydrothermal treatment to improve CNC yield. It is speculated that glucose subunit undergoes structural change from gauche–trans (gt, left) to trans–gauche (tg, right) conformation, which induces crystallization. The figure showing glucose at different torsion angles were reprinted from Solvent Interactions Determine Carbohydrate Conformation, Kirschner, K.N. and Woods, R.J., Proc. Natl. Acad. Sci. USA, 98, Copyright (2001) National Academy of Sciences.

Furthermore, removal of hemicellulose side chains or even partial hydrolysis can cause deformation, which promotes the mobility of para–crystalline cellulose chains to re–structure to a higher level of ordering [187][189]. Increase in cellulose fibril aggregate crystal size has been reported with the degradation of lignin and hemicellulose in wood pulp [114][115].

B. Furfural production from hemicellulose degradation

Substantial hemicellulose degradation in wood begins at 160 °C during hydrothermal treatment [190]. At the initial stage, ionized water attacks hemicelluloses to release acetyl groups and oligosaccharides from side chains and heterocyclic ether bonds, respectively [38]. Subsequently, hydronium ions from the organic acids initiate an autocatalytic process for further degradation [42]. Pentose sugars released such as xylose can undergo dehydration to form furfural (Figure 15) [38][191].

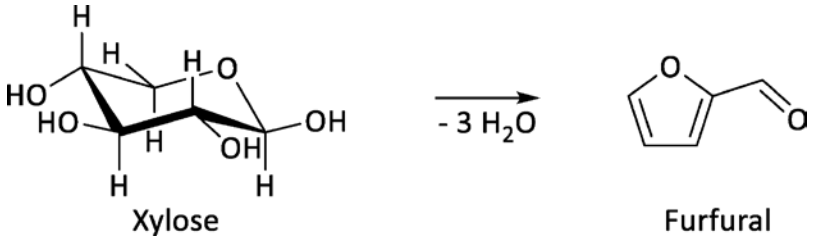

Figure 15 Dehydration of xylose to furfural. This figure was republished with permission of Royal Society of Chemistry, from Process Analytical Technology (PAT) Applied to Biomass Valorisation: A Kinetic Study on the Multiphase Dehydration of Xylose to Furfural, Eifert, T. and Liauw, React Chem Eng., 1, 2016; permission conveyed through Copyright Clearance Center, Inc.

Furfural is an important precursor for the synthesis of various bio-based chemicals, solvents and fuels [44]. It is used as a solvent for the removal of certain aromatics during refining of lubricating oils and fuels [43]. Furfural is an ingredient for the production of pharmaceutical, fragrances, food flavorings, insecticides, fungicides, pesticides, herbicides, antiseptics, disinfectants, detergents, and rust-removers [44]. Furfural is currently produced by high temperature (150–240 ˚C) dilute acid catalyzed digestion of hemicellulose rich biomass such as oat hull and corn cob [192][193]. However, commercial production of furfural faces multiple challenges due to low yields, high energy demand for digestion and recovery, acid corrosion, environmental safety concerns over waste handling and inability to produce a valuable co-product [44]. Co-production

of other value–added products through biorefinery strategy can improve the economic feasibility of furfural production [193]. There are suggestions for the pulp industry to carryout hydrothermal treatment of virgin wood prior to pulping to produce furfurals from hemicelluloses [38]. Alternatively, hydrothermal treatment of the pulp is more attractive as it allows both furfural production and cellulose crystallization that improves CNC yield simultaneously.

3. Methodology

3.1. Materials

3.1.1. Feedstock

Whatman™ No. 1 Qualitative filter paper (110 mm diameter, Whatman™ supplied by Fisher Scientific, Whitby, ON, Canada) was used as a model cellulose substrate. It was cut into approximately 4 × 27 mm strips with a paper shredder (Aurora AS 650 C, Torrance, CA, USA) for cellulase treatment studies. Northern Bleached Hardwood Kraft (NBHK) pulp, predominantly composed of aspen, was kindly provided by Alberta Pacific Forest Industries Inc. (Al–Pac Inc, Edmonton, AB, Canada). The pulp was supplied as pressed and dried squares (approximately 6 mm × 8 mm) produced by a pulp chopper (Pierret Cutting Machine G45L1, Corbion, LX, Belgium). This material was chosen as it is the same cellulose–based feedstock used for CNC production at the CNC pilot plant facility at InnoTech Alberta (a research collaborator, Edmonton, AB, Canada). The pulp was composed of 79.1 ± 1.0% cellulose, 21.2 ± 0.6% hemicellulose (xylan) and 4.0 ± 0.1% lignin, as determined by a two–step acid hydrolysis procedure [106]. It is likely that this lignin content (acid soluble lignin) from UV absorption analysis was overestimated due to interferences from sugar degradation products [194].

3.1.2. Enzyme and chemicals

Non–commercial and proprietary cellulase (NS 51129, composed of endoglucanase, cellobiohydrolase and β–glucosidase cellulases) supplemented with xylanase enzyme were kindly provided by Novozymes® A/S (Bagsvaerd, Denmark). Dinitrosalicylic acid (DNS) reagent was prepared from water (1416 mL), 3,5–DNS ($C_7H_4N_2O_7$, 10.6 g), sodium hydroxide (NaOH, 19.8 g), Rochelle salt ($KNaC_4H_4O_6$, 306 g), phenol (C_6H_6O, 7.6 mL) and sodium metabisulfite ($Na_2S_2O_5$, 8.3 g) [195]. Water, 3,5–DNS and NaOH were dissolved prior to adding the rest of the reagents. 3,5–DNS (98%), Rochelle salt (100%), sodium metabisulfite (98%), NaOH (98.8%), sodium chloride (NaCl, ≥99%) and acetic acid (CH_3COOH, 99.7%) were procured from Fisher Scientific (Whitby, ON, Canada). Phenol (99%), glucose ($C_6H_{12}O_6$, ≥95%), xylose ($C_5H_{10}O_5$, ≥99%), furfural ($C_5H_4O_2$, 99%), 5–methyl furfural ($C_6H_6O_3$, 99%), formic acid (CH_2O_2, >95%), citric acid ($C_6H_8O_7$, 99%),

sulfuric acid (H_2SO_4, 72% and 95–98%) and calcium carbonate ($CaCO_3$, >99%) were purchased from Sigma–Aldrich (St. Louis, MO, USA).

3.2. Experimental treatments

3.2.1. Cellulase treatment

3.2.1.1. Activity assay

A filter paper assay protocol based on the DNS method for reducing sugar analysis was adopted to determine cellulase activity [195]. Filter paper strips (1 x 6 cm, equivalent to approximately 50 mg), soaked in sodium citrate buffer (pH 4.8, 0.05 M, 1 mL), were hydrolysed with cellulase at 50 °C for 1 h. Suitably diluted (0.5 mL final volume) cellulase solutions were prepared to release slightly above and below 2 mg (absolute weight) of reducing sugar whereby the activity as a function of concentration is expected to be linear under the study conditions. DNS reagent (3 mL) was added to terminate the reaction and a reddish–brown color was developed by heating in boiling water for 5 min. The tubes were cooled to room temperature and absorbance was measured at 540 nm. Cellulase activities were expressed in filter paper units (FPU). One unit of enzyme activity was defined based on international units as the amount of cellulase required to release 1 µmol of sugar per min under the assay conditions.

3.2.1.2. Dosage response curve

A dosage response curve was generated from the hydrolysis of filter paper (Whatman) and wood pulp substrates with a range of cellulase loadings (in terms of activity) for 24 h. This study was used to identify a cellulase dose with the most effective activity, which was defined as the least loading with the maximum increase in glucose yield. Each substrate (10% w/v solid loading) was hydrolyzed with 5–35 FPU/g cellulase loading, buffered in 0.05 M sodium citrate solution at pH 4.8 in a shake flask. The flask was incubated for 24 h at 50 °C with 100 rpm shaking.

3.2.1.3. Treatment as a function of time

Filter paper and wood pulp substrates were treated with effective cellulase loadings (25 and 15 FPU/g of substrate, respectively) over a period of 2–10 h. Cellulase hydrolysis was carried out in

shake flasks under the same conditions as described in section 3.2.1.2. For the controls, untreated substrates were suspended in buffer (without addition of cellulases) and mock treated under the same conditions. Cellulase activity was terminated by heating in boiling water for 15 min.

3.2.2. Hydrothermal treatments

A Parr® High Pressure/High Temperature reactor (Parr series 4570, 1 L capacity, Parr Instrument Company, Moline, IL, USA) was used to carry out hydrothermal treatments. The reaction was controlled with SpecView® 32 Version 2.5 (SpecView Corporation, Gig Harbor, WA, USA). The reactor vessel and the lines in the system were purged with nitrogen 3 times for 5 min at 3.4 MPa. Hydrothermal treatment of the wood pulp suspension in water (10g in 400 mL) was carried out in batch mode at 150–225 °C for 1 h with stirring (100 rpm). The starting pressure and hold time were 0.1MPa (atmospheric pressure) and 1.5 h, respectively in all cases. The reaction was cooled to room temperature overnight.

3.2.3. Acid hydrolysis for cellulose nanocrystal isolation

Cellulase and hydrothermally treated fibers were used as feedstock for CNC isolation via acid hydrolysis. The slurry produced from cellulase and hydrothermal treatments was centrifuged at 33,700x *g* for 15 min at 20 °C. The precipitated solid was re–suspended in water, washed 3 times by centrifugation and freeze dried. Solid recovery (wt % original feedstock) was calculated using Equation (1) in which W_1 is the mass of substrate before treatment (g) and W_2 is the mass of freeze–dried solid recovered after treatment (g).

$$\text{Solid recovery} = \frac{W_2}{W_1} \times 100\% \quad (1)$$

A standard operating procedure developed by InnoTech Alberta for bench–scale acid hydrolysis and CNC purification was adopted for CNC isolation [57][124]. The freeze dried cellulase– and hydrothermally–treated fibers were hydrolyzed with 64 wt % H_2SO_4 in a shake flask (8% pulp–to–acid ratio, w/v). The reaction was carried out in a water bath at 45 °C for 2 h with overhead stirring at 200 rpm. The acid was diluted 10 fold (v/v) with cold water to terminate the reaction.

The suspension was centrifuged at 6400x *g* for 10 min to reduce the dilute acid volume. The pellet was re–suspended in water and neutralized with NaOH (30%, w/v) to pH 7 on an ice bath. The suspension was centrifuged at 3700x *g* for 10 min to remove salts in the liquid phase, formed by neutralization. The pellet was further washed by re–suspending in water followed by centrifugation. The pellet was again re–suspended in water and dialyzed against water in regenerated cellulose membrane tube (Spectrum™ Spectra/Por™, Rancho Dominguez, California, USA, 12–14 kDa molecular weight cut off). Dialysis was monitored for 3–5 days using a conductometer until the ionic strength of the liquid dropped to 100–150 µS/cm, which allows CNC particles to suspend. The suspension was centrifuged at 8900x *g* for 10 min to precipitate over–sized particles. The CNCs in the supernatant were collected as colloid and the pellet was re–suspended in water and centrifuged again to extract any remnant CNC at lower ionic strength. The supernatants were pooled and an aliquot sample (by weight) was oven dried overnight at 103–105 °C. The precipitated pellets were also pooled together and freeze–dried to analyze the amount of over–sized reject cellulosic material that were not hydrolyzed by the acid to CNC.

Equations (2)–(4) were used to calculate: a) CNC yield$_1$ which was defined as the yield from a fixed mass of feedstock that enters the acid hydrolysis process (wt % feedstock for acid hydrolysis); b) over–sized rejects (wt % original feedstock); and c) CNC yield$_2$ which was defined as the yield from the initial feedstock by accounting for the mass loss due to the treatments (wt % original feedstock), respectively in which W_3 is the mass of oven dried CNC from an aliquot sample (g), F_1 is the ratio of total mass of colloid to mass of aliquot, W_4 is the mass of the feedstock added to the acid hydrolysis reaction (g), W_5 is the freeze–dried mass of the un–hydrolyzed pellet collected after acid hydrolysis (g), and solid recovery (wt % original feedstock) as determined in Equation (1).

$$\text{CNC yield}_1 = \frac{W_3 \times F_1}{W_4} \times 100\% \quad (2)$$

$$\text{Over sized reject} = \frac{W_5}{W_4} \times 100\% \quad (3)$$

$$\text{CNC yield}_2 = \frac{\text{CNC yield}_1 \times \text{solid recovery}}{100} \quad (4)$$

3.2.4. Characterization of products

3.2.4.1. Sugars and other degradation products

The liquid fractions from cellulase dosage response curve study, cellulase and hydrothermal treatments were analyzed for glucose, xylose and sugar degradation product yields using a high performance liquid chromatography system (HPLC, Agilent 1200, Santa Clara, CA, USA) coupled with a refractive index detector (RID, Agilent 1100 series, Agilent Technologies, Santa Clara, CA, USA). Sugars (glucose and xylose) in the sample (30 µL injection volume) were separated on an HPX–87P column (Bio–Rad Aminex, Hercules, CA, USA) with water as the mobile phase at a flow rate of 0.5 mL/min at 80 °C for 40 min. Sugar degradation products (furfural, hydroxymethyl furfural, acetic acid and formic acid) in the liquid fraction from hydrothermal treatment were separated on an HPX–87H column (Bio–Rad Aminex, Hercules, California, USA). Samples were carried through the column with 5 mM H_2SO_4 at a flow rate of 0.5 mL/min at 60 °C for 90 min. Refractive index and ultraviolet detectors were used to analyze organic acids (acetic and formic acids) and sugar degradation products (hydroxymethyl furfural at 284 nm and furfural at 275 nm), respectively [196]. Sugars (0.25–16 mg/mL) and their degradation product (0.01–0.25 mg/mL) standards were also simultaneously run on HPLC to generate a calibration curve (R^2 > 0.99). Individual product yield (wt % original feedstock) was calculated using Equation 5, in which W_6 is the mass of product as determined from HPLC analysis (g) and W_7 is the mass of sample used for the analysis.

$$\text{Product yield} = \frac{W_6}{W_7} \times 100\% \quad (5)$$

3.2.4.2. Compositional analysis

The composition of structural carbohydrates and lignin of control and hydrothermally–treated wood pulp fibers were determined by a 2–step acid hydrolysis procedure [106]. Samples were powdered on a Retsch ZM 200 Ultra Centrifugal Mill (Newton, PA, USA) operated at 8000 rpm and passed through a 0.5 mm screen. A sample of wood pulp was hydrolyzed with 72% H_2SO_4 (10% solid loading) in a pressure tube at 30 °C for 1 h while continuously stirring with a glass rod. The reaction was terminated by diluting the acid to 4% with water. The sample, along with sugar recovery standard tubes (to account for sugar degradation), were further hydrolyzed in an

autoclave at 121 °C for 1 h at 0.1 MPa. After cooling the tubes, the solution was vacuum filtered on pre–weighted filtering crucibles. An aliquot of the filtrate was neutralized to pH 7 with $CaCO_3$ powder. The suspension was centrifuged 3300x *g* for 5 min and the liquid supernatant was analyzed for sugars on HPLC (under conditions described in section 3.2.4.1.). Cellulose and xylan compositions (wt % original feedstock) were determined using Equation 6 in which W_8 is the absolute sugar mass (mg) from HPLC analysis, F_2 is the anhydro correction factor (0.90 for glucose and 0.88 for xylose), W_9 is the mass of sample used for acid hydrolysis (mg) and R is the % recovered sugar from HPLC analysis of sugar recovery standards. In the case of polysaccharide content analysis of pulp after hydrothermal treatment, the mass of sample of W_9 represents the hydrothermally treated pulp instead of the initial feedstock. Hence, cellulose and xylan composition were calculated as wt % hydrothermally treated feedstock. Another aliquot of the filtrate was directly analyzed on a UV spectrophotometer (205 nm) to determine the acid soluble lignin (%) using Equation 7 in which, A_{205} is the absorbance reading at 205 nm, V_1 is the total volume of the filtrate (mL), ε is the absorptivity constant (L/g cm) and l is the path length under which the absorbance measurement was made (cm). The solids recovered on the filtering crucibles were washed with water to remove any soluble sugars and oven dried. Acid insoluble lignin (%) was calculated using Equation 8 in which, W_{10} and W_{11} are the weights of the filtering crucible before and after filtration, respectively. The total lignin (%) was determined from Equation 9.

$$\text{Polysaccharide} = \frac{W_8 \times F_2}{W_9 \times R} \times 100\% \quad (6)$$

$$\text{Acid soluble lignin} = \frac{A_{205} \times V_1}{\varepsilon \times W_9 \times l} \times 100\% \quad (7)$$

$$\text{Acid insoluble lignin} = \frac{W_{11} - W_{10}}{W_9} \times 100\% \quad (8)$$

$$\text{Total lignin} = \text{Acid soluble lignin} + \text{Acid insoluble lignin} \quad (9)$$

3.2.4.3. Fiber structure and dimensions

A. SEM imaging

Cellulase–treated fibers were soaked in water (25 mg in 2.5 mL H_2O, 1% w/v) and vortexed at high speed. A drop of the fiber suspension was mounted onto stubs and dried in a desiccator overnight. Samples were carbon coated using a Leica EM SCD005 (Leica Microsystems Inc., Wetzlar, Germany). Scanning electron microscope (SEM) (Carl Zeiss AG, Oberkochen, Germany) images were generated on a Zeiss Sigma 300 Variable Pressure–Field Emission SEM (VP–FESEM) (Department of Earth and Atmospheric Sciences, University of Alberta) whereby electrons were accelerated at 10 kV and images were magnified 1000x.

B. Dimensions from pulp quality monitoring system analysis

Control fibers (0 h cellulase–treated) were pre–soaked in water (24 g in 2 L H_2O, 1.2% w/v) for 4 h. Since the fibers are intertwined in these feedstocks, a pulp disintegrator (Messmer pulp disintegrator MK111C, Messmer Instruments Ltd., Gravesend, UK) operating at 3000 rpm for 1 min was used to separate individual fibers. Cellulase–treated fibers were in powder form; hence, separation was simply conducted by stirring a fiber suspension (2 g in 200 mL H_2O, 1% w/v) at low speed with a magnetic stirrer overnight.

The fiber suspensions were further topped up with water to a final volume of 600 mL and loaded into the pulp quality monitoring system (PQM 1000, Metso Sweden AB, Sundsvall, Sweden) to analyze the average length, width, and length distribution. The system measured the dimensions of fibers (70,000 to 240,000 counts) passing through a glass cell, based on image analysis of transmitted variable light beam distribution [197]. The instrument use was kindly facilitated by InnoTech Alberta (Edmonton, AB, Canada).

3.2.4.4. Degree of crystallinity of fibers and cellulose nanocrystals

Cellulase– and hydrothermally–treated fibers were powdered as described in 3.2.4.2. while CNCs generated from the respective treatments were already in powder form after freeze drying. The degree of crystallinity was analyzed on a Rigaku Ultima IV diffractometer (Rigaku Corporation, Tokyo, Japan), at the nanoFAB fabrication and characterization center (University of Alberta). Powdered samples were scanned with an X–ray beam generated from a Cu tube (at 40 kV and 44

mA and controlled via 10 mm divergent slit), over 5–45° Bragg angles (2θ) and at a scan speed of 2° per min. The spectra were processed through JADE software (Jade Software Corporation Limited, Christchurch, Australia) to format and access the intensity measurements. The degree of crystallinity was assessed from the crystallinity index (%) that was calculated based on the peak height method using Equation (10) in which I_{am} is the intensity count of the minimum valley between the 110 and 200 planes (around 2θ = 18°) (Figure 16), representing the less ordered cellulose, and I_{total} is the intensity count at the maximum height of the peak at 200 plane (2θ in the range between 22°–24°), representing both crystalline and non–crystalline cellulose [198][199].

$$\text{Crystallinity index} = \frac{I_{total} - I_{am}}{I_{total}} \times 100\% \quad (10)$$

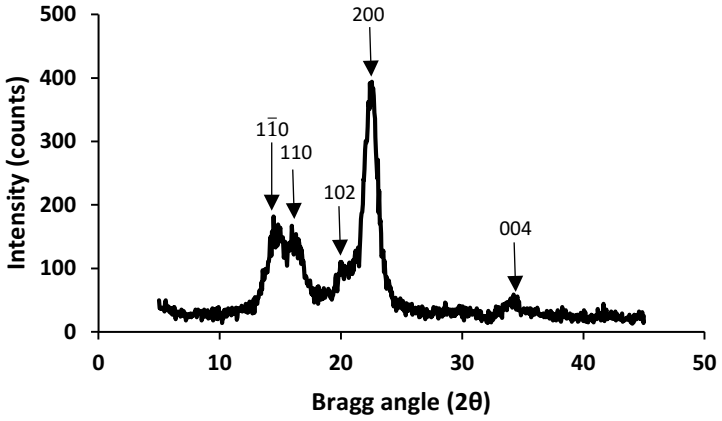

Figure 16 X–ray diffraction (XRD) spectra of filter paper showing characteristic intensity peaks for cellulose.

3.2.4.5. Particle size and zeta potential of cellulose nanocrystals

A. Dynamic light scattering

The hydrodynamic diameter and the colloidal stability of CNCs isolated from cellulase– and hydrothermally treated fibers were estimated from dynamic light scattering and zeta potential analyses on a Malvern Zetasizer Nano–ZS (Malvern Panalytical Ltd., Almelo, Netherlands) at the InnoTech Alberta facility (Edmonton, AB, Canada).

A.1. Hydrodynamic diameter

Small particles in colloid exhibit Brownian movement. When a colloid sample is scanned with a laser, the motion causes light scattering, whereby the intensity fluctuates over time. A translation diffusion coefficient (D_t) can be derived from a correlation function (mathematical functions not shown here). This coefficient can be used to calculate the hydrodynamic diameter (d_H) of spherical particles using the Stoke–Einstein relation in Equation (11):

$$d_H = \frac{kT}{3\pi\eta D_t} \quad (11)$$

where k is the Boltzmann's constant, T is the absolute temperature, and η is the viscosity of the colloid [200][201].

CNC colloid was diluted with NaCl (10 mM) solution to a final CNC and salt concentration of approximately 0.05 wt % and 5 mM NaCl, respectively. Salt was added to prevent overestimation of hydrodynamic diameter by increasing the ionic strength to reduce the thickness of the electric double layer surrounding the CNC particles [200].

Colloid samples were loaded in a cuvette and scanned with a 633 nm light beam generated from a 4.0 mW He–Ne laser. The intensity of scattered light was measured with an avalanche photodiode detector positioned at 173° to estimate the light scattering intensity fluctuations.

A.2. Colloid stability

Zeta potential is a good indicator of the stability of colloids based on electrostatic repulsive forces on the surface charges. When a colloid is subjected to an electric field, the particles move toward the opposite charge. While in motion, a hypothetical plane called the slipping plane is formed within the electric double layer between the moving charged particle and the dispersant layer. The potential difference formed at this plane is called the zeta potential. In estimating zeta potential, the particle velocity is derived from the frequency shift of the scattering light. Electrophoretic mobility (μ_e) is determined from the particle velocity (mathematical function not shown here) and is used to calculate zeta potential (ζ) from Henry's equation (Equation 12):

$$\zeta = \frac{\mu_e 3\eta}{2\varepsilon_r \varepsilon_0 f(Ka)} \quad (12)$$

where ε_r is the dielectric constant of the medium, ε_0 is the permittivity of vacuum, $f(Ka)$ is Henry's function, and η is the viscosity of the colloid [200][202].

An electric field was induced by an electrode (dip cell) inserted into the cuvette containing the same CNC colloid aliquot for hydrodynamic diameter analysis to estimate the frequency shift of the scattering light. Light scattering data were automatically analyzed and computed on the built–in Zetasizer software to generate hydrodynamic diameter and zeta potential estimations.

B. Particle size from TEM analysis

Freeze dried CNCs isolated from cellulase–treated fibers were re–suspended in water (0.1 g in 100 mL H_2O, 0.1% w/v) and sonicated for 15 min. A droplet of the CNC colloid was mounted on a copper grid (300 mesh) coated with formvar film (Ted Pella Inc., Redding, CA, USA) for 20–30 min. Excess liquid was removed with filter paper and the grid was negatively stained with phospho–tungstic acid (2% w/v) for 15 sec. Excess stain was removed with filter paper and the copper grid was loaded on a transmission electron microscope (Philips/FEI Morgagni 268, Hillsboro, OR, USA), at the Advanced Microscopy Facility (Department of Biological Sciences, University of Alberta) to generate CNC images. The instrument was operated at 80 kV electron speed and 110,000x magnification. Length and width of well separated CNC rods (total count of 75 from all triplicates), with distinguishable tip ends and widths, were analysed using image J software (National Institute of Health, Rockville, MD, USA). A straight–line tool, standardized by the scale bar generated from the TEM micrograph, was used for manual measurement of individual particles on the software. The aspect ratio of an individual CNC particle was calculated from the ratio of the longest side to the shortest side.

3.2.4.6. Thermal stability of cellulose nanocrystals

A thermogravimetric analyzer Q50 (Thermal Analyzers, Newcastle, DE, USA) at the Lipid Chemistry Group Laboratory (Department of Agricultural, Food and Nutritional Science, University of Alberta) was used to analyze the thermal stability of CNC. Freeze–dried CNCs isolated from cellulase–treated filter paper (5–17 mg) and wood pulp (3–10 mg) were heated in a furnace under nitrogen gas (60 mL/min flow rate), with temperature increasing at a rate of 10 °C/min from room temperature up to 500 °C. The onset of degradation temperature (°C) was

identified from the intersection of an initial line tangent to the constant weight line and a final line tangent to the inflection point, implicating weight loss from thermal degradation. The temperature (°C) corresponding to the maximum rate of change in weight was attained from the derivative plot.

3.2.4.7. Elemental analysis of cellulose nanocrystals

Freeze dried CNCs isolated from hydrothermally–treated wood pulp were kept in a vacuum oven at room temperature for 8 h [203]. Carbon, hydrogen, nitrogen and sulfur compositions were determined based on the Pregl–Dumas method. The analysis was carried out on a Thermo Scientific Flash 2000 Elemental Analyzer (Themo Fisher Scientific Inc, Rodano, Milan, Italy) at the Analytical and Instrumentation Laboratory in the Department of Chemistry, University of Alberta. The oxygen content was calculated by taking the difference of the sum of all other elements from 100%. Approximately 1.5–1.8 mg of sample was combusted at 1000 °C in the presence of oxygen. The combustion products were carried through a gas chromatographic column (Porapak QS, 4 mm internal diameter and 2 m long) with Helium (mobile phase). Signals of the separated gases identified by a thermal conductivity detector were analyzed on Eager Xperience software (Themo Fisher Scientific Inc, Rodano, Milan, Italy).

3.3. Data analysis

All reported data (mean ± standard deviation) represent analyses from experimental triplicate analysis, unless specified. One–way ANOVA combined with Tukey's test, at a 95% confidence interval (CI) was used for pairwise comparison of means on Minitab 17 and 18 software, versions 17.3.1 and 18.1, respectively (Minitab Inc., State College, PA, USA). Outliers were detected from the data set using an interquartile range test.

4. Results and discussion

4.1. Cellulase–treatment mediated cellulose nanocrystal isolation

In the following sections, all findings from efforts to develop a biorefinery strategy that integrates cellulase treatment with acid hydrolysis to efficiently co-generate fermentable sugars and CNC will be discussed.

4.1.1. Effective cellulase loading for hydrolysis

This study was conducted to select an effective cellulase loading, which is a dosage with an activity that does not further increase significantly with higher concentration. Glucose yield (wt % original feedstock) curves from 24 h hydrolysis of filter paper and wood pulp as a function of cellulase loadings were evaluated (Figure 17). The enzyme dosage at the point when glucose yield levelled off was identified as an effective cellulase loading. There was no significant increase in glucose yield from hydrolysis of filter paper and wood pulp at enzyme dosages above 25 and 15 FPU/g, respectively. At these points, all of the enzyme–accessible binding sites would have been saturated [204]. Further addition of enzyme would not contribute to cellulose hydrolysis and only incur unnecessary additional cost to the process. Therefore, these effective cellulase loadings for the respective feedstocks were selected for subsequent cellulase treatment investigations. It was evident that higher dosage (1.7 fold) was required for the filter paper substrate relative to wood pulp. Whatman™ No. 1 filter paper is made from cotton pulp and has a greater crystallinity (83%) than hard wood pulp (73% CI) [99][205]. It has been previously suggested that the hydrolysis of crystalline cellulose requires higher loading for synergistic action of cellulases catalyzed by certain classes of exoglucanases [87].

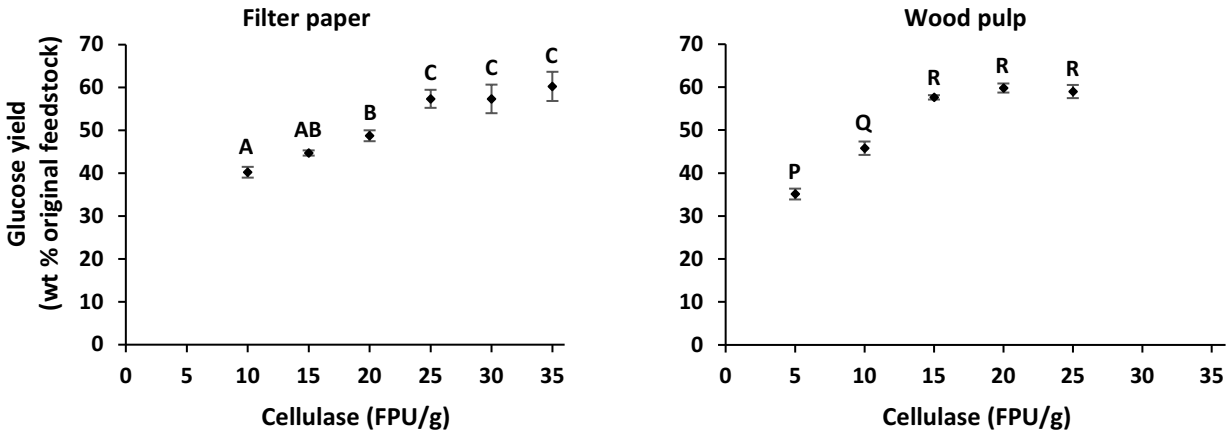

Figure 17 Glucose yield response curve as a function of cellulase dosage. Each data represents the mean of the total value–added products with standard deviation denoted by error bars from experimental triplicates. Values that are denoted by different letters within each plot are significantly different ($p < 0.05$).

4.1.2. Cellulase saccharification profile

Filter paper and wood pulp were treated with cellulase (25 and 15 FPU/g, respectively) for 2–10 h, prior to acid hydrolysis with the objectives of identifying treatment period for: (a) recovering fermentable sugars efficiently from preferential degradation of non–crystalline celluloses and xylan with minimal loss to CNC pecursors; and (b) generating a feedstock with accumulated CNC precursors (large crystalline cellulose that is fragmented to CNC by acid) for an efficient acid hydrolysis. Cellulase treatment hydrolysis rates over time were assessed to identify efficient saccharification. Glucose yields from cellulase treatment of filter paper ranged from 23.7 ± 0.2 to 42.0 ± 2.2 (wt % original feedstock) (Table 5). Hydrolysis rate plateaued after 6 h with no significant increase in yield. Therefore, 2–6 h cellulase treatment can be considered as an efficient saccharification period. A plateau in the hydrolysis rate is also a signal for recalcitrance of the residual substrate due to accumulation of crystalline cellulose after substantial hydrolysis of the easily accessible non–crystalline celluloses [35][87][206]. Consequently, there could be an increase in CNC precursor concentration in the solid residue, which can be exploited to isolate CNC efficiently. However, there is the possibility that CNC precursors are also simultaneously degraded at this point. This is because some crystalline chains exposed to enzyme binding are susceptible to hydrolysis even in the presence of non–crystalline celluloses if the latter domains are buried between crystalline chains making them inaccessible to cellulases or acid hydrolysis

[95][96]. Xylose yield from filter paper was relatively poor and did not exceed 1.3%. This is because cotton is almost entirely composed of cellulose (98%) with only a small fraction of hemicelluloses (0.5%) [47].

Table 5 Sugar yields and solid recovery from cellulase treatment of filter paper and wood pulp over a period of 2–10 h

Cellulase treatment (h)	Filter paper (wt % original feedstock)			Wood pulp (wt % original feedstock)		
	Glucose	Xylose	Solid recovery	Glucose	Xylose	Solid recovery
0	0.0 ± 0.0	0.0 ± 0.0	99.5 ± 0.5^{A}	0.0 ± 0.0	0.0 ± 0.0	100.5 ± 0.5^{a}
2	23.7 ± 0.2^{A}	1.0 ± 0.0^{A}	79.2 ± 0.2^{B}	21.0 ± 0.6^{a}	6.1 ± 0.2^{a}	74.5 ± 0.7^{b}
4	32.4 ± 0.6^{B}	1.1 ± 0.0^{B}	70.4 ± 0.4^{C}	30.6 ± 1.1^{b}	8.5 ± 0.3^{b}	62.7 ± 1.3^{c}
6	36.5 ± 0.3^{BC}	1.2 ± 0.0^{BC}	65.4 ± 0.2^{D}	36.6 ± 0.8^{c}	9.8 ± 0.2^{c}	54.0 ± 1.4^{d}
8	40.2 ± 2.0^{C}	1.3 ± 0.0^{C}	62.5 ± 2.3^{E}	39.9 ± 2.2^{c}	11.1 ± 0.6^{d}	50.7 ± 0.2^{e}
10	42.0 ± 2.2^{C}	1.0 ± 0.1^{A}	60.0 ± 0.2^{E}	44.2 ± 1.4^{d}	12.1 ± 0.3^{e}	45.4 ± 1.8^{f}

Each data represents the mean ± standard deviation from experimental triplicates. Values within each column that are denoted by different letters (in superscript) are significantly different ($p < 0.05$). The effective cellulase loading for filter paper and wood pulp treatment were 25 and 15 FPU/g to ensure that enzyme concentration is not a limiting factor based on dosage response curve analysis.

Wood pulp hydrolysis released glucose (21.0 ± 0.6 to 44.2 ± 1.4 wt % original feedstock) and xylose (6.1 ± 0.2 to 12.1 ± 0.3 wt % original feedstock) from cellulose and xylan degradation during 2–10 h treatment. Hydrolysis rate did not plateau over the treatment period with a significant increase in yields for both sugars (except for glucose at 8 h). Crystallinity may not be a rate–limiting factor during the treatment period evaluated in the present study. This is most likely due to the high non–crystalline cellulose and xylan composition of wood pulp relative to filter paper [99][205]. Yet, it is probable that the cellulase treatment during this period can preferentially saccharify the abundantly available non–crystalline cellulose and xylan leading to accumulation of CNC precursors. An efficient treatment will be dependent on the extent of damage to CNC precursors and consequently the loss in CNC yields.

Xylan degradation suggests that the cellulase preparation contains xylanase enzyme with high activity. Generally, residual hemicelluloses in wood pulp are not easily accessible to enzymatic

degradation. The degradation of side chains during the pulping process facilitates the xylan linear chains to attain a high level of ordering that promotes integration of xylan into crystalline cellulose domains [116]. Hence, xylan in wood pulp cannot be completely degraded at the initial stages due to inaccessibility. The hydrolysis profile confirms this hypothesis as xylose yield (12.1 ± 0.3 wt % original feedstock) after 10 h accounted for only 50% conversion of the available xylan (21.2 ± 0.6 wt % original feedstock). Addition of a supplementary xylanase may be required to develop an enzyme formulation that is even more aggressive to xylan. This has been suggested for other commercial preparations when hydrolyzing feedstock with high xylan content [147].

Glucose and xylose sugars generated can be fermented to ethanol using genetically engineered yeast strains, as demonstrated in commercial cellulosic ethanol facilities [169]. Hence, this study provides insights on how cellulase treatment mediated CNC isolation pathway can efficiently recover fermentable sugars for cost effective production of ethanol. This biorefinery strategy can be integrated into pulp mills to offset CNC production cost and co–generate ethanol sustainably.

Residual solids after cellulase treatment were separated from the liquid hydrolysate by centrifugation, washed and freeze dried to determine the solid recovery (wt % original feedstock {Table 5}). The mass loss due to cellulase hydrolysis was close to the total sugar release.

4.1.3. Characteristics of cellulase–treated fibers

The following sections discuss the characteristics of cellulase–treated fibers to make inferences on the mechanism and impact of cellulase treatment on the overall structure, dimension and crystallinity of filter paper and wood pulp.

4.1.3.1. Fiber structure and dimension

SEM and pulp quality monitoring (PQM) system analyses were conducted to study the structure and size of cellulase–treated fibers, respectively. Despite substantial degradation (with solid recovery of only 45.4 ± 1.8 wt % original feedstock {Table 5}), fibers with lengths up to millimeters in length were apparent in SEM micrographs of both feedstocks (Figure 18, 10 h). This implies that the cellulases did not entirely cut the fiber length into very short fragments or fines. PQM system analysis showed that cellulase treatment significantly reduced the average fiber length

from 1.21 ± 0.10 down to 0.68 ± 0.03 mm in filter paper and from 1.10 ± 0.01 down to 0.75 ± 0.06 mm in wood pulp (Table 6). No significant change was observed in the length as a function of cellulase treatment period (except at 10 h for filter paper).

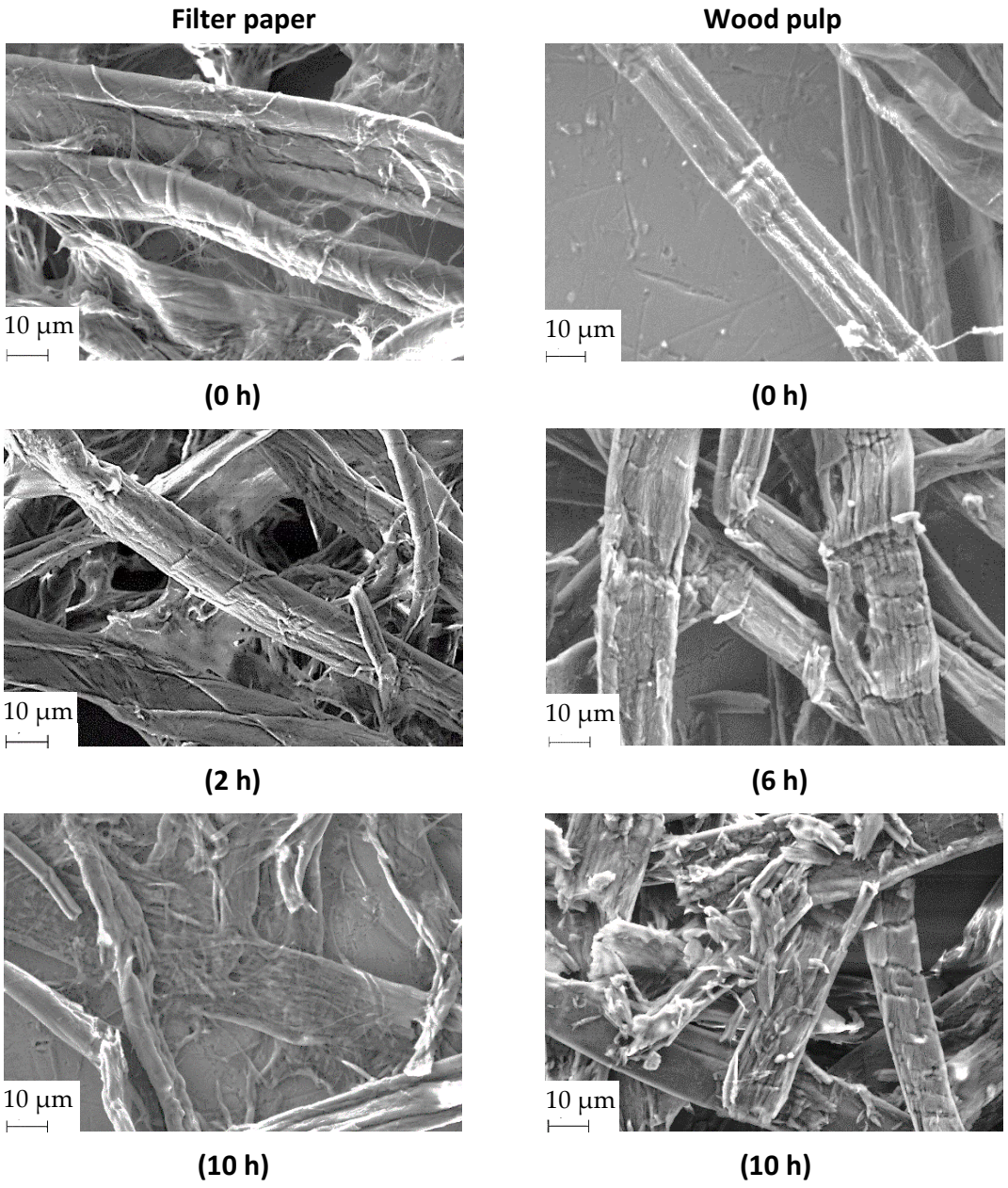

Figure 18 Scanning electron microscopy (SEM) micrographs of cellulase–treated filter paper (left) and wood pulp (right) fibers at different times

Table 6 Average length and width of cellulase–treated filter paper and wood pulp fibers based on pulp quality monitoring system analysis

Cellulase treatment (h)	Filter Paper		Wood Pulp	
	Length (mm)	Width (μm)	Length (mm)	Width (μm)
0	1.21 ± 0.10^{A}	29 ± 1^{A}	1.10 ± 0.01^{a}	32 ± 0^{a}
2	0.90 ± 0.11^{B}	33 ± 1^{B}	0.88 ± 0.07^{b}	37 ± 1^{b}
6	$0.71 \pm 0.01^{B,C}$	36 ± 1^{B}	0.75 ± 0.07^{b}	42 ± 1^{c}
10	0.68 ± 0.03^{C}	35 ± 2^{B}	$0.75 \pm 0.06^{b,*}$	41 ± 1^{c}

Each data represents the mean ± standard deviation from experimental triplicates (*is an exception calculated from duplicates after removing an outlier). Values with different letters (in superscripts) within each column are significantly different ($p < 0.05$).

The length distribution data shows that the abundance of short fragments (0–0.2 and 0.2–0.5 mm) significantly increased as a function of enzyme hydrolysis period until 6 h (Figure 19). However, these fragments only accounted for 19% of the total distribution. Fiber lengths in the range of 0.5–1.0 mm dominated the distribution (29–37%) of cellulase–treated fibers. These findings were in correspondence with observations from SEM. Conversely, the abundance of 1–3 mm fibers, which was the most prominent in the untreated wood pulp (37–42%), was significantly reduced (10–16%) by cellulase treatment until 6 h. The abundance of 3.0–7.0 mm long fibers did not change throughout the treatment period. The degradation of long fibers ≤7 mm to fragments >3 mm long was likely masked due to the broadness of the distribution range.

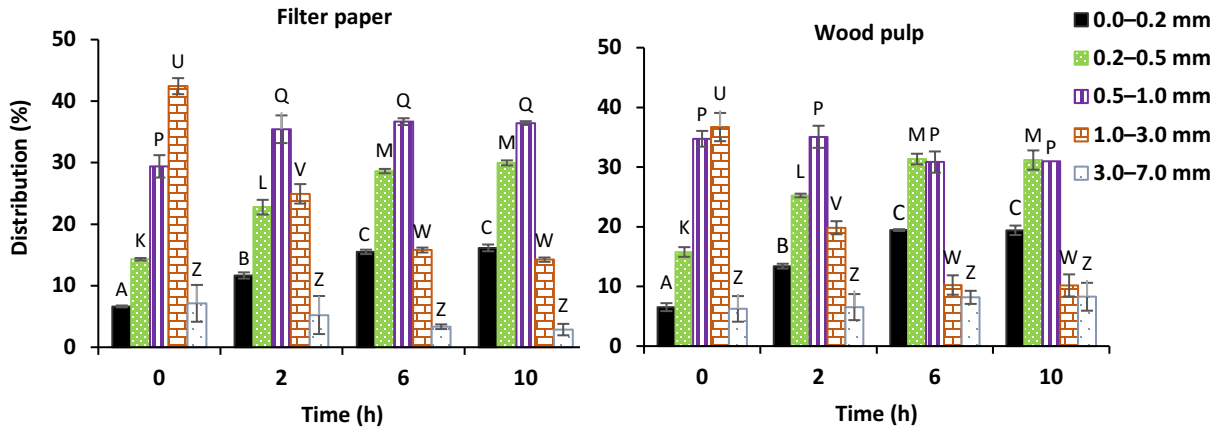

Figure 19 Length distribution of cellulase–treated (a) filter paper and (b) wood pulp fibers. Each data represents the mean with standard deviation denoted by error bars from experimental triplicates (*is an exception calculated from duplicates). Values with different letters are significantly different ($p < 0.05$) from comparisons within a given fiber length size as a function of time for each chart.

Remarkably, fiber width was not reduced even with longer treatment periods, with broad fibers (up to 24 µm) still visible in the SEM micrographs (Figure 18). PQM system analysis revealed that the width of filter paper and wood pulp fibers significantly increased from 29 ± 1 to 36 ± 1 µm and 32 ± 0 to 42 ± 1 µm, respectively due to cellulase treatment (Table 6). In the case of wood pulp, a significant increase in width as a function of cellulase treatment period (until 6 h) was observed. Song *et al*. reported significant reduction in lengths but no changes in the diameter (several micrometers in dimension) of cellulase–treated fibers [207]. During cellulase hydrolysis, the fibers have likely undergone swelling by the action of cellulose–binding domains and non–hydrolytic enzymes, which induce amorphogenesis [131].

Detailed investigation on the structure of individual cellulase–treated pulp fibers under SEM revealed weak junctions along the length (Figure 18, 2 h), which appeared deeper with longer enzyme treatment periods (Figure 18, 10 h). After prolonged treatment (10 h), the erosion of smaller fragments from these degradation sites was also visible, while some long fibers were still apparent (Figure 18, 10 h). In summary, analysis of cellulase–treated fibers revealed interesting findings such as the prevalence of very long fibers, low abundance of very short fragments, implications of fiber swelling, and indications of progressive weakening of the fiber structure

along the length. These observations suggest that during enzymatic treatment of cellulose fibers, fragmentation and peeling were simultaneously in effect, facilitated by amorphogenesis [145].

4.1.3.2. Degree of crystallinity of cellulase–treated fibers

The crystallinity indices of fibers from cellulase–treated feedstock were assessed by XRD spectra analyses based on the peak height method. Increase in the crystallinity of residual cellulose would imply concentration of crystalline cellulose composed of CNC precursors. The fiber crystallinity indices of cellulase–treated filter paper at 6 h (88.6% ± 0.6%) and 10 h (88.4% ± 0.4%) improved significantly, relative to the original, untreated feedstock (85.9% ± 0.7%) (Table 7). The non–crystalline cellulose was likely preferentially hydrolyzed by the cellulases, which led to an increase in the concentration of crystalline domains. The tightly packed chains in the crystalline regions were not hydrolysed rapidly due to inaccessibility to not only enzymes, but also water and even acids [81][207]. This finding corresponds with the plateau in cellulase hydrolysis rate of filter paper after 6 h (Table 5).

Table 7 Degree of crystallinity of cellulase–treated filter paper and wood pulp fibers

Cellulase treatment (h)	Crystallinity Index (%)	
	Filter Paper	Wood Pulp
0	85.9 ± 0.7^{A}	76.6 ± 0.8^{a}
2	$87.3 \pm 1.0^{A,B}$	75.9 ± 1.8^{a}
6	88.6 ± 0.6^{B}	76.0 ± 1.4^{a}
10	$88.4 \pm 0.4^{B,*}$	78.0 ± 1.8^{a}

Each data represents the mean ± standard deviation from experimental triplicates (*is an exception calculated from duplicates). Values with different letters (in superscripts) within each column are significantly different ($p < 0.05$).

As a function of hydrolysis time, no significant difference was observed in the fiber crystallinity index of cellulase–treated filter paper (Table 7). There was also no significant change in crystallinity index of wood pulp fiber due to cellulase treatment. It can be suggested that either there was simultaneous hydrolysis of non–crystalline and crystalline cellulose or accumulation of crystalline cellulose was not significant to be detectible from the analysis. Ramos *et al*. observed

no changes in the fiber crystallinity index of cellulase–treated cellulose and suggested that the enzymes were peeling off the crystalline domains on the exposed surfaces [208]. As discussed previously, non–crystalline cellulose embedded in the core of crystalline chains are inaccessible to hydrolysis [95][96]. Simultaneous amorphogenesis and gradual erosion of layers, also evident from the fiber structures on SEM (Figure 18), are likely to expose the crystalline celluloses to enzymatic hydrolysis [95][145]. Therefore, enzymatic treatment, in the presence of exoglucanases that also act on crystalline cellulose, may not be entirely selective to non–crystaline cellulose [29]. In addition, filter paper could have a very low composition of non–crystalline cellulose. This was evident from the requirement of higher effective cellulase loading (as discussed in section 4.1.1.) to degrade the more prevalent crystalline cellulose. Despite being recalcitrant, these abundant crystalline regions are likely to be the only available substrate for cellulase adsorption and hydrolysis. Hence, the simultaneous degradation of crystalline and non–crystalline cellulose has led to a constant crystallinity index as a function of enzyme treatment period.

Generally, conflicting findings have been reported in the literature regarding the correlation between enzyme hydrolysis and degree of crystallinity. Some studies have reported that fiber cellulose crystallinity index improved due to cellulase treatment [176][209][210]. In contrast, other studies did not find any change in fiber crystallinity indices, even after 90% hydrolysis, using a more sensitive (CP/MAS) ^{13}C–nuclear magnetic resonance (NMR) spectroscopy analysis [34][208][211]. After investigating multiple XRD and NMR analyses, Park *et al*. concluded that in order to make inferences about preferential hydrolysis, the non–crystalline cellulose in the substrate must be severely degraded [95]. The longest treatment in the present study, with the highest extent of degradation (45.4 ± 1.8 wt % original feedstock solid recovery from 10 h hydrolysis), may not have reached the level of severity required to make interpretations. In addition, the limitations in the XRD data interpretations via the empirical method could mask changes in crystallinity index. In Equation 10 (section 3.2.4.4.), the 200 plane is the only position that was accounted for in the crystalline cellulose domains. However, 4 other planes ($1\bar{1}0$, 110, 102, and 004) also display characteristic crystalline XRD peaks in the spectra (Figure 16) [95]. The improvement in crystalline content in these regions may have been overlooked. XRD

deconvolution is an alternative method for calculating the crystallinity index from XRD spectra. The contributions by the amorphous peaks can be identified using a curve fitting software using a reference amorphous cellulose spectra [95]. However, curve fitting was found to be subjective and non–reproducible from multiple efforts to deconvolute XRD spectra generated in the present study.

4.1.4. Cellulose nanocrystal isolation from cellulase–treated fiber

4.1.4.1. Cellulose nanocrystal yield$_1$ (wt % feedstock for acid hydrolysis)

The cellulase–treated undigested solid recovered (washed and freeze dried) was acid–hydrolyzed at a constant solid–to–acid ratio to isolate CNCs. The effect of the cellulase treatment on the acid hydrolysis process was determined by calculating the yield (CNC yield$_1$) from a fixed mass of feedstock that enters the acid hydrolysis reactor (wt % feedstock for acid hydrolysis). The CNC yield$_1$ from 0–10 h cellulase–treated filter paper and wood pulp ranged from 59.3 ± 0.1 to 69.9 ± 1.8 and 10.3 ± 0.1 to 19.2 ± 1.5%, respectively (Table 8). Cellulase treatment increased the CNC yield$_1$ by up to 1.2 and 1.9 fold for filter paper and wood pulp, respectively, compared with the untreated feedstock. It can be suggested that there was significant accumulation of recalcitrant CNC precursor in the residual solids due to the rapid degradation of non–crystalline cellulose and xylan (for wood pulp) by cellulase treatment during the study period [32]–[34][36]. The increase in the crystallinity index of cellulase–treated filter paper further supports this hypothesis. Therefore, it is likely that the cellulase–treated fiber feedstock with concentrated CNC precursors improved the acid hydrolysis efficiency to isolate more CNC relative to the untreated filter paper or pulp. It was surprising that despite such strong implications of significant CNC precursors accumulation from the CNC yield$_1$ data, no change in the crystallinity index was identified in cellulase–treated wood pulp. The limitations of XRD analysis (as discussed in section 4.1.3.2.) may have hindered the detection of any improvement.

Table 8 CNC yield$_1$ from cellulase–treated filter paper and wood pulp

Cellulase treatment (h)	Filter paper		Wood pulp	
	CNC yield$_1$ (wt % acid–hydrolyzed feedstock)	Improvement in CNC yield$_1$ (fold)	CNC yield$_1$ (wt % acid–hydrolyzed feedstock)	Improvement in CNC yield$_1$ (fold)
0	59.3 ± 0.1^{A}	–	10.3 ± 0.1^{a}	–
2	63.8 ± 2.7^{B}	1.1	16.2 ± 1.5^{b}	1.6
4	65.2 ± 0.8^{B}	1.1	17.7 ± 0.9^{b}	1.7
6	66.7 ± 1.6^{BC}	1.1	19.2 ± 1.5^{b}	1.9
8	67.2 ± 0.6^{BC}	1.1	17.3 ± 1.9^{b}	1.7
10	69.9 ± 1.8^{C}*	1.2	18.4 ± 0.7^{b}	1.8

Each data represents the mean ± standard deviation from experimental triplicates (*is an exception calculated from duplicates). Values within columns that are denoted by different letters (in superscript) are significantly different ($p < 0.05$)

The improvement in CNC yield$_1$ due to cellulase treatment will proportionally decrease the input requirement for an acid hydrolysis process to isolate a given amount of CNC. The volumes of water and H_2SO_4 for acid hydrolysis will be correspondingly reduced. Improvement in CNC yield$_1$ from the reactor will concequently decrease water and NaOH requirements and enhance the throughput of the downstream purification operations, which conserves time and energy. Hence, the number of costly operation cycles for processes such as centrifugation, tangential flow filtration and drying can possibly be reduced. Alternatively, a more efficient acid hydrolysis process can reduce the capital expenditure to establish a new CNC plant with the requirement of lower capacity reactors and systems to generate CNC with equivalent productivity. Furthermore, fewer sugars and their degradation products will be disposed into the acid waste stream, which eases acid recovery. The cellulase treatment mediated process will require more filter paper and wood pulp substrate relative to the control, to generate the feedstock with concentrated CNC precursors. This is due to the mass loss from cellulase degradation of the substrates to sugars, which is proportional with the decrease in solid recovery (Table 5). Overall, the biorefinery strategy that integrates cellulase treatment with CNC isolation can reduce CNC production cost that will boost commercial production and use of CNC.

When the two feedstocks were compared, irrespective of the cellulase treatment, CNC yield$_1$ from filter paper was significantly higher (up to 6 fold) than wood pulp. This is likely due to the higher content of CNC precursors in filter paper (85.9 ± 0.7%), which is more crystalline relative to wood pulp (76.6 ± 0.8%) (Table 7). Previous studies have reported CNC yield$_1$ from cotton in the range of 23–65% [47][176].

During the course of cellulase treatment, there was no significant improvement in CNC yield$_1$ over time from acid hydrolysis of cellulase–treated substrates (except at 10 h for filter paper). The constant crystallinity index values as a function of time (Table 7) also support these findings. This implies that the cellulase treatment did not show exclusive preference to non–crystalline cellulose due to inaccessibility [95]. Therefore, it is likely that CNC precursors exposed to cellulase attack are simultaneously disintegrated by amorphogenesis inducing proteins and hydrolytic cellulases. On the other hand, the improvement in CNC yield$_1$ relative to the untreated substrate suggest that the disintegration and/or dissolution rate of the CNC precursors, is relatively much slower due to recalcitrance [36]. During this delay, peeling off due to amorphogenesis could have possibly exposed non–crystalline cellulose layers, that were buried in crystalline sheets for simultaneous degradation but at a faster rate. It is also possible that acid hydrolysis conditions were too aggressive and led to dissolution of CNC precursors that are more accessible in the cellulase–treated fiber. The original feedstock has layers of amorphous and para–crystalline cellulose enclosing the CNC crystalline core [19][93]. In cellulase–treated substrates, these layers were likely softened (amorphogenesis) and/or completely removed with longer treatments exposing more CNC precursors for acid hydrolysis. Improved accessibility to acid could cause dissolution of cellulose chains, instead of fragmentation, along the length or the surface of the CNC precursor and thus reduce CNC yield$_1$. Therefore, milder acid hydrolysis conditions for a cellulase–treated feedstock should be investigated in the future.

Following the findings of the present study, our group also investigated cellulase mediated CNC isolation using purified endoglucanase (NS 51137, Novozymes® A/S) that has specific activity towards non–crystalline cellulose [29][133][212]. The aim was to develop a cellulase treatment strategy that prevents loss of CNC precursors due to exoglucanase activity in the enzyme preparation (NS 51129) used in the present study. Since endoglucanase hydrolysis primarily cuts

chains and releases oligosaccharides, a secondary hydrolysis with the complete cellulase preparation composed of endoglucanase, cellobiohydrolase and β–glucosidase (NS 51129) was introduced to generate monosaccharides [29][133]. The glucan conversion from endoglucanase treatment (5 U/g, 72 h) integrated with secondary hydrolysis (72 h) was 14.1 ± 1.2 wt % glucan. There was no xylose yield as the endoglucanase lacks xylanase activity. The CNC yield$_1$ from acid hydrolysis of endoglucanase–treated wood pulp (16.9 ± 0.7) significantly improved (1.3 fold) relative to the control (13.2 ± 0.6). The crystallinity index of endoglucanase–treated wood pulp (83%) was significantly higher than the control (77 %), which implies selective non–crystalline cellulose degradation that led to accumulation of crystalline cellulose and increase in CNC yield$_1$. These findings demonstrate the potential of endoglucanase mediated CNC isolation to co–produce fermentable sugars and CNC with improved recovery. However, very high enzyme dosage (volume), long treatment time (72 h) and a secondary cellulase hydrolysis were required to generate glucose yields and improve CNC yield$_1$ at a lower magnitude relative to the present study.

4.1.4.2. Cellulose nanocrystal yield$_2$ (wt % original feedstock)

The CNC yield$_2$ was defined as the yield from the initial feedstock, accounting for the mass loss due to enzymatic saccharification of cellulose chains (wt % original feedstock). These data give an indication of CNC precursor disintegration or dissolution during enzymatic and/or acid hydrolysis relative to the untreated feedstock. The CNC yield$_2$ from cellulase–treated filter paper significantly decreased compared with the untreated substrate and stabilized after 4 h (Table 9). The implication is that cellulase treatment and/or acid hydrolysis conditions have led to significant degradation of CNC precursors in the filter paper substrates. This finding also corresponds with the stable CNC yield$_1$ as a function of cellulase treatment period. However, in the case of cellulase–treated wood pulp, there was no significant difference in the CNC yield$_2$ from 2–8 h relative to the untreated feedstock. This was apparent despite almost 50% weight loss of original feedstock after 8 h cellulase treatment (solid recovery was 50.7 ± 0.2 wt % original feedstock, Table 5). It can be suggested that there was a relatively more preferential degradation of the more abundant non–crystalline cellulose in wood pulp substrate. The 10 h time period was possibly the turning point when CNC precursors were substantially more accessible to

disintegration or dissolution by the enzymes and/or acid hydrolysis. The endoglucanase mediated CNC isolation strategy also did not significantly change the CNC $yield_2$ from wood pulp, which also implied selective non–crystalline cellulose degradation [212].

Table 9 CNC $yield_2$ and over–sized rejects from cellulase–treated filter paper and wood pulp

Cellulase treatment (h)	Filter paper (wt % original feedstock)		Wood pulp (wt % original feedstock)	
	CNC $yield_2$	Over–sized rejects	CNC $yield_2$	Over–sized rejects
0	59.0 ± 0.4^{A}	2.6 ± 1.4	10.3 ± 0.1^{ab}	1.0 ± 0.3
2	50.5 ± 2.2^{B}	ND	12.1 ± 1.0^{a}	0.9 ± 0.2
4	45.9 ± 0.6^{C}	ND	11.1 ± 0.7^{a}	1.1 ± 0.1
6	43.6 ± 1.1^{C}	1.1 ± 0.8	10.3 ± 0.7^{ab}	1.1 ± 0.3
8	42.0 ± 2.0^{C}	1.2 ± 0.5	8.8 ± 1.0^{bc}	0.9 ± 0.3
10	42.0 ± 1.2^{C}*	0.8 ± 0.2	8.3 ± 0.2^{c}	0.7 ± 0.0

Each data represents the mean ± standard deviation from experimental triplicates (*is an exception calculated from duplicates). Values with different letters (in superscripts) within each column are significantly different ($p < 0.05$). ND, not determined.

As discussed previously (section 4.1.3.2.), filter paper has significantly more CNC precursors than wood pulp. There is a very high probability for the CNC precursors in filter paper to serve as substrates for cellulase dissolution due to the higher relative abundance. This was apparent even during the very early stages of cellulase hydrolysis (2 h) of filter paper, which consequently reduced the CNC $yield_2$ by 17% relative to the yield from the untreated feedstock. There was no significant change in CNC $yield_2$ from 4–10 h cellulase treatment, possibly due to the recalcitrance of the residual CNC precursors. The plateau in cellulase hydrolysis rate after 6 h (Table 5) further supports this argument.

Beltramino *et al*. studied the effect of cellulase treatment of cotton linter on the CNC $yield_2$ [176]. Significant yield improvement was reported from hydrolysis of cellulase–treated cotton with 62 wt % H_2SO_4 for 45 min. It was suggested that selective degradation of non–crystalline cellulose by the enzymes improved the accessibility of the CNC precursors to acid hydrolysis. Interestingly, the cellulase treatment did not significantly change the CNC $yield_2$ when 64 wt % acid concentration was used. In the present study, acid resistant solids recovered after acid hydrolysis

of cellulase–treated feedstock ranged from only 0.7 ± 0.0 to 2.6 ± 1.4 (wt % original feedstock) (Table 9). This suggests that accessibility to CNC precursors is unlikely to be a limitation to isolate CNCs at longer acid hydrolysis time (2 h) relative to the shorter period (45 min) in the study by Beltramino *et al*. Cellulase treatment in the present study was not expected to improve the CNC $yield_2$. This is because preferential hydrolysis of non–crystalline celluloses by the cellulase cannot increase the native CNC precursor content in the original feedstock. The aim of cellulase treatment was to concentrate the CNC precursors to improve the acid hydrolysis efficiency, which was implied in the CNC $yield_1$.

CNC and fermentable sugar yields from the cellulase–mediated process were added to assess the % total value–added product yield from the original feedstock. This total yield rose from 59.0 ± 0.4 up to 85.0 ± 3.3% for filter paper and from 10.3 ± 0.1 up to 64.6 ± 1.8% for wood pulp, relative to the untreated feedstock (Figure 20). There was no significant difference in the total yield between 6–10 h for filter paper substrate while further cellulase hydrolysis of wood pulp to sugars at 10 h showed a significant increase. Co–generation of sugars and enhanced acid hydrolysis efficiency can improve the process economics of the CNC industry. However, reduction in the CNC $yield_2$ could likely affect the economic feasibility of using filter paper as feedstock. The market value of CNC can reach up to $1000 USD/kg (Blue Goose Biorefineries Inc., Saskatoon, SK, Canada), which is substantially higher compared with $0.84 USD/kg cost for dextrose [213][214]. In the case of the wood pulp substrate, over the course of the 2–8 h cellulase treatment, the CNC $yield_2$ was not compromised. Overall, cellulase treatment for 8 h is the most feasible pathway that demonstrated an efficient saccharification (with the highest glucose and xylose yields) and improvement in CNC $yield_1$ (1.7 fold that was not significantly different from 2–10 h treatments) without compromising CNC $yield_2$. Techno–economic assessments can give insights on the potential of commercializing the cellulase–mediated CNC isolation pathway in pulp mills for co–production of ethanol and CNC. This study is the first report of an effort to efficiently integrate saccharification with CNC isolation in the biorefinery strategy.

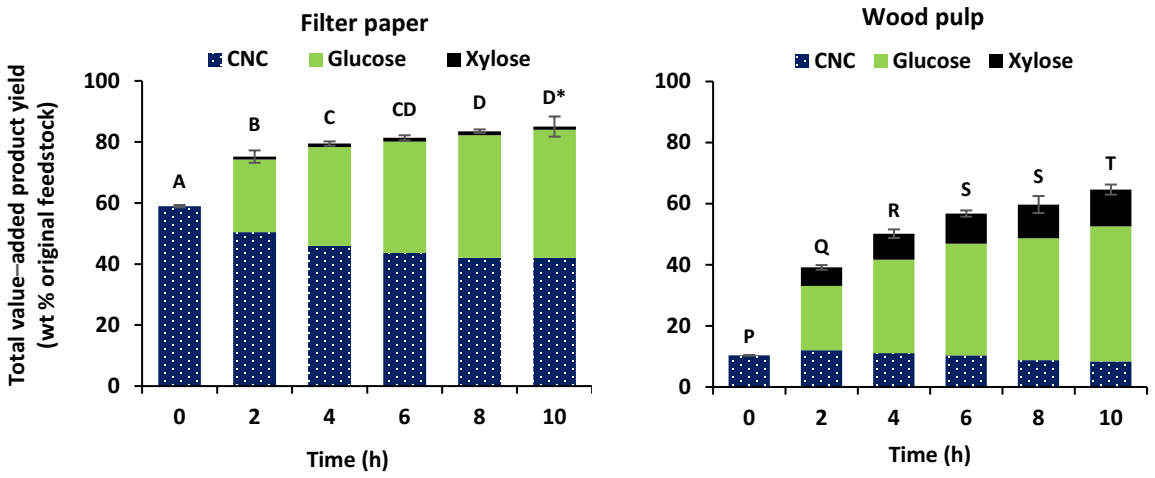

(a) (b)

Figure 20 Total value–added products (CNC and sugars, wt % original feedstock) extracted from (a) filter paper and (b) wood pulp, via cellulase–mediated CNC production process. Each data represents the mean of the total value–added products (wt % original feedstock) with standard deviation denoted by error bars from experimental triplicates (*is an exception calculated from duplicates). Values with different letters (in superscripts) within each column are significantly different ($p < 0.05$).

4.1.5. Characteristics of cellulose nanocrystals isolated from cellulase–treated fibers

CNCs were successfully isolated from cellulase–treated filter paper and wood pulp with improved recovery. The following sections discuss characterization studies to evaluate the quality of the isolated CNCs relative to the control and determine if cellulase treatment affected any property.

4.1.5.1. Particle size

A. Dynamic light scattering analysis

The average hydrodynamic diameter of CNC was estimated from dynamic light scattering analysis. The particle size of CNCs from cellulase–treated filter paper and wood pulp ranged from 221 ± 34 to 294 ± 51 nm and 196 ± 31 to 245 ± 63 nm, respectively (Table 10). The effect of cellulase treatment was only observed on the filter paper feedstock with a significant decrease in the average hydrodynamic diameter of CNC particles starting from 2 h cellulase–treated cellulose. The CNC crystals in filter paper were possibly more accessible to cellulase degradation, which reduced the dimension of the CNC precursors. This is likely due to the relatively higher degree of crystallinity of filter paper fibers (85.9 ± 0.7%) relative to wood pulp (76.6 ± 0.8%).

Cellulase hydrolysis had no significant effect as a function of cellulase treatment period. Beltramino *et al*. studied the characteristics of CNCs from cellulase–treated cotton linter and reported that the particle size did not change due to enzymatic hydrolysis [176].

Table 10 Particle size and colloidal stability of CNCs isolated from cellulase–treated filter paper and wood pulp based on dynamic light scattering and zeta potential analyses

Cellulase treatment (h)	Filter Paper		Wood Pulp	
	Average hydrodynamic diameter (nm) †	Zeta potential (mV)	Average hydrodynamic diameter (nm)	Zeta potential (mV)
0	294 ± 51^{A}	-40.5 ± 2.5^{P}	245 ± 63^{a}	-39.8 ± 3.6^{p}
2	229 ± 53^{B}	$-41.9 \pm 1.5^{P,Q}$	225 ± 12^{a}	-42.6 ± 1.4^{p}
6	213 ± 9^{B}	-43.8 ± 0.8^{Q}	243 ± 45^{a}	-42.6 ± 3.5^{p}
10	$209 \pm 14^{B,*}$	$-43.8 \pm 0.6^{Q,*}$	205 ± 16^{a}	-38.9 ± 2.7^{p}

Each data represents the mean ± standard deviation from experimental triplicates (*is an exception calculated from duplicates). Values with different letters (in superscripts) within each column are significantly different ($p < 0.05$). †average diameter of the peak showing the highest intensity abundance (81–99%). The conductivity, pH, and temperature of the colloid were 0.7–0.9 mS/cm, 4.6–4.8, and 25 °C, respectively. The polydispersity indices that measures the broadness of the size distribution ranged from 0.3–0.6. Colloid with an index value <0.05 is monodisperse, <0.08 is nearly monodisperse, 0.08–0.7 is midrange value, and >0.7 has a broad distribution [215].

Dynamic light scattering analysis is a valuable tool for measuring the size of nanoparticles in a colloid system. The hydrodynamic diameters are estimated from light scattering analysis based on the Stoke–Einstein relation (Equation 11). However, there are limitations in analysis of rod–shaped particles like CNCs as this equation works best for measuring the diameter of a spherical particle in a colloid as a function of the translational diffusion coefficient. CNCs have a rod/needle shape structure with two unequal dimensions of length and width (Table 1). Boluk and Christophe compared the length estimations from the Stoke–Einstein equation with TEM image measurements [200]. A substantial difference was found in the length, most likely due to the influence of the width on the overall diffusion rate. The translation diffusion rate parallel to the longitudinal axis is known to be faster than the motion perpendicular to it. Hence, the estimation from dynamic light scattering analysis is an interdependent parameter referred to as

hydrodynamic diameter. Yet, this measurement is still useful for relative comparison of CNC particle size.

B. Transmission Electron Microscopy image analysis

CNC particles from both feedstocks had an elongated needle–like shape under TEM (Figure 21). The lengths and widths of the CNCs were measured from the micrographs. The average lengths of CNCs isolated from untreated (0 h) filter paper and wood pulp feedstock were 116 ± 30 and 113 ± 30 nm, respectively. Cellulase treatment did not have any significant effect on CNC lengths in both feedstocks (except at 2 h for filter paper) with sizes ranging from 123 ± 45 to 138 ± 44 nm for CNC from filter paper and 109 ± 33 to 126 ± 42 nm for CNC from wood pulp (Table 11). As expected, these length measurements were substantially different from the hydrodynamic diameter as the latter is only an indirect estimation (as discussed in section 4.1.5.1.A.). The widths of CNCs from cellulase–treated filter paper were uniform (9.5 ± 3.0 to 10.2 ± 3.0 nm) and similar with CNCs from untreated (0 h) filter paper (8.8 ± 2.5 nm) (except at 2 h). However, cellulase treatment significantly decreased the width of wood pulp CNC from 9.2 ± 3.3 nm (untreated, 0 h) to up to 6.8 ± 2.1 (6 h). Studies in literature have reported the particle size of CNC from TEM analysis of wood and cotton in the range of 70 to 300 nm in length and 4 to 20 nm in width [46][47][51][127][177][216]–[218]. Siqueira *et al*. isolated CNC by acid hydrolysis of cellulase–treated and mechanically sheared pulp with particle size of 230–250 nm in length and 7 nm wide [160].

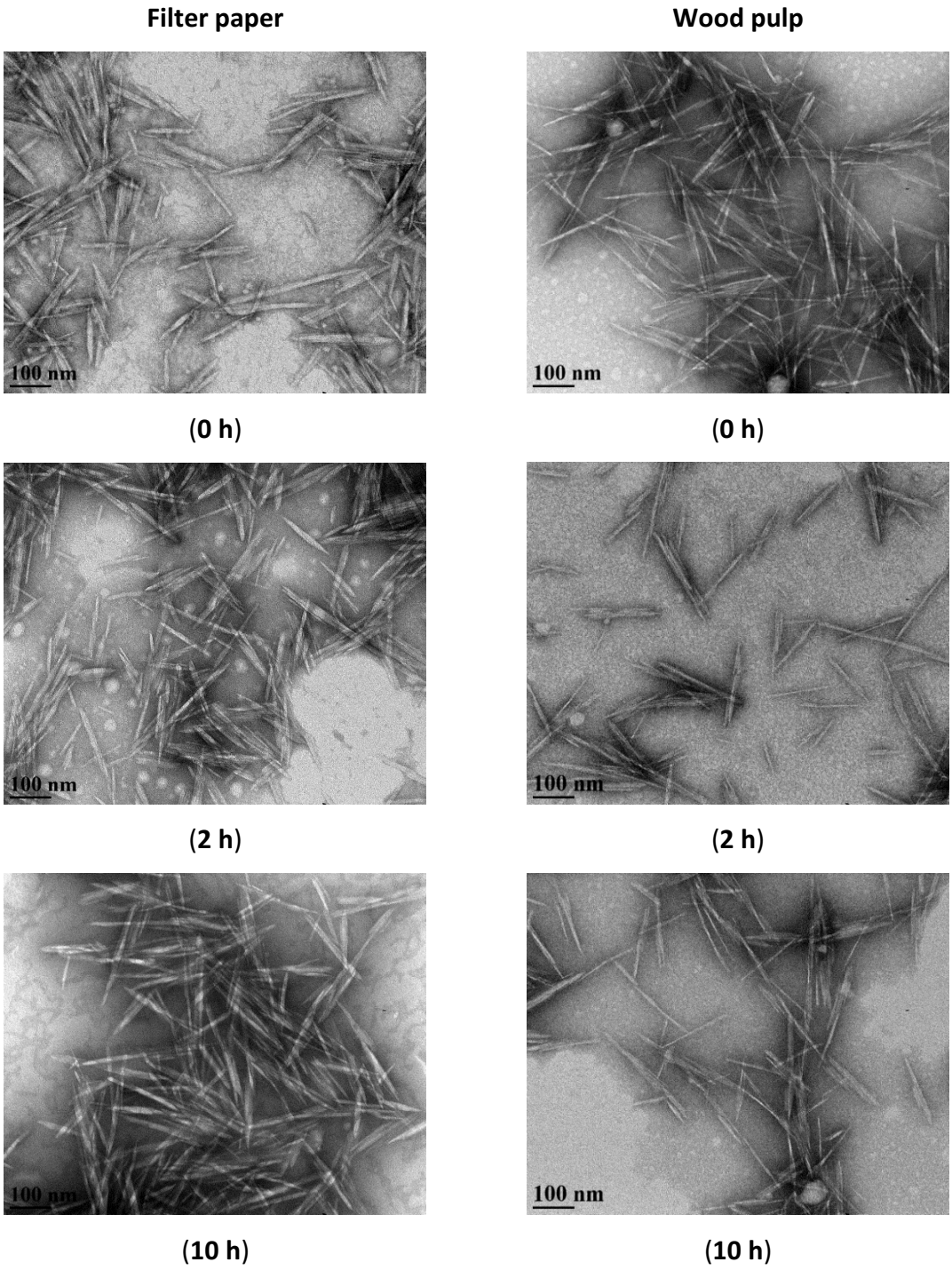

Figure 21 Transmission electron microscopy (TEM) micrographs of CNC isolated from cellulase–treated filter paper (left) and wood pulp (right) at different times.

Table 11 Particle size of CNC isolated from cellulase–treated filter paper and wood pulp based on transmission electron microscopy (TEM) micrograph analysis

Cellulase treatment (h)	Filter Paper			Wood Pulp		
	Length (nm)	Width (nm)	Aspect Ratio	Length (nm)	Width (nm)	Aspect Ratio
0	116 ± 30^{A}	8.8 ± 2.5^{P}	$13.2 \pm 3.6^{W,X}$	$113 \pm 30^{a,b}$	9.2 ± 3.3^{p}	13.4 ± 5.1^{w}
2	138 ± 44^{B}	10.2 ± 3.0^{Q}	$13.5 \pm 3.8^{W,X}$	126 ± 42^{a}	6.8 ± 2.1^{r}	18.8 ± 5.4^{x}
6	$123 \pm 45^{A,B}$	$9.8 \pm 3.0^{P,Q}$	12.0 ± 3.7^{X}	109 ± 33^{b}	7.9 ± 1.9^{q}	14.0 ± 4.4^{w}
10	$134 \pm 40^{A,B,*}$	$9.5 \pm 3.1^{P,Q,*}$	$15.1 \pm 7.0^{W,*}$	123 ± 32^{a}	$7.6 \pm 2.3^{q,r}$	17.5 ± 7.3^{x}

Each data represents the mean ± standard deviation from experimental triplicates (*is an exception calculated from duplicates). Values with different letters (in superscripts) within each column are significantly different ($p < 0.05$).

The aspect ratios (calculated from the ratio of length to width) of filter paper CNCs ranged from 12.0 ± 3.7 to 15.1 ± 7.0 nm, with no significant change in size due to cellulase treatment relative to the control (Table 11). No clear trend was observed in the aspect ratios of wood pulp CNC, which ranged from 13.4 ± 5.9 to 18.8 ± 5.4 nm. The aspect ratios of CNC from wood pulp were relatively lower than those reported (23–31 nm) by Beck–Candanedo *et al*. [46]. Bias in the selection of particles from the TEM micrograph may have affected the average length and width measured in the present study. Despite the repulsive forces from the negative surface charge, self–aggregation was apparent on the copper grid (Figure 21), as reported in literature [123][218]. In addition, CNC particles isolated from cotton and wood are likely to form more aggregates compared with crystals from other sources such as tunicate [51][217]. In the present study, it was observed that longer particles aggregated more than smaller size particles. This is most likely due to the relatively higher surface area for hydrogen bond formation. Therefore, the preferential selection of shorter length particles due to the characteristic dispersion probably led to an overall underestimation of the length and hence lowered the aspect ratio values. Aspect ratios were also calculated from the dataset without removing outliers to retain the longer CNC particle sizes, assuming that these particles were not apparent in the micrograph due to experimental error or by chance. However, no substantial change in the value of the aspect ratio and interpretation were observed.

4.1.5.2. Zeta potential analysis

The stability of a colloid due to electrostatic repulsive forces of the charged surfaces was assessed from zeta potential measurement. A stable colloid is desirable to prevent self aggregation, which is critical for the reinforcement filler to impart strength properties to the composite material [4]. The zeta potential absolute values of CNC colloids extracted from filter paper (−40.5 ± 2.5 to −43.8 ± 0.8 mV) and wood pulp (−38.9 ± 2.7 to −42.6 ± 3.5 mV) (Table 10) were above the minimum threshold (±30 mV) for electrostatic stability [219]. Studies have reported zeta potential values of −15 mV from controlled microbial hydrolysis of filter paper, −25 to −31 mV from acid hydrolysis of cotton fibers, −31 mV from cellulase treatment of recycled paper, and −52 to −58 mV from acid hydrolysis of filter paper [25][47][200][220]. Large zeta potential values do not always guarantee stability, as strong van der Waals attractive forces may cause agglomeration [202]. Based on visual observation of some samples, the colloids in the present study did not show precipitation for several days and hence support the stability implications from the estimated zeta potential values.

Similar to the particle size estimations, only the zeta potential values of filter paper CNC were affected by cellulase treatment. The zeta potential values of CNC isolated from filter paper treated with cellulase for 6 and 10 h were significantly lower than the control. The enzymes likely altered the hydroxyl groups distribution on the CNC surface, which could affect the esterification of the sulfate group and hence the charge density on the surface [176].

4.1.5.3. Cellulose nanocrystal degree of crystallinity

Isolation of CNC by acid hydrolysis increased the crystallinity indices of filter paper and wood pulp celluloses (0 h, untreated) from 85.9 ± 0.7% (fiber, Table 7) up to 88.2 ± 0.5% (CNC, Table 12) and 76.6 ± 0.8% (fiber, Table 7) up to 80.2 ± 0.9% (CNC, Table 12), respectively. This implies that the strong acid substantially hydrolyzed the non–crystalline celluloses during CNC isolation. The crystallinity index of filter paper CNC (86.0 ± 0.6–88.9% ± 0.3%) was much higher compared with wood pulp CNC (78.5 ± 2.2–80.9 ± 0.8%). This implies that the level of ordering of the crystalline fractions in the filter paper CNC is higher relative to wood pulp. It can be suggested that acid hydrolysis of non–crystalline cellulose does not guarantee a uniform CNC crystallinity index from

any given feedstock. The CNC degree of crystallinity is a function of the level of crystalline cellulose chain ordering in the native structure of the feedstock. The substantially higher fiber crystallinity index of the original untreated filter paper cellulose (85.9% ± 0.7%) relative to wood pulp (76.6% ± 0.8%) also supports this suggestion. Variable CNC crystallinity indices, from XRD analysis of acid hydrolyzed cotton (87%–91%), rice straw (86%–91%), wood (75%–85%), bagasse (73%), and coconut fiber (66%) have been reported in literature [47][48][50][123][177][221].

Table 12 Degree of crystallinity of CNCs isolated from cellulase–treated fibers

Cellulase treatment (h)	Crystallinity Index (%)	
	Filter Paper	Wood Pulp
0	88.2 ± 0.5^{A}	80.2 ± 0.9^{a}
2	$87.6 \pm 0.9^{A,B}$	80.7 ± 3.5^{a}
6	86.0 ± 0.6^{B}	78.5 ± 2.2^{a}
10	$88.9 \pm 0.3^{A,*}$	80.9 ± 0.8^{a}

Each data represents the mean ± standard deviation from experimental triplicates (*is an exception calculated from duplicates). Values with different letters (in superscripts) within each column are significantly different ($p < 0.05$).

The crystallinity index of cellulase–treated fibers at a given treatment period (for instance, 2 h, Table 7) was compared with the crystallinity index of CNCs isolated from acid hydrolysis of the same fiber (2 h cellulase–treated feedstock, Table 12). In the case of the filter paper feedstock, no substantial differences in crystallinity indices of fibers and CNCs were identified. There could have been a subtle change in the degree of crystallinity that was not detected from the XRD analysis due to the limitations discussed in section 4.1.3.2. On the other hand, it is possible that a value close to the maximum achievable degree of crystallinity of fiber was attained due to the substantial cellulase degradation of poorly ordered cellulose, even within 2 h. Hence, during acid hydrolysis, the exposed/ available CNC precursors in the cellulase–treated fibers were likely attacked, which led to the dissolution to sugars (Table 5) and decrease in CNC $yield_2$ (Table 9). In contrast, the CNC crystallinity indices from cellulase–treated wood pulp improved by up to 5%, relative to the cellulase–treated wood pulp fiber across the same time period. Even though the concentration of CNC precursors in cellulase–treated pulp was evident from the improvement in

CNC $yield_1$, the feedstock still had substantial composition of non–crystalline cellulose. As discussed previously, this is likely due to the inaccessibility of non–crystalline cellulose chains that are trapped in the core structure [95].

CNC crystallinity indices did not show any significant difference due to cellulase treatment or as a function of time in both feedstocks (except for CNC from 6 h cellulase–treated filter paper) (Table 12). This implies that despite some evident crystalline cellulose degradation in the fiber, cellulase treatment does not change the quality of the CNC precursor crystals.

4.1.5.4. Thermal stability

Thermogravimetric analysis was conducted to assess the degradation profile of CNC particles as a function of temperature. Ideally, CNC as a reinforcement filler should have high thermal stability to withstand the high temperatures in composite processing [22][121]. The onset temperature of degradation could not be quantified as the change in slope of the weight (%) for majority of the samples was ambiguous (Figure 22). The derivative plots did not show clearly distinguishable peaks that led to highly subjective sketching of the final tangential line. Hence, the estimations of the onset temperature of degradation could not be accurately reported in this comparative study. However, it was evident from the curves on the plot that there was no substantial difference due to cellulase treatment and/or as a function of time for both feedstocks with the onset temperature of degradation falling between 250–300 °C. Conversely, the derivative plots distinctly showed the temperature profile for maximum rate of weight loss of CNCs from the steepest peaks. The peak degradation temperatures for filter paper and wood pulp CNCs were between 290 ± 32 to 311 ± 1 °C and 301 ± 2 to 305 ± 1 °C, respectively (Table 13). Yildirim *et al*. reported a maximum rate of CNC weight loss at 247.9 °C [222]. Cellulase treatment had no significant effect on this rate in both feedstocks (except at 10 h for wood pulp).

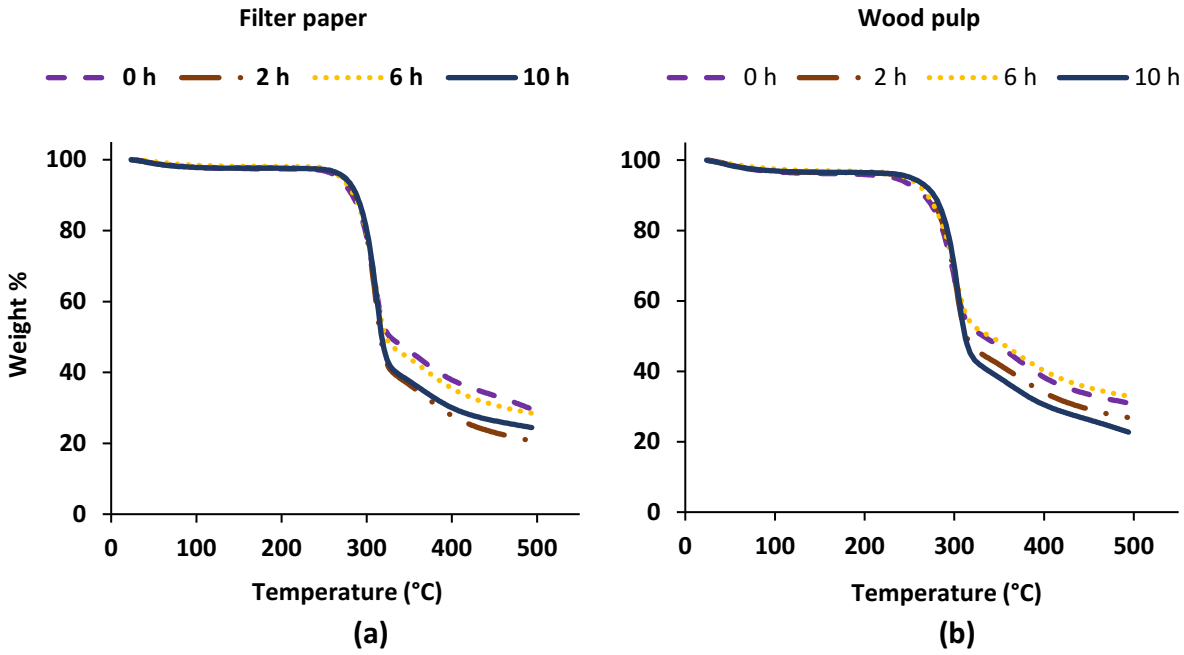

Figure 22 Onset temperature of degradation of CNC isolated from (a) filter paper and (b) wood pulp cellulase–treated for 0, 2, 6 and 10 h.

Table 13 Rate of CNC weight loss as a function of temperature

Cellulase treatment (h)	Temperature for Maximum Rate of Weight Loss (°C)	
	Filter Paper	Wood Pulp
0	290 ± 32^{A}	301 ± 2^{a}
2	310 ± 1^{A}	$303 \pm 0^{a,b}$
6	311 ± 1^{A}	$302 \pm 1^{a,b}$
10	310 ± 2^{A}*	305 ± 1^{b}

Each data represents the mean ± standard deviation from experimental triplicates (*is an exception calculated from duplicates). Values with different letters (in superscripts) within each column are significantly different ($p < 0.05$).

4.2. Hydrothermal treatment mediated cellulose nanocrystal isolation

The following sections discuss the results and interpretations from hydrothermal treatment experiments on wood pulp to generate furfural as a value-added product from xylan degradation and form new CNC precursors to improve CNC yields from acid hydrolysis.

4.2.1. Degradation profile of wood pulp fiber

Square cut wood pulp suspended in water (2.5% solid loading) was hydrothermally treated in batch mode for 1 h. The pressure in the reactor vessel rose from 0.414–2.551 MPa as the temperature increased from 150–225 °C (Table 14). The water heated at 150 and 175 °C was not subcritical as the recorded pressures (0.414 and 0.827 MPa, respectively) were below the saturation vapor pressures (0.478 and 0.894 MPa, respectively) for these temperatures [223]. The pressures at 200 and 225 °C (1.551 and 2.551 MPa, respectively) were very close to the saturation vapor pressures (1.553 and 2.548 MPa) and hence, the heated water was on the borderline with the subcritical region.

Table 14 Characteristics of the hydrothermally treated pulp

Hydrothermal treatment (°C)	Recorded pressure (MPa)	Solid recovery (wt % original feedstock)	Polysaccharide composition (wt % hydrothermally treated feedstock)		Crystallinity Index (%)
			Cellulose	Xylan	
RT	*	98.9 ± 0.4^{A}	74.3 ± 0.1^{H}	19.2 ± 0.1^{P}	76.7 ± 0.8^{W}
150	0.414	97.3 ± 0.6^{A}	75.6 ± 2.6^{H}	18.8 ± 0.7^{P}	77.5 ± 1.7^{WX}
175	0.827	92.2 ± 0.3^{B}	78.0 ± 3^{HI}	15.5 ± 0.6^{Q}	81.4 ± 1.5^{XY}
200	1.551	78.5 ± 0.6^{C}	83.6 ± 2.3^{I}	7.2 ± 0.3^{R}	83.8 ± 2.4^{Y}
225	2.551	46.6 ± 1.2^{D}	73.4 ± 0.5^{H}	1.9 ± 0.2^{S}	80.2 ± 0.8^{WXY}

Each data represents the mean ± standard deviation from experimental triplicates. Values with different letters (in superscripts) within each column are significantly different ($p < 0.05$). *carried out at atmospheric pressure. RT–room temperature as a control.

Solid recovery ≥ 175 °C hydrothermal treatment was significantly reduced due to wood pulp degradation (Table 14). Consequently, the square cut dimension (approximately 6 × 8 mm) of wood pulp was reduced to coarse and fine powder at 200 and 225 °C, respectively (Figure 23). Furthermore, the hydrothermally treated pulps were faint yellow, light brown and dark brown colored at 175, 200 and 225 °C, respectively. The color could arise from insoluble dark sugar degradation products produced by caramelization [224][225]. The pH of the liquid hydrolysate was reduced from pH 5 (control) down to pH 2.5 (225 °C) due to the release of acetic and formic acids from xylose degradation (Table 15) [79][226][227].

Room temperature **150** **175** **200** **225**

Hydrothermal treatment temperature (°C)

Figure 23 Color imparted on wood pulp due to hydrothermal treatment

Degradation products were analyzed using HPLC to study the composition of hydrothermally treated pulp (after 2 step acid hydrolysis of the polysaccharides to sugars, Table 14) and the liquid hydrolysate (Table 15). There were no changes in xylan and cellulose contents of hydrothermally treated wood pulp at 150 °C. Very poor peak intensities of oligo–, monosaccharide and other degradation products were detected in the liquid hydrolysate at this temperature. Pulp degradation was initiated at 175 °C with significant xylan hydrolysis. Hemicelluloses generally solubilize at 180 °C and are relatively less stable because of accessibility of glycosidic bonds with lower levels of crystallinity than celluloses [79]. The xylan composition in the hydrothermally treated wood pulp (wt % hydrothermally treated feedstock) significantly decreased at 200 °C (7.2 ± 0.3 %) and 225 °C (1.9 ± 0.2 %) relative to the original feedstock (19.2 ± 0.1 %). Bizikis *et al*. also reported significant loss in hemicellulose from 25–28% down to 4, 9 and 12% due to hydrothermal treatment of birch wood, aspen and alder wood, respectively for 1 h at 180 °C [190]. The formation of an acidic medium by organic acids, evident from the low pH, has likely facilitated autohydrolysis reactions [42].

Table 15 Composition of the liquid fraction from hydrothermal treatment

Hydrothermal treatment (°C)	pH	Sugars and degradation product recovery (wt % original feedstock)					
		Glucose	Xylose	Hydoxy–methyl furfural	Furfural	Formic acid	Acetic acid
RT	5.0	0.0 ± 0.0	0.0 ± 0.0	0.0 ± 0.0	0.0 ± 0.0	0.0 ± 0.0	0.0 ± 0.0
150	4.5	0.0 ± 0.0	0.1 ± 0.0	0.0 ± 0.0	0.1 ± 0.0^{A}	0.0 ± 0.0	0.0 ± 0.0
175	3.9	0.1 ± 0.0	0.8 ± 0.0	0.0 ± 0.0	0.3 ± 0.0^{A}	0.1 ± 0.0^{P}	0.0 ± 0.0
200	3.3	1.6 ± 0.1	1.7 ± 0.1	0.0 ± 0.0	3.7 ± 0.2^{B}	0.2 ± 0.0^{P}	0.2 ± 0.0^{W}
225	2.5	7.0 ± 1.5	0.0 ± 0.0	0.0 ± 0.0	4.1 ± 0.8^{B}	1.4 ± 0.2^{Q}	0.4 ± 0.0^{X}

Each data represents the mean ± standard deviation from experimental triplicates. Values with different letters (in superscripts) within each column are significantly different ($p < 0.05$). *carried out at atmospheric pressure. RT–room temperature as a control.

The xylose sugars recovered in the liquid hydrolysate were not proportional to the xylan degradation in the recovered solid at these temperatures. Substantial concentrations of furfural and traces of formic and acetic acids were detected, which imply xylose degradation at 200 and 225 °C. Acetic acid and secondary products such as furfural, carboxylic acids (formic, lactic and oxalic acids), aldehydes, dihydroxyacetone and dark insoluble brown product from xylan degradation have been reported from treatments at subcritical temperatures [225][228][229].

Among the degradation products, furfural has versatile applications as a solvent, platform chemical or ingredient in oil refinery, agriculture, pharmaceutical and cosmetic industries [43][44]. It is produced by thermal hydrolysis of lignocellulosic biomass catalyzed by dilute acid as a sole product at low yields below 50% with high energy consumption for processing [44][193]. Improvements in the recovery process has increased the yields by up to 70%. Furfural was the major sugar degradation product (except for glucose at 225 ˚C) generated from the hydrothermal treatment. Hydrothermal treatment at 200 and 225 °C produced 3.7 ± 0.2 and 4.1 ± 0.8 furfural (wt % original feedstock), respectively that is equivalent to 19 and 21% xylan conversion (wt %). Hence, there is a potential to generate furfural as a value–added co–product with CNC through hydrothermal treatment mediated acid hydrolysis process as a biorefinery strategy.

An unidentified peak, with substantial intensity was separated at 35 min retention time and detected by UV analysis at 284 and 275 nm. Pinkowska *et al.* also detected unknown peaks from xylan degradation at 180–300 °C and suggested that these could be aldehydes, carboxylic acids or other sugar degradation products [229]. If this product was quantified and the concentrations of other degradation products were pooled, a complete mass balance may be achieved.

Cellulose accumulation became apparent in the hydrothermally treated pulp with significant xylan degradation at 200 °C. There was only minor cellulose loss as very low glucose content (1.6 ± 0.1 wt %) and oligosaccharide peak intensities were detected from analysis of the liquid hydrolysate at 200 °C. Cellulose was significantly degraded at 225 °C with glucose yields of 7.0 ± 1.5 wt % original feedstock. The recovery of glucose and lack of hydroxymethyl furfural peaks in the hydrolysate at 225 °C suggest that glucose was relatively stable to thermal decomposition. Interestingly, the mass balance from the 225 °C hydrothermal treatment was far from complete. Insoluble dark brown products that were not accounted for in the analysis of the 2 step acid hydrolysis procedure could make up for the mass difference.

4.2.2. Crystallinity of hydrothermally treated wood pulp

Hydrothermal treatments at 175–225 °C significantly improved the crystallinity index of wood pulp from 76.7 ± 0.8 up to 83.8 ± 2.4% (Table 14). Crystallinity could have improved as a result of concentration of crystalline chains due to degradation of xylan and some non–crystalline cellulose as indicated in the findings from cellulase treatment. Significant thermal degradation of xylan and cellulose to some extent at 225 °C (as discussed in section 4.2.1.) supports this assumption. The other hypothesis is that hydrothermal treatment can also promote the reorientation of para–crystalline celluloses to form new compact crystals [185][187]. Heat can also rotate bond angles in the functional groups involved in hydrogen bonding between crystalline chains that facilitate higher level crystalline ordering [39]. Isogai *et al.* reported an increase in crystallinity index of hydrothermally treated amorphous cellulose [186]. Inagaki *et al*. also observed that heat–treatment (140 °C, up to 100 h) of raw wood conferred increase in the crystallite thickness [185]. In addition, it is likely that xylan degradation promotes cellulose crystallization [114][115][189]. The removal of the non–crystalline xylan interspersed between

the cellulose chains can give more freedom of mobility for the semi–crystalline celluloses to reorient and form compact crystals [189]. If the newly formed crystals are as compact as CNC precursors, then this hydrothermal treatment strategy has the potential to improve not only CNC $yield_1$ but also CNC $yield_2$. The newly formed crystals conferred by hydrothermal treatment have been reported to be stable to subsequent soaking or washing [230].

4.2.3. Cellulose nanocrystal yields from hydrothermally treated wood pulp

CNC was isolated from hydrothermally treated wood pulp (washed and freeze dried) by acid hydrolysis. CNC $yield_1$ (wt % feedstock for acid hydrolysis) improved by 1.4 fold, doubled and quadrupled due to heat treatment at 175 °C (13.9 ± 0.4%), 200 °C (19.8 ± 0.6%) and 225 °C (38.3 ± 2.4%), respectively, relative to the control (9.8 ± 1.3%) (Table 16). It can be suggested that heat treatment increased the CNC precursor composition of the feedstock going to the acid hydrolysis reactor. An efficient CNC $yield_1$ reduces the consumption of chemicals, water and, operational costs in upstream and downstream process as in the case of cellulase mediated acid hydrolysis.

Table 16 CNC yields from hydrothermally treated wood pulp

Hydrothermal treatment (°C)	CNC $yield_1$ (wt % feedstock for acid hydrolysis)	Improvement in CNC $yield_1$ (fold)	CNC $yield_2$ (wt % original feedstock)	Improvement in CNC $yield_2$ (fold)
25	9.8 ± 1.3^{A}	–	9.7 ± 1.3^{P}	–
150	10.1 ± 0.8^{A}	1.0	9.8 ± 0.8^{P}	1.0
175	13.9 ± 0.4^{B}	1.4	12.8 ± 0.4^{Q}	1.3
200	19.8 ± 0.6^{C}	2.0	15.5 ± 0.6^{R}	1.6
225	38.3 ± 2.4^{D}	3.9	17.8 ± 1.4^{R}	1.8

Each data represents the mean ± standard deviation from experimental triplicates. Values with different letters (in superscripts) within each column are significantly different ($p < 0.05$).

The CNC $yield_2$, which was calculated by accounting for the mass loss due to hydrothermal degradation, was significantly improved above 150 °C from 9.7 ± 1.3% (control) to up to 17.8 ± 1.4% (225 °C). If the effect of hydrothermal treatment was only to concentrate the crystalline cellulose, then the CNC $yield_2$ should have been constant. Therefore, the increase in CNC yield

implies that heat treatment of wood pulp induced crystalline ordering that led to the formation new CNC precursors. It can be suggested that these newly formed crystals in the hydrothermally treated wood pulp significantly amplified the XRD intensities (Table 14). It is worth noting that, XRD analysis was not sensitive to the changes in cellulase–treated wood pulp (Table 7) due to the concentration of CNC precursor implied from the improvements in CNC yield$_1$ (Table 8). Agarwal *et al.* reported 8–19% CNC yield$_2$ (lignin containing CNC) from hydrothermally–treated (167–225 °C) raw poplar wood, while the yield was negligible without the treatment [39]. Therefore, partial crystallization of wood pulp cellulose by hydrothermal treatment improves the carbon use efficiency of the acid hydrolysis process. This strategy not only improves CNC productivity, which potentially generates more revenue, but also minimizes the sugar degradation products entering the acid stream to ease recovery. It was not surprising that CNC yields did not improve at 150 °C as no transformation was evident from both compositional and crystallinity analysis of the hydrothermally treated wood pulp (Table 14 and 15). This is the first report of a biorefinery strategy that integrated hydrothermal treatment with CNC isolation for the co–production of furfural and CNC with improved CNC yield.

4.2.4. Characteristics of cellulose nanocrystals from hydrothermally treated wood pulp

Hydrothermal treatment did not change the crystallinity of CNC and increasing the temperature also did not have any effect (Table 17). This suggests that the newly formed crystals had equivalent level of crystalline ordering as the native crystals in wood pulp. Hence, fragmentation of these newly formed CNC precursors with the acid generated CNCs with similar degree of crystallinity. Agarwal *et al*. reported that crystallinity of CNC at 200 °C was not substantially different from treatment at 170 °C from XRD analysis, while 13.8 % improvement due to hydrothermal treatment was identified from Raman spectroscopy [231].

Table 17 Crystallinity, particle size and colloidal stability of CNCs isolated from hydrothermally treated wood pulp

Hydrothermal treatment (°C)	Crystallinity Index (%)	Average hydrodynamic diameter (nm)[†]	Zeta potential (mV)
RT	80.9 ± 2.5^{A}	242 ± 58^{PQ}	–41.3 ± 1.0^{W}
150	81.0 ± 1.2^{A}	199 ± 75^{Q}	–41.8 ± 0.8^{W}
175	81.1 ± 2.0^{A}	255 ± 54^{PQ}	–41.8 ± 0.5^{W}
200	74.3 ± 9.2^{A}	320 ± 42^{P}	–41.7 ± 1.9^{W}
225	79.0 ± 1.5^{A}	254 ± 75^{PQ}	–38.8 ± 2.0^{X}

Each data represents the mean ± standard deviation from experimental triplicates. Values with different letters (in superscripts) within each column are significantly different ($p < 0.05$). [†]average diameter of the peak showing the highest abundance intensity (67–79%). The conductivity, pH, and temperature of the colloid were 0.7 to 0.8 mS/cm, 4.6 to 4.8, and 25 °C, respectively. The polydispersity indices ranged from 0.6 to 0.8, which measures the broadness of the size distribution. Colloid with an index value below 0.05 is monodisperse, below 0.08 is nearly monodisperse, 0.08–0.7 is midrange value, and above 0.7 is a broad distribution [215]. Data represent mean ± standard deviation of analytical triplicates of treatment triplicates.

The hydrodynamic diameter of CNC was not affected by hydrothermal treatment of wood pulp. The visually observed reduction in size of the square cut pulp to coarse and fine powder at 170 and 200 °C, respectively, did not influence the CNC dimensions after acid hydrolysis. These results were also in agreement with CNCs from cellulase–treated pulp. This implies that the permeability of CNC precursors to the acid under these conditions (64 wt % H_2SO_4, 2 h, 45 °C) were conserved irrespective of the fiber size. Zeta potential, which is an indicator of surface charge that confers colloid stability by electrostatic repulsion, did not change due to hydrothermal treatment until 225 °C. This was also supported by the significantly low sulfur content (0.9 ± 0.1 wt % at 225 °C) of CNC relative to the untreated pulp (1.3 ± 0.1 wt %) (Table 18). Degradation products bound to the surface of the hydrothermally treated pulp (as shown in Figure 23) may have prevented esterification of sulfonate groups. Elemental analysis of CNC at 225 °C had significantly higher carbon content (44.2 ± 1.5 wt %) and lower hydrogen and oxygen contents (5.56 ± 0.05 and 49.3 ± 1.4 wt %) relative to the untreated CNC (40.4 ± 0.4, 5.75 ± 0.05 and 52.5 ± 0.4 wt %, respectively). This data and the intense dark brown coloration also observed from CNC isolated

from pulp treated at this temperature (Figure 24) indicate caramelization. Boonstra and Tjeerdsma also reported an increase in carbon content and reduction in oxygen content in hydrothermally treated wood [224]. It was suggested that such changes from hydrothermal treatment are due to dehydration, decarboxylation and condensation. Colored CNC could be undesirable for certain applications and caramelized products bound on the surface could likely affect the chemistry of the CNC and hence the reactivity with polymer matrices.

Table 18 Elemental analysis of CNCs isolated from hydrothermally treated wood pulp

Hydrothermal treatment (°C)	Elemental analysis (wt % CNC)				
	Carbon	Hydrogen	Nitrogen	Sulfur	Oxygen
RT	40.4 ± 0.4^{A}	5.75 ± 0.05^{H}	0	1.3 ± 0.1^{P}	52.5 ± 0.4^{W}
150	40.5 ± 0.3^{A}	5.76 ± 0.03^{H}	0	1.2 ± 0.1^{P}	52.5 ± 0.3^{W}
175	40.4 ± 0.1^{A}	5.77 ± 0.02^{H}	0	1.3 ± 0.1^{P}	52.5 ± 0.1^{W}
200	41.1 ± 0.2^{A}	5.82 ± 0.03^{H}	0	1.2 ± 0.1^{P}	51.9 ± 0.2^{W}
225	44.2 ± 1.5^{B}	5.56 ± 0.05^{I}	0	0.9 ± 0.1^{Q}	49.3 ± 1.4^{X}

Each data represents the mean ± standard deviation from experimental triplicates. Values with different letters (in superscripts) within each column are significantly different ($p < 0.05$).

Figure 24 CNC isolated from hydrothermally treated wood pulp at 175, 200 and 225 °C

5. Conclusions and recommendations

This thesis study demonstrated 2 novel biorefinery strategies that can be consolidated in pulp mills to generate new value–added product streams while improving the efficiency of the CNC isolation process. The transformation to diverse multi–purpose renewable materials, chemicals and fuels is vital for the sustainability of the industry in overcoming declining markets for conventional products. In this study, cellulase and hydrothermal treatments were introduced prior to CNC isolation via acid hydrolysis. The integrated pathways generated fermentable sugars and furfural, respectively, as new value–added co–products. These treatments were also specifically chosen to confer structural modifications in the feedstock that improve the efficiency of acid hydrolysis for CNC isolation without compromising the quality of the CNC.

In the cellulase–mediated CNC isolation biorefinery strategy, filter paper (as a model substrate) and wood pulp were treated with cellulases for 2–10 h prior to acid hydrolysis. Substantial glucose (20–40 %) and xylose (6–12 %) yields (wt % original feedstock), which can be readily fermented to ethanol, were recovered within a short period. Efficient saccharification with increasing hydrolysis rates was attained until 6 h for filter paper and throughout the 10 h treatment for wood pulp. Hence it was demonstrated that fermentable sugars can be recovered efficiently from preferential degradation of non–crystalline cellulose and hemicellulose components. This strategy of preserving the crystalline cellulose lowers ethanol production cost as there is no need for expensive and energy intensive pretreatment and saccharification processes that are currently employed in the biofuel industry to reduce crystallinity. Consequently, CNC $yield_1$ per acid hydrolysis reaction was successfully improved by 1.2 and almost 2 fold from cellulase–treated filter paper and wood pulp, respectively. Hence a cellulase treatment pathway that accumulates CNC precursors in the feedstock for efficient acid hydrolysis was established in this study. This strategy can decrease CNC production cost from the reduced requirement of reagents and operations, both upstream and downstream, or it could lower capital expenditure for establishing a plant with equivalent production capacity. Furthermore, cellulase treatment did not attack CNC precursors in wood pulp and hence CNC $yield_2$ was not compromised until 10 h. Hence, a biorefinery system was developed with efficient saccharification and CNC isolation pathways for the co–generation of fermentable sugars and

CNCs from wood pulp. There was a substantial decrease in CNC $yield_2$ due to the degradation of CNC precursors in filter paper, which were much more abundant in the substrate and hence accessible for hydrolysis. However, the feedstock conversion to value–added product was improved from 60 to 84 % (wt % original feedstock).

This cellulase treatment pathway can be further optimized to achieve an even more efficient and selective saccharification process. Substrate swelling in buffer and high solid loading could be investigated to increase the surface area and throughput, respectively. Cellulase composition (particularly endoglucanase and cellobiohydrolase concentrations, and oxidative enzyme supplementation) can also be manipulated to develop a highly selective enzyme formulation. This novel approach of selectively degrading non–crystalline cellulose with minimal loss to CNC precursor can give life to cellulase extracts or formulations that have been shelved due to poor activity on crystalline cellulose that was conventionally desirable by the cellulosic ethanol industry. Acid hydrolysis reaction conditions used in the present study were adopted from the CNC pilot plant operations at InnoTech Alberta (Edmonton, AB, Canada) at the start of the project in 2014. However, these conditions can be optimized for cellulase–treated feedstock, which has a different structural composition relative to the parent material, to preserve more CNC precursors and achieve higher CNC yields.

The second novel biorefinery strategy developed in this study integrated hydrothermal treatment and CNC isolation. This is the first demonstration of a pathway that co–produces furfural along with CNC from wood pulp feedstock. Hydrothermal treatment at 175–225 °C degraded xylan and significant dehydration of the resulting xylose sugars to furfural was achieved with 20% conversion efficiency (wt % xylan) at 200 and 225 °C. Even though established furfural production processes generate higher yields (50–70% xylan conversion) from acid catalyzed thermal degradation, other lignocellulosic components are not utilized. The hydrothermal treatment mediated biorefinery approach thus has a competitive advantage in transforming the cellulosic feedstock to CNC as a high value co–product. The addition of furfural into the product stream will open up new and growing markets for the pulp and paper industry as the molecule is a platform chemical and solvent for diverse products in various industries. In addition to furfural co–production, this is the first report of an improvement in CNC $yield_1$ and $yield_2$ due to

crystallization of cellulose in a kraft pulp feedstock. These findings suggest that in addition to CNC precursor accumulation from degradation of xylan (for furfural generation), hydrothermal treatment can re–orient para–crystalline cellulose to form crystals that are equivalent to CNC precursors. Significant CNC yield$_1$ (up to 4 fold) and CNC yield$_2$ improvements (up to 2 fold) were achieved from 175–225 °C. This will have significant impact not only in improving the process cost but also production capacity, which makes integration of this pathway in CNC plants highly attractive and feasible. It is possible to further optimize furfural production and crystallization by investigating parameters such as solid loading, treatment period, and reactor cooling time and method. The prospect of integrating cellulase hydrolysis to preferentially degrade residual amorphous cellulose in the hydrothermally treated wood pulp to co–generate not only furfural but also fermentable sugars will also be interesting to explore.

Pulp mills can adopt both biorefinery strategies developed in this thesis to offset CNC production cost from: (a) the additional revenue streams that can be generated from the co–products and (b) improvements in CNC yields. This is a step forward in realizing the commercial production and application of CNC as a renewable and sustainable material in various products. This study was carried out in collaboration with research facilities and industry partners including InnoTech Alberta and Al–Pac Forestry Industries, which are on the verge of establishing a demonstration scale CNC plant. Therefore, there is an opportunity to consider integrating the biorefinery strategies after evaluating scaled–up operations and assessing technoeconomic feasibility.

Similarly, generation of ethanol and furfural as co–products from the biorefinery stream is a potentially viable production strategy that would substantially reduce the production cost of the chemicals. In recent times, the cellulosic ethanol industry has been struggling to survive with the closure or transformation of major plants established by companies such as DuPont and Abengoa. This is a result of competition with the low price of gasoline and high production costs. The coproduction pathway from a biorefinery is a sustainable approach for biofuel production to maintain the global efforts to reduce greenhouse gas emissions and dependency of petroleum oil. Furfural production from a biorefinery is also more feasible as current production processes have high energy requirements and other processing costs. Both pathways in the present study also achieved better carbon use efficiency of amorphous and para–crystalline celluloses, as well

as hemicelluloses, that would have otherwise entered the acid stream. Hence, acid recovery efficiency will also be improved, which reduces recycling process cost and operations.

Overall, the findings and implications from this study on cellulase and hydrothermal treatment mediated CNC production processes are promising for establishing potentially viable biorefinery systems. This strategy can be integrated in the pulp and paper industry for the coproduction of CNC, furfural, and ethanol at reduced cost, which will help the industry enter diverse and bigger growing markets to maintain sustainability.

References

1. Bajpai, P. Global Pulp and Paper Production and Consumption. In *Pulp and Paper Industry: Energy Conservation*; Elsevier Inc.: Oxford, 2016; pp 9–14.

2. Resolute Forest Products. 2016 Annual Report http://www.pfresolu.com/uploadedFiles/Media/Publications/RFP_2016-Annual-Report.pdf (accessed Sep 8, 2017).

3. Moon, R. J.; Martini, A.; Nairn, J.; Simonsen, J.; Youngblood, J. Cellulose Nanomaterials Review: Structure, Properties and Nanocomposites. *Chem. Soc. Rev.* **2011**, *40* (7), 3941–3994. https://doi.org/10.1039/c0cs00108b.

4. Mariano, M.; El Kissi, N.; Dufresne, A. Cellulose Nanocrystals and Related Nanocomposites: Review of Some Properties and Challenges. *J. Polym. Sci. Part B Polym. Phys.* **2014**, *52* (12), 791–806. https://doi.org/10.1002/polb.23490.

5. Cao, Y.; Zavaterri, P.; Youngblood, J.; Moon, R.; Weiss, J. Cement & Concrete Composites The Influence of Cellulose Nanocrystal Additions on the Performance of Cement Paste. *Cem. Concr. Compos.* **2015**, *56*, 73–83. https://doi.org/10.1016/j.cemconcomp.2014.11.008.

6. Fortunati, E.; Armentano, I.; Zhou, Q.; Iannoni, A.; Saino, E.; Visai, L.; Berglund, L. A. Multifunctional Bionanocomposite Films of Poly (Lactic Acid), Cellulose Nanocrystals and Silver Nanoparticles. *Carbohydr. Polym.* **2012**, *87* (2), 1596–1605. https://doi.org/10.1016/j.carbpol.2011.09.066.

7. Kong, X.; Zhao, L.; Curtis, J. M. Polyurethane Nanocomposites Incorporating Biobased Polyols and Reinforced with a Low Fraction of Cellulose Nanocrystals. *Carbohydr. Polym.* **2016**, *152*, 487–495. https://doi.org/10.1016/j.carbpol.2016.07.032.

8. Kaboorani, A.; Riedl, B.; Blanchet, P.; Fellin, M.; Hosseinaei, O.; Wang, S. Nanocrystalline Cellulose (NCC): A Renewable Nano-Material for Polyvinyl Acetate (PVA) Adhesive. *Eur. Polym. J.* **2012**, *48* (11), 1829–1837. https://doi.org/10.1016/j.eurpolymj.2012.08.008.

9. Boluk, Y.; Zhao, L. Aircraft Anti-Icing Fluids Formulated with Nanocrystalline Cellulose. U.S. Patent. 8,105,430 B2, January 31, 2012.

10. Hu, Z.; Patten, T.; Pelton, R.; Cranston, E. D. Synergistic Stabilization of Emulsions and Emulsion Gels with Water-Soluble Polymers and Cellulose Nanocrystals. *ACS Sustain. Chem. Eng.* **2015**, *3* (5), 1023–1031. https://doi.org/10.1021/acssuschemeng.5b00194.

11. Li, M. C.; Wu, Q.; Song, K.; De Hoop, C. F.; Lee, S.; Qing, Y.; Wu, Y. Cellulose Nanocrystals and Polyanionic Cellulose as Additives in Bentonite Water-Based Drilling Fluids: Rheological Modeling and Filtration Mechanisms. *Ind. Eng. Chem. Res.* **2016**, *55* (1), 133–143. https://doi.org/10.1021/acs.iecr.5b03510.

12. De Souza Lima, M. M.; Borsali, R. Rodlike Cellulose Microcrystals: Structure, Properties, and Applications. *Macromol. Rapid Commun.* **2004**, *25* (7), 771–787. https://doi.org/10.1002/marc.200300268.

13. Shopsowitz, K. E.; Qi, H.; Hamad, W. Y.; Maclachlan, M. J. Free-Standing Mesoporous Silica Films with Tunable Chiral Nematic Structures. *Nature* **2010**, *468* (7322), 422–425. https://doi.org/10.1038/nature09540.

14. Chen, X.; Deng, X.; Shen, W.; Jiang, L. Controlled Enzymolysis Preparation of Nanocrystalline Cellulose from Pretreated Cotton Fibers. *BioResources* **2012**, *7* (3), 4237–4248. https://doi.org/10.15376/biores.7.3.4237-4248.

15. Fortunati, E.; Peltzer, M.; Armentano, I.; Torre, L.; Jiménez, A.; Kenny, J. M. Effects of Modified Cellulose Nanocrystals on the Barrier and Migration Properties of PLA Nano-Biocomposites. *Carbohydr. Polym.* **2012**, *90*, 948–956. https://doi.org/10.1016/j.carbpol.2012.06.025.

16. Pereira, A. L. S.; Nascimento, D. M. do; Souza Filho, M. de sá M.; Morais, J. P. S.; Vasconcelos, N. F.; Feitosa, J. P. A.; Brígida, A. I. S.; Rosa, M. de F. Improvement of Polyvinyl Alcohol Properties by Adding Nanocrystalline Cellulose Isolated from Banana Pseudostems. *Carbohydr. Polym.* **2014**, *112*, 165–172. https://doi.org/10.1016/j.carbpol.2014.05.090.

17. Jin, L.; Li, W.; Xu, Q.; Sun, Q. Amino-Functionalized Nanocrystalline Cellulose as an Adsorbent for Anionic Dyes. *Cellulose* **2015**, *22* (4), 2443–2456. https://doi.org/10.1007/s10570-015-0649-4.

18. Batmaz, R.; Mohammed, N.; Zaman, M.; Minhas, G.; Berry, R. M.; Tam, K. C. Cellulose Nanocrystals as Promising Adsorbents for the Removal of Cationic Dyes. *Cellulose* **2014**, *21* (3), 1655–1665. https://doi.org/10.1007/s10570-014-0168-8.

19. Larsson, P. T.; Wickholm, K.; Iversen, T. A CP/MAS Carbon-13 NMR Investigation of Molecular Ordering in Celluloses. *Carbohydr. Res.* **1997**, *302*, 19–25. https://doi.org/10.1016/S0008-6215(97)00130-4.

20. Nickerson, R. F.; Habrle, J. A. Cellulose Intercrystalline Structure. *Ind. Eng. Chem.* **1947**, *39* (11), 1507–1512. https://doi.org/10.1021/ie50455a024.

21. Chen, L.; Wang, Q.; Hirth, K.; Baez, C.; Agarwal, U. P.; Zhu, J. Y. Tailoring the Yield and Characteristics of Wood Cellulose Nanocrystals (CNC) Using Concentrated Acid Hydrolysis. *Cellulose* **2015**, *22* (3), 1753–1762. https://doi.org/10.1007/s10570-015-0615-1.

22. Chen, L.; Zhu, J. Y.; Baez, C.; Kitin, P.; Elder, T. Highly Thermal-Stable and Functional Cellulose Nanocrystals and Nanofibrils Produced Using Fully Recyclable Organic Acids. *Green Chem.* **2016**, *18* (13), 3835–3843. https://doi.org/10.1039/C6GC00687F.

23. Luong, C. W.; Luong, J. H. T.; Lam, E.; Liu, Y.; Male, K. B.; Mahmoud, K.; Rho, D. Cellulose Nanocrystals from Renewable Biomass. U.S. Patent. 8900706 B2, December 02, 2014.

24. Novo, L. P.; Bras, J.; Garcia, A.; Belgacem, N.; Curvelo, A. A. S. Subcritical Water: A Method for Green Production of Cellulose Nanocrystals. *ACS Sustain. Chem. Eng.* **2015**, *3* (11), 2839–2846. https://doi.org/10.1021/acssuschemeng.5b00762.

25. Filson, P. B.; Dawson-Andoh, B. E.; Schwegler-Berry, D. Enzymatic-Mediated Production of Cellulose Nanocrystals from Recycled Pulp. *Green Chem.* **2009**, *11* (11), 1808. https://doi.org/10.1039/b915746h.

26. Bondancia, T. J.; Mattoso, L. H. C.; Marconcini, J. M.; Farinas, C. S. A New Approach to

Obtain Cellulose Nanocrystals and Ethanol from Eucalyptus Cellulose Pulp via the Biochemical Pathway. *Biotechnol. Prog.* **2017**, *33* (4), 1085–1095. https://doi.org/10.1002/btpr.2486.

27. Trache, D.; Hussin, M. H.; Haafiz, M. K. M.; Thakur, V. K. Recent Progress in Cellulose Nanocrystals: Sources and Production. *Nanoscale* **2017**, *9* (5), 1763–1786. https://doi.org/10.1039/C6NR09494E.

28. Marcoccia, B.; Edwards, M.; Cooper, M. D. Methods for the Manufacture of Cellulose Nanocrystals. U.S. Patent. 9297111 B1, March 29, 2016.

29. Lynd, L. R.; Weimer, P. J.; van Zyl, W. H.; Pretorius, I. S. Microbial Cellulose Utilization: Fundamentals and Biotechnology. *Microbiol. Mol. Biol. Rev.* **2002**, *66* (3), 506–577. https://doi.org/10.1128/MMBR.66.3.506-577.2002.

30. Kazi, F. K.; Fortman, J. A.; Anex, R. P.; Hsu, D. D.; Aden, A.; Dutta, A.; Kothandaraman, G. Techno-Economic Comparison of Process Technologies for Biochemical Ethanol Production from Corn Stover Q. *Fuel* **2010**, *89*, S20–S28. https://doi.org/10.1016/j.fuel.2010.01.001.

31. Zhao, X.; Xiong, L.; Zhang, M.; Bai, F. Towards Efficient Bioethanol Production from Agricultural and Forestry Residues: Exploration of Unique Natural Microorganisms in Combination with Advanced Strain Engineering. *Bioresour. Technol.* **2016**, *215*, 84–91. https://doi.org/10.1016/j.biortech.2016.03.158.

32. Sasaki, T.; Tanaka, T.; Nanbu, N.; Sato, Y.; Kainuma, K. Correlation between X-Ray Diffraction Measurements of Cellulose Crystal Structure and the Suceptibility to Microbial Cellulase. *Biotechnol. Bioeng.* **1979**, *21*, 1031–1042.

33. Fan, L. T.; Lee, Y.-H.; Beardmore, D. R. The Influence of Major Structural Features of Cellulose on Rate of Enzymatic Hydrolysis. *Biotechnol. Bioeng.* **1981**, *23* (2), 419–424. https://doi.org/10.1002/bit.260230215.

34. Hall, M.; Bansal, P.; Lee, J. H.; Realff, M. J.; Bommarius, A. S. Cellulose Crystallinity - A Key

Predictor of the Enzymatic Hydrolysis Rate. *FEBS J.* **2010**, *277* (6), 1571–1582. https://doi.org/10.1111/j.1742-4658.2010.07585.x.

35. Fan, L. T.; Lee, Y.-H.; David, H. Mechanism of the Enzymatic Hydrolysis of Cellulose - Effects of Major Structural Features of Cellulose on Enzymatic Hydrolysis. *Biotechnol. Bioeng.* **1980**, *22*, 177–199. https://doi.org/10.1002/bit.260220113.

36. Lee, S. B.; Kim, I. H.; Ryu, D. D.; Taguchi, H. Structural Properties of Cellulose and Cellulase Reaction Mechanism. *Biotechnol. Bioeng.* **1983**, *25* (1), 33–51. https://doi.org/10.1002/bit.260250105.

37. Möller, M.; Nilges, P.; Harnisch, F.; Schröder, U. Subcritical Water as Reaction Environment: Fundamentals of Hydrothermal Biomass Transformation. *ChemSusChem* **2011**, *4* (5), 566–579. https://doi.org/10.1002/cssc.201000341.

38. Garrote, G.; Domínguez, H.; Parajo, J. C. Hydrothermal Processing of Lignocellulosic Materials. *Holz als Roh-und Werkst.* **1999**, *57*, 191–202. https://doi.org/https://doi.org/10.1007/s001070050039.

39. Agarwal, U. P.; Ralph, S. A.; Reiner, R. S.; Baez, C. Production of Cellulose Nanocrystals from Raw Wood via Hydrothermal Treatment. U.S. Patent. 20170260692A1, September 14, 2017.

40. Gümüskaya, E.; Usta, M.; Kirci, H. The Effects of Various Pulping Conditions on Crystalline Structure of Cellulose in Cotton Linters. *Polym. Degrad. Stab.* **2003**, *81* (3), 559–564. https://doi.org/10.1016/S0141-3910(03)00157-5.

41. Evans, R.; Newman, R. H.; Roick, U. C.; Suckling, I. D.; Wallis, A. F. A. Changes in Cellulose Crystallinity During Kraft Pulping. Comparison of Infrared, X-Ray Diffraction and Solid State NMR Results. *Holzforschung* **2009**, *49* (6), 498–504. https://doi.org/10.1515/hfsg.1995.49.6.498.

42. Kumar, S.; Gupta, R. B. Hydrolysis of Microcrystalline Cellulose in Subcritical and Supercritical Water in a Continuous Flow Reactor. *Ind. Eng. Chem.* **2008**, *47*, 9321–9329.

https://doi.org/10.1021/ie801102j.

43. Mandalika, A.; Runge, T. Enabling Integrated Biorefineries through High-Yield Conversion of Fractionated Pentosans into Furfural. *Green Chem.* **2012**, *14*, 3175. https://doi.org/10.1039/c2gc35759c.

44. Peleteiro, S.; Rivas, S.; Alonso, J. L.; Santos, V.; Parajó, J. C. Furfural Production Using Ionic Liquids: A Review. *Bioresour. Technol.* **2016**, *202*, 181–191. https://doi.org/10.1016/J.BIORTECH.2015.12.017.

45. Habibi, Y.; Lucia, L. A.; Rojas, O. J. Cellulose Nanocrystals: Chemistry, Self-Assembly, and Applications. *Chem. Rev.* **2010**, *110* (6), 3479–3500. https://doi.org/10.1021/cr900339w.

46. Beck-Candanedo, S.; Roman, M.; Gray, D. G. Effect of Reaction Conditions on the Properties and Behavior of Wood Cellulose Nanocrystal Suspensions. *Biomacromolecules* **2005**, *6* (2), 1048–1054. https://doi.org/10.1021/bm049300p.

47. de Morais Teixeira, E.; Corrêa, A. C.; Manzoli, A.; de Lima Leite, F.; de Ribeiro Oliveira, C.; Mattoso, L. H. C. Cellulose Nanofibers from White and Naturally Colored Cotton Fibers. *Cellulose* **2010**, *17* (3), 595–606. https://doi.org/10.1007/s10570-010-9403-0.

48. Rosa, M. F.; Medeiros, E. S.; Malmonge, J. A.; Gregorski, K. S.; Wood, D. F.; Mattoso, L. H. C.; Glenn, G.; Orts, W. J.; Imam, S. H. Cellulose Nanowhiskers from Coconut Husk Fibers: Effect of Preparation Conditions on Their Thermal and Morphological Behavior. *Carbohydr. Polym.* **2010**, *81* (1), 83–92. https://doi.org/10.1016/j.carbpol.2010.01.059.

49. Lu, P.; Hsieh, Y. Lo. Preparation and Characterization of Cellulose Nanocrystals from Rice Straw. *Carbohydr. Polym.* **2012**, *87* (1), 564–573. https://doi.org/10.1016/j.carbpol.2011.08.022.

50. Kumar, A.; Negi, Y. S.; Choudhary, V.; Bhardwaj, N. K. Characterization of Cellulose Nanocrystals Produced by Acid-Hydrolysis from Sugarcane Bagasse as Agro-Waste. *J. Mater. Phys. Chem.* **2014**, *2* (1), 1–8. https://doi.org/10.12691/jmpc-2-1-1.

51. Sacui, I. A.; Nieuwendaal, R. C.; Burnett, D. J.; Stranick, S. J.; Jorfi, M.; Weder, C.; Foster, E.

J.; Olsson, R. T.; Gilman, J. W. Comparison of the Properties of Cellulose Nanocrystals and Cellulose Nanofibrils Isolated from Bacteria, Tunicate, and Wood Processed Using Acid, Enzymatic, Mechanical, and Oxidative Methods. *ACS Appl. Mater. Interfaces* **2014**, *6* (9), 6127–6138. https://doi.org/10.1021/am500359f.

52. Mahfoudhi, N.; Boufi, S. Nanocellulose as a Novel Nanostructured Adsorbent for Environmental Remediation: A Review. *Cellulose* **2017**, *24* (3), 1171–1197. https://doi.org/10.1007/s10570-017-1194-0.

53. Rusli, R.; Eichhorn, S. J. Determination of the Stiffness of Cellulose Nanowhiskers and the Fiber-Matrix Interface in a Nanocomposite Using Raman Spectroscopy. *Appl. Phys. Lett.* **2008**, *93* (3), 033111. https://doi.org/10.1063/1.2963491.

54. Salas, C.; Nypelö, T.; Rodriguez-Abreu, C.; Carrillo, C.; Rojas, O. J. Nanocellulose Properties and Applications in Colloids and Interfaces. *Curr. Opin. Colloid Interface Sci.* **2014**, *19* (5), 383–396. https://doi.org/10.1016/J.COCIS.2014.10.003.

55. Revol, J. F.; Bradford, H.; Giasson, J.; Marchessault, R. H.; Gray, D. G. Helicoidal Self-Ordering of Cellulose Microfibrils in Aqueous Suspension. *Int. J. Biol. Macromol.* **1992**, *14* (3), 170–172. https://doi.org/10.1016/S0141-8130(05)80008-X.

56. Nair, S. S.; Zhu, J.; Deng, Y.; Ragauskas, A. J. High Performance Green Barriers Based on Nanocellulose. *Sustain. Chem. Process.* **2014**, *2* (1), 23. https://doi.org/10.1186/s40508-014-0023-0.

57. Ngo, T.-D.; Danumah, C.; Ahvazi, B. Production of Cellulose Nanocrystals at InnoTech Alberta. In *Nanocellulose and Sustainability: Production, Properties, Applications, and Case Studies*; Lee, K.-Y., Ed.; CRC Press: Milton, 2018; pp 1–26.

58. Ni, H.; Zeng, S.; Wu, J.; Cheng, X.; Luo, T.; Wang, W. Cellulose Nanowhiskers : Preparation , Characterization and Cytotoxicity Evaluation. *Biomed. Mater. Eng.* **2012**, *22*, 121–127. https://doi.org/10.3233/BME-2012-0697.

59. Roman, M. Toxicity of Cellulose Nanocrystals: A Review. *Ind. Biotechnol.* **2015**, *11* (1), 25–

33. https://doi.org/10.1089/ind.2014.0024.

60. Lordan, S.; Kennedy, J. E.; Higginbotham, C. L. Cytotoxic Effects Induced by Unmodified and Organically Modified Nanoclays in the Human Hepatic HepG2 Cell Line. *J. Appl. Toxicol.* **2011**, *31* (1), 27–35. https://doi.org/10.1002/jat.1564.

61. Kovacs, T.; Naish, V.; O'Connor, B.; Blaise, C.; Gagné, F.; Hall, L.; Trudeau, V.; Martel, P. An Ecotoxicological Characterization of Nanocrystalline Cellulose (NCC). *Nanotoxicology* **2010**, *4* (3), 255–270. https://doi.org/10.3109/17435391003628713.

62. George, J.; Sabapathi, S. N. Cellulose Nanocrystals: Synthesis, Functional Properties, and Applications. *Nanotechnol. Sci. Appl.* **2015**, *8*, 45–54. https://doi.org/10.2147/NSA.S64386.

63. Evdokimova, O.; Svensson, F.; Agafonov, A.; Håkansson, S.; Seisenbaeva, G.; Kessler, V. Hybrid Drug Delivery Patches Based on Spherical Cellulose Nanocrystals and Colloid Titania—Synthesis and Antibacterial Properties. *Nanomaterials* **2018**, *8* (4), 228. https://doi.org/10.3390/nano8040228.

64. Yang, J.; Han, C. R.; Duan, J. F.; Xu, F.; Sun, R. C. Mechanical and Viscoelastic Properties of Cellulose Nanocrystals Reinforced Poly(Ethylene Glycol) Nanocomposite Hydrogels. *ACS Appl. Mater. Interfaces* **2013**, *5* (8), 3199–3207. https://doi.org/10.1021/am4001997.

65. Treaty Biotech LLC. FogKicker: A High-Performance Anti-fog Solution https://www.fogkickerdefog.com/ (accessed Apr 30, 2019).

66. Domtar Corporation. Domtar and CelluForce: Innovating with Cellulose Nanocrystals https://newsroom.domtar.com/cellulose-nanocrystals/ (accessed Apr 30, 2019).

67. InnoTech Alberta. Cellulose Nanocrystals (CNC) Pilot Plant – InnoTech Alberta https://innotechalberta.ca/research-facilities/cellulose-nanocrystals-cnc-pilot-plant/ (accessed Apr 24, 2019).

68. CelluForce. NanoCrystalline Cellulose applications | CelluForce https://www.celluforce.com/en/applications/ (accessed Apr 24, 2019).

69. Blue Goose Biorefineries Inc. Blue Goose Biorefineries, Purchase Cellulose Nanocrystals, Nanocellulose https://bluegoosebiorefineries.com/ (accessed Apr 24, 2019).

70. Forest Products Laboratory. Forest Products Laboratory - USDA Forest Service https://www.fpl.fs.fed.us/research/facilities/nanocellulose_pilot-plant.php (accessed Apr 24, 2019).

71. InnoTech Materials LLC. Oxidized Nanocellulose http://www.innotechmaterials.com/oxidized-nanocellulose/ (accessed May 2, 2019).

72. Melodea Ltd. Melodea | Bio Based Solutions,NCC Production,Nano Crystalline Cellulose,microfibrillated cellulose http://www.melodea.eu/Default.asp?sType=0&PageId=104256 (accessed May 2, 2019).

73. Guilin Qihong Technology Co. Ltd. Nanocellulose expert | Guilin Qihong Tech. http://qh-tech.cn/en/ (accessed May 2, 2019).

74. Caspian Nanocellulose Polymer Development Co. Products - Caspian Nanocellulose Polymer Development Co. https://sites.google.com/site/caspiannanocelluloseco/products (accessed May 2, 2019).

75. Rowell, R. M.; Pettersen, R.; Tshabalala, M. A. Cell Wall Chemistry. In *Handbook of Wood Chemistry and Wood Composites*; Rowell, R. M., Ed.; CRC Press: Boca Raton, 2013. https://doi.org/10.1016/j.jclepro.2015.07.070.

76. Sun, Y.; Cheng, J. Hydrolysis of Lignocellulosic Materials for Ethanol Production: A Review. *Bioresour. Technol.* **2002**, *83* (1), 1–11. https://doi.org/10.1016/S0960-8524(01)00212-7.

77. Sjostrom, E. Wood Polysaccharides. In *Wood Chemistry Fundamentals and Applications*; Academic Press Inc: Helsinki, 1993; pp 51–70. https://doi.org/10.1016/B978-0-08-092589-9.50001-2.

78. Chen, H. Chemical Composition and Structure of Natural Lignocellulose. In *Biotechnology of Lignocellulose- Theory and Practice*; Chemical Industry Press and Springer: Beijing and Dordrecht, 2014; pp 25–71. https://doi.org/10.1007/978-94-007-6898-7.

79. Bobleter, O. Hydrothermal Degradation of Polymers Derived from Plants. *Prog. Polym. Sci.* **1994**, *19* (5), 797–841. https://doi.org/10.1016/0079-6700(94)90033-7.

80. Pinkert, A.; Marsh, K. N.; Pang, S.; Staiger, M. P. Ionic Liquids and Their Interaction with Cellulose. *Chem. Rev.* **2009**, *109* (12), 6712–6728. https://doi.org/10.1021/cr9001947.

81. Sinitsyn, A. P.; Gusakov, A. V.; Vlasenko, E. Y. Effect of Structural and Physico-Chemical Features of Cellulosic Substrates on the Efficiency of Enzymatic Hydrolysis. *Appl. Biochem. Biotechnol.* **1991**, *30* (1), 43–59. https://doi.org/10.1007/BF02922023.

82. Koyama, M.; Helbert, W.; Imai, T.; Sugiyama, J.; Henrissat, B. Parallel-up Structure Evidences the Molecular Directionality during Biosynthesis of Bacterial Cellulose. *Proc. Natl. Acad. Sci. U. S. A.* **1997**, *94* (17), 9091–9095. https://doi.org/10.1073/pnas.94.17.9091.

83. French, A.; Johnson, G. P. Cellulose Shapes. In *Cellulose: Molecular and Structural Biology*; Brown, R. M., Saxena, I. M., Eds.; Springer: Texas, 2007; pp 257–284. https://doi.org/10.1007/978-1-4020-5380-1_1.

84. Doblin, M. S.; Kurek, I.; Jacob-Wilk, D.; Delmer, D. P. Cellulose Biosynthesis in Plants: From Genes to Rosettes. *Plant Cell Physiol.* **2002**, *43* (12), 1407–1420. https://doi.org/10.1093/pcp/pcf164.

85. Somerville, C. Cellulose Synthesis in Higher Plants. *Annu. Rev. Cell Dev. Biol.* **2006**, *22*, 53–78. https://doi.org/10.1146/annurev.cellbio.22.022206.160206.

86. O'Sullivan, A. C. Cellulose: The Structure Slowly Unravels. *Cellulose* **1997**, *4* (3), 173–207. https://doi.org/10.1023/A:1018431705579.

87. Mansfield, S. D.; Mooney, C.; Saddler, J. N. Substrate and Enzyme Characteristics That Limit Cellulose Hydrolysis. *Biotechnol. Prog.* **1999**, *15* (5), 804–816. https://doi.org/10.1021/bp9900864.

88. Zhang, Y. H. P.; Lynd, L. R. Toward an Aggregated Understanding of Enzymatic Hydrolysis of Cellulose: Noncomplexed Cellulase Systems. *Biotechnol. Bioeng.* **2004**, *88* (7), 797–824.

https://doi.org/10.1002/bit.20282.

89. Fengel, D. Ideas on the Ultrastructural Organization of the Cell Wall Components. *J. Polym. Sci. Part C Polym. Symp.* **2007**, *36* (1), 383–392. https://doi.org/10.1002/polc.5070360127.

90. Blomqvist, K.; Djerbi, S.; Henrik, A.; Teeri, T. T. Cellulose Biosynthesis in Forest Trees. In *Cellulose: Molecular and Structural Biology*; Brown, R. M., Saxena, I. M., Eds.; Springer: Texas, 2007; pp 85–106. https://doi.org/10.1007/978-1-4020-5380-1.

91. Cosgrove, D. J. Enzymes and Other Agents That Enhance Cell Wall Extensibility. *Annu. Rev. Plant Physiol. Plant Mol. Biol.* **1999**, *50* (1), 391–417. https://doi.org/10.1146/annurev.arplant.50.1.391.

92. Nishiyama, Y.; Sugiyama, J.; Chanzy, H.; Langan, P. Crystal Structure and Hydrogen Bonding System in Cellulose Iα from Synchrotron X-Ray and Neutron Fiber Diffraction. *J. Am. Chem. Soc.* **2003**, *125* (47), 14300–14306. https://doi.org/10.1021/ja037055w.

93. Langan, P.; Petridis, L.; O'Neill, H. M.; Pingali, S. V.; Foston, M.; Nishiyama, Y.; Schulz, R.; Lindner, B.; Hanson, B. L.; Harton, S.; et al. Common Processes Drive the Thermochemical Pretreatment of Lignocellulosic Biomass. *Green Chem.* **2014**, *16* (1), 63. https://doi.org/10.1039/c3gc41962b.

94. Clarke, K.; Li, X.; Li, K. The Mechanism of Fiber Cutting during Enzymatic Hydrolysis of Wood Biomass. *Biomass and Bioenergy* **2011**, *35* (9), 3943–3950. https://doi.org/10.1016/j.biombioe.2011.06.007.

95. Park, S.; Baker, J. O.; Himmel, M. E.; Parilla, P. A.; Johnson, D. K. Cellulose Crystallinity Index: Measurement Techniques and Their Impact on Interpreting Cellulase Performance. *Biotechnol. Biofuels* **2010**, *3* (1), 10. https://doi.org/10.1186/1754-6834-3-10.

96. Zhao, H.; Kwak, J. H.; Conrad Zhang, Z.; Brown, H. M.; Arey, B. W.; Holladay, J. E. Studying Cellulose Fiber Structure by SEM, XRD, NMR and Acid Hydrolysis. *Carbohydr. Polym.* **2007**, *68* (2), 235–241. https://doi.org/10.1016/j.carbpol.2006.12.013.

97. Abraham, R. E.; Wong, C. S.; Puri, M. Enrichment of Cellulosic Waste Hemp (Cannabis

Sativa) Hurd into Non-Toxic Microfibres. *Materials (Basel).* **2016**, *9* (7), 562. https://doi.org/10.3390/MA9070562.

98. Huang, S.; Zhou, L.; Li, M. C.; Wu, Q.; Zhou, D. Cellulose Nanocrystals (CNCs) from Corn Stalk: Activation Energy Analysis. *Materials (Basel).* **2017**, *10* (1), 1–13. https://doi.org/10.3390/ma10010080.

99. Cao, Y.; Tan, H. Study on Crystal Structures of Enzyme-Hydrolyzed Cellulosic Materials by X-Ray Diffraction. *Enzyme Microb. Technol.* **2005**, *36*, 314–317. https://doi.org/10.1016/j.enzmictec.2004.09.002.

100. Zhao, Y.; Li, J. Excellent Chemical and Material Cellulose from Tunicates: Diversity in Cellulose Production Yield and Chemical and Morphological Structures from Different Tunicate Species. *Cellulose* **2014**, *21*, 3427–3441. https://doi.org/10.1007/s10570-014-0348-6.

101. Park, S.; Johnson, D. K.; Ishizawa, C. I.; Parilla, P. A.; Davis, M. F. Measuring the Crystallinity Index of Cellulose by Solid State 13C Nuclear Magnetic Resonance. *Cellulose* **2009**, *16* (4), 641–647. https://doi.org/10.1007/s10570-009-9321-1.

102. Nishimura, T.; Ishihara, M.; Ishii, T.; Kato, A. Structure of Neutral Branched Xylooligosaccharides Produced by Xylanase from in Situ Reduced Hardwood Xylan. *Carbohydr. Res.* **1998**, *308* (1–2), 117–122. https://doi.org/10.1016/S0008-6215(98)00069-X.

103. Liu, C.-G.; Xiao, Y.; Xia, X.-X.; Zhao, X.-Q.; Peng, L.; Srinophakun, P.; Bai, F.-W. Cellulosic Ethanol Production: Progress, Challenges and Strategies for Solutions. *Biotechnol. Adv.* **2019**, *37* (3), 491–504. https://doi.org/10.1016/j.biotechadv.2019.03.002.

104. Pettersen, R. C. The Chemical Compostition of Wood. In *The Chemistry of Solid Wood*; Rowell, R., Ed.; American Chemical Society: Washington DC, 1984; pp 57–126.

105. Le Floch, A.; Jourdes, M.; Teissedre, P. L. Polysaccharides and Lignin from Oak Wood Used in Cooperage: Composition, Interest, Assays: A Review. *Carbohydr. Res.* **2015**, *417*, 94–

102. https://doi.org/10.1016/j.carres.2015.07.003.

106. Sluiter, A.; Hames, B.; Ruiz, R.; Scarlata, C.; Sluiter, J.; Templeton, D. *Determination of Structural Carbohydrates and Lignin in Biomass Determination of Structural Carbohydrates and Lignin in Biomass*; Denver, 2012.

107. Biermann, C. J. Pulping Fundamentals. In *Handbook of Pulping and Papermaking*; Academic Press Inc: Corvallis, 1996; pp 55–100. https://doi.org/10.1016/b978-012097362-0/50007-8.

108. Bajpai, P. Pulp and Paper Production Processes and Energy Overview. In *Pulp and Paper Industry: Energy Conservation*; Elsevier: Oxford, 2016; pp 15–49. https://doi.org/10.1016/b978-0-12-803411-8.00003-2.

109. Dyer, T. J. Elucidating the Formation and Chemistry of Chromophores during Kraft Pulping, University of Wisconsin-Stevens Point, 2004, Vol. 1.

110. Johnsson, S.; Wansbrough, H.; Lindstrom, M. Forestry-C-The Pulp and Paper Industry. In *Industrial and Engineering Chemistry*; Packer, J. ., Robertson, J., Wansbrough, H., Eds.; New Zealand Institute of Chemistry: Auckland, 1998.

111. U.S. Congress Office of Technology Assessment. The Pulp and Paper Making Process. In *Technologies for Reducing Dioxin in the Manufacture of Bleached Wood Pulp*; U.S. Government Printing Office: Washington, 1989; pp 17–25.

112. Alberta-Pacific Forest Industries Inc. Fibreline - Alberta-Pacific Forest Industries Inc. https://alpac.ca/index.php/pulp-operations/fibreline (accessed Apr 19, 2019).

113. Patt, R.; Kordsachia, O.; Fehr, J. European Hardwoods versus Eucalyptus Globulus as a Raw Material for Pulping. *Wood Sci. Technol.* **2006**, *40* (1), 39–48. https://doi.org/10.1007/s00226-005-0042-9.

114. Hult, E.-L.; Larsson, P. .; Iversen, T. Cellulose Fibril Aggregation an Inherent Property of Kraft Pulp. *Poly* **2001**, *42*, 3309–3314.

115. Wan, J.; Wang, Y.; Xiao, Q. Effects of Hemicellulose Removal on Cellulose Fiber Structure

and Recycling Characteristics of Eucalyptus Pulp. *Bioresour. Technol.* **2010**, *101* (12), 4577–4583. https://doi.org/10.1016/J.BIORTECH.2010.01.026.

116. Saul, D. J.; Gibbs, M. D.; Bergquist, P. L. Enzymatic Bleaching of Wood Pulp. In *Chemical Processes in New Zealand*; Packer, J. ., Robertson, J., Wansbrough, H., Eds.; New Zealand Institute of Chemistry: Auckland, 1998.

117. Rånby, B. G. Aqueous Colloidal Solutions of Cellulose Micelles. *Acta Chem. Scand.,* **1949**, *3*, 649–650. https://doi.org/10.3891/acta.chem.scand.03-0649.

118. Dong, X. M.; Revol, J.-F.; Gray, D. G. Effect of Microcrystallite Preparation Conditions on the Formation of Colloid Crystals of Cellulose. *Cellulose* **1998**, *5*, 19–32. https://doi.org/10.1023/A:1009260511939.

119. Bondeson, D.; Mathew, A.; Oksman, K. Optimization of the Isolation of Nanocrystals from Microcrystalline Cellulose by Acid Hydrolysis. *Cellulose* **2006**, *13* (2), 171–180. https://doi.org/10.1007/s10570-006-9061-4.

120. Araki, J.; Wada, M.; Kuga, S.; Okano, T. Flow Properties of Microcrystalline Cellulose Suspension Prepared by Acid Treatment of Native Cellulose. *Colloids Surfaces A Physicochem. Eng. Asp.* **1998**, *142* (1), 75–82. https://doi.org/10.1016/S0927-7757(98)00404-X.

121. Lorenz, M.; Sattler, S.; Reza, M.; Bismarck, A.; Kontturi, E. Cellulose Nanocrystals by Acid Vapour: Towards More Effortless Isolation of Cellulose Nanocrystals. *Faraday Discuss.* **2017**, *202*, 315–330. https://doi.org/10.1039/C7FD00053G.

122. Peng, B. L.; Dhar, N.; Liu, H. L.; Tam, K. C. Chemistry and Applications of Nanocrystalline Cellulose and Its Derivatives: A Nanotechnology Perspective. *Can. J. Chem. Eng.* **2011**, *89* (5), 1191–1206. https://doi.org/10.1002/cjce.20554.

123. Lu, P.; Hsieh, Y. Lo. Preparation and Properties of Cellulose Nanocrystals: Rods, Spheres, and Network. *Carbohydr. Polym.* **2010**, *82* (2), 329–336. https://doi.org/10.1016/j.carbpol.2010.04.073.

124. Lorenz, H. *Nanocrystalline Cellulose Preparation by Sulfuric Acid (Bench Top Scale)*; Alberta Innovtes Technology Futures, Bioresource Technologies Bioconversion, 2014.

125. Wang, Q. Q.; Zhu, J. Y.; Reiner, R. S.; Verrill, S. P.; Baxa, U.; McNeil, S. E. Approaching Zero Cellulose Loss in Cellulose Nanocrystal (CNC) Production: Recovery and Characterization of Cellulosic Solid Residues (CSR) and CNC. *Cellulose* **2012**, *19* (6), 2033–2047. https://doi.org/10.1007/s10570-012-9765-6.

126. Wang, Q.; Zhao, X.; Zhu, J. Y. Kinetics of Strong Acid Hydrolysis of a Bleached Kraft Pulp for Producing Cellulose Nanocrystals (CNCs). *Ind. Eng. Chem. Res.* **2014**, *53* (27), 11007–11014. https://doi.org/10.1021/ie501672m.

127. Revol, J.-F.; Godbout, L.; Gray, D. G. Solid Self-Assembled Films of Cellulose with Chiral Nematic Order and Optically Variable Properties. *J. Pulp Pap. Sci.* **1998**, *24* (5), 146–149.

128. Roman, M.; Winter, W. T. Effect of Sulfate Groups from Sulfuric Acid Hydrolysis on the Thermal Degradation Behavior of Bacterial Cellulose. *Biomacromolecules* **2004**, *5* (5), 1671–1677. https://doi.org/10.1021/bm034519+.

129. Moreau, J. Driving Innovation to Market Cellulose Nanomaterials – A Path to Commercialization https://www.nano.gov/sites/default/files/moreau_washington_dc_may_20_2014.pdf (accessed May 8, 2019).

130. Mascheroni, E.; Rampazzo Riccardo; Ortenzi Marco Aldo; Piva, G.; Bonetti, S.; Piergiovanni, L. Comparison of Cellulose Nanocrystals Obtained by Sulfuric Acid Hydrolysis and Ammonium Persulfate, to Be Used as Coating on Flexible Food-Packaging Materials. *Cellulose* **2016**, *23*, 779–793. https://doi.org/10.1007/s10570-015-0853-2.

131. Arantes, V.; Saddler, J. N. Access to Cellulose Limits the Efficiency of Enzymatic Hydrolysis: The Role of Amorphogenesis. *Biotechnol. Biofuels* **2010**, *3* (4), 1–11. https://doi.org/10.1186/1754-6834-3-4.

132. Gupta, V. K.; O'Donovan, A.; Tuohy, M. G.; Sharma, G. D. Trichoderma in Bioenergy

Research: An Overview. In *Biotechnology and Biology of Trichoderma*; Gupta, V. K., Schmoll, M., Herrera-Estrella, Upadhyay, R. S., Druzhinina, I., Maria G, T., Eds.; Elsevier B.V.: Waltham, 2014; pp 325–336. https://doi.org/10.1016/B978-0-444-59576-8.00023-0.

133. Do Vale, L. H. F.; Filho, E. X. F.; Miller, R. N. G.; Ricart, C. A. O.; de Sousa, M. V. Cellulase Systems in Trichoderma: An Overview. In *Biotechnology and Biology of Trichoderma*; Gupta, V. K., Schmoll, M., Herrera-Estrella, Upadhyay, R. S., Druzhinina, I., Maria G, T., Eds.; Elsevier B.V.: Waltham, 2014; pp 229–244. https://doi.org/10.1016/B978-0-444-59576-8.00016-3.

134. Gusakov, A. V. Alternatives to Trichoderma Reesei in Biofuel Production. *Trends Biotechnol.* **2011**, *29* (9), 419–425. https://doi.org/10.1016/j.tibtech.2011.04.004.

135. Shoseyov, O.; Shani, Z.; Levy, I. Carbohydrate Binding Modules: Biochemical Properties and Novel Applications. *Microbiol. Mol. Biol. Rev.* **2006**, *70* (2), 283–295. https://doi.org/10.1128/mmbr.00028-05.

136. Sandgren, M.; Shaw, A.; Ropp, T. H.; Wu, S.; Bott, R.; Cameron, A. D.; Ståhlberg, J.; Mitchinson, C.; Jones, T. A. The X-Ray Crystal Structure of the Trichoderma Reesei Family 12 Endoglucanase 3, Cel12A, at 1.9 Å Resolution. *J. Mol. Biol.* **2001**, *308* (2), 295–310. https://doi.org/10.1006/jmbi.2001.4583.

137. Nakamura, A.; Ishida, T.; Kusaka, K.; Yamada, T.; Fushinobu, S.; Tanaka, I.; Kaneko, S.; Ohta, K.; Tanaka, H.; Inaka, K.; et al. “Newton’s Cradle” Proton Relay with Amide–Imidic Acid Tautomerization in Inverting Cellulase Visualized by Neutron Crystallography. *Sci. Adv.* **2015**, *1* (7). https://doi.org/10.1126/SCIADV.1500263.

138. Datta, S.; Sapra, R. Cellulases and Hemicellulases for Biomass Degradation: An Introduction. In *Chemical and Biochemical Catalysis for Next Generation Biofuels*; Simmons, B. A., Ed.; Royal Society of Chemistry: Cambridge, 2011; pp 115–135. https://doi.org/https://doi.org/10.1039/9781849732857-FP001.

139. Boraston, A. B.; Bolam, D. N.; Gilbert, H. J.; Davies, G. J. Carbohydrate-Binding Modules: Fine-Tuning Polysaccharide Recognition. *Biochem. J.* **2004**, *382* (3), 769–781.

https://doi.org/10.1042/bj20040892.

140. Beguin, P.; Lemaire, M. The Cellulosome: An Exocellular, Multiprotein Complex Specialized in Cellulose Degradation. *Crit. Rev. Biochem. Mol. Biol.* **1996**, *31* (3), 201–236. https://doi.org/10.3109/10409239609106584.

141. Tamaru, Y.; Doi, R. H. Three Surface Layer Homology Domains at the N Terminus of the Clostridium Cellulovorans Major Cellulosomal Subunit EngE. *J. Bacteriol.* **1999**, *181* (10), 3270–3276.

142. Harris, P. V.; Welner, D.; McFarland, K. C.; Re, E.; Navarro Poulsen, J. C.; Brown, K.; Salbo, R.; Ding, H.; Vlasenko, E.; Merino, S.; et al. Stimulation of Lignocellulosic Biomass Hydrolysis by Proteins of Glycoside Hydrolase Family 61: Structure and Function of a Large, Enigmatic Family. *Biochemistry* **2010**, *49* (15), 3305–3316. https://doi.org/10.1021/bi100009p.

143. Hu, J.; Arantes, V.; Pribowo, A.; Gourlay, K.; Saddler, J. N. Substrate Factors That Influence the Synergistic Interaction of AA9 and Cellulases during the Enzymatic Hydrolysis of Biomass. *Energy Environ. Sci.* **2014**, *7* (7), 2308–2315. https://doi.org/10.1039/c4ee00891j.

144. Phillips, C. M.; Beeson, W. T.; Cate, J. H.; Marletta, M. A. Cellobiose Dehydrogenase and a Copper-Dependent Polysaccharide Monooxygenase Potentiate Cellulose Degradation by Neurospora Crassa. *ACS Chem. Biol.* **2011**, *6* (12), 1399–1406. https://doi.org/10.1021/cb200351.

145. Arantes, V.; Gourlay, K.; Saddler, J. N. The Enzymatic Hydrolysis of Pretreated Pulp Fibers Predominantly Involves “Peeling/Erosion” Modes of Action. *Biotechnol. Biofuels* **2014**, *7* (1), 87. https://doi.org/10.1186/1754-6834-7-87.

146. Hu, J.; Arantes, V.; Pribowo, A.; Saddler, J. N. The Synergistic Action of Accessory Enzymes Enhances the Hydrolytic Potential of a “Cellulase Mixture” but Is Highly Substrate Specific. *Biotechnol. Biofuels* **2013**, *6* (1). https://doi.org/10.1186/1754-6834-6-112.

147. Novozymes. Cellulosic ethanol Novozymes Cellic ® CTec3-Secure your plant's lowest total cost Application sheet http://s3.amazonaws.com/zanran_storage/bioenergy.novozymes.com/ContentPages/2546502386.pdf (accessed Apr 17, 2019).

148. Subramaniyan, S.; Prema, P. Biotechnology of Microbial Xylanases: Enzymology, Molecular Biology, and Application. *Crit. Rev. Biotechnol.* **2002**, *22* (1), 33–64. https://doi.org/10.1080/07388550290789450.

149. Kumar, V.; Marín-Navarro, J.; Shukla, P. Thermostable Microbial Xylanases for Pulp and Paper Industries: Trends, Applications and Further Perspectives. *World J. Microbiol. Biotechnol.* **2016**, *32* (2), 34. https://doi.org/10.1007/s11274-015-2005-0.

150. Poutanen, K. Enzymes: An Important Tool in the Improvement of the Quality of Cereal Foods. *Trends in Food Science and Technology*. 1997, pp 300–306. https://doi.org/10.1016/S0924-2244(97)01063-7.

151. Bajaj, B. K.; Manhas, K. Production and Characterization of Xylanase from Bacillus Licheniformis P11(C) with Potential for Fruit Juice and Bakery Industry. *Biocatal. Agric. Biotechnol.* **2012**, *1* (4), 330–337. https://doi.org/10.1016/J.BCAB.2012.07.003.

152. Battan, B.; Dhiman, S. S.; Ahlawat, S.; Mahajan, R.; Sharma, J. Application of Thermostable Xylanase of Bacillus Pumilus in Textile Processing. *Indian J. Microbiol.* **2012**, *52* (2), 222–229. https://doi.org/10.1007/s12088-011-0118-1.

153. Goyal, A.; Ghosh, B.; Eveleigh, D. Characteristics of Fungal Cellulases. *Bioresour. Technol.* **1991**, *36* (1), 37–50. https://doi.org/10.1016/0960-8524(91)90098-5.

154. Gudmundsson, M.; Kaper, T.; Mikkelsen, N.-E.; Sandgren, M.; Scott-Craig, J. S.; Karkehabadi, S.; Fujdala, M.; Phillips, G. N.; Helmich, K. E.; Walton, J. D.; et al. Biochemical Characterization and Crystal Structures of a Fungal Family 3 β-Glucosidase, Cel3A from Hypocrea Jecorina . *J. Biol. Chem.* **2014**, *289* (45), 31624–31637. https://doi.org/10.1074/jbc.m114.587766.

155. Berlin, A.; Maximenko, V.; Gilkes, N.; Saddler, J. Optimization of Enzyme Complexes for Lignocellulose Hydrolysis. *Biotechnol. Bioeng.* **2007**, *97* (2), 287–296. https://doi.org/10.1002/bit.21238.

156. Teter, S. A. DECREASE Final Technical Report- Development of a Commercial Ready Enzyme Application System for Ethanol https://www.osti.gov/servlets/purl/1039767/ (accessed Apr 17, 2019).

157. Ferreira, N. L.; Margeot, A.; Blanquet, S.; Berrin, J.-G. Use of Cellulases from Trichoderma Reesei in the Twenty-First Century—Part II. In *Biotechnology and Biology of Trichoderma*; Gupta, V. K., Schmoll, M., Herrera-Estrella, Upadhyay, R. S., Druzhinina, I., Maria G, T., Eds.; Elsevier: Waltham, 2014; pp 245–261. https://doi.org/10.1016/B978-0-444-59576-8.00018-7.

158. Anderson, S. R.; Esposito, D.; Gillette, W.; Zhu, J. Y.; Baxa, U.; Mcneil, S. E. Enzymatic Preparation of Nanocrystalline and Microcrystalline Cellulose. *Tappi J.* **2014**, *13* (Copyright (C) 2015 American Chemical Society (ACS). All Rights Reserved.), 35–42.

159. Teixeira, R. S. S.; Silva, A. S. da; Jang, J.-H.; Kim, H.-W.; Ishikawa, K.; Endo, T.; Lee, S.-H.; Bon, E. P. S. Combining Biomass Wet Disk Milling and Endoglucanase/β-Glucosidase Hydrolysis for the Production of Cellulose Nanocrystals. *Carbohydr. Polym.* **2015**, *128*, 75–81. https://doi.org/10.1016/j.carbpol.2015.03.087.

160. Siqueira, G.; Tapin-Lingua, S.; Bras, J.; da Silva Perez, D.; Dufresne, A. Morphological Investigation of Nanoparticles Obtained from Combined Mechanical Shearing, and Enzymatic and Acid Hydrolysis of Sisal Fibers. *Cellulose* **2010**, *17*, 1147–1158. https://doi.org/10.1007/s10570-010-9463-1.

161. Xu, Y.; Salmi, J.; Kloser, E.; Perrin, F.; Grosse, S.; Denault, J.; Lau, P. C. K. Feasibility of Nanocrystalline Cellulose Production by Endoglucanase Treatment of Natural Bast Fibers. *Ind. Crops Prod.* **2013**, *51*, 381–384. https://doi.org/10.1016/j.indcrop.2013.09.029.

162. George, J.; Ramana, K. V.; Bawa, A. S.; Siddaramaiah. Bacterial Cellulose Nanocrystals Exhibiting High Thermal Stability and Their Polymer Nanocomposites. *Int. J. Biol.*

Macromol. **2011**, *48* (1), 50–57. https://doi.org/10.1016/j.ijbiomac.2010.09.013.

163. de Campos, A.; Correa, A. C.; Cannella, D.; de M Teixeira, E.; Marconcini, J. M.; Dufresne, A.; Mattoso, L. H. C.; Cassland, P.; Sanadi, A. R. Obtaining Nanofibers from Curauá and Sugarcane Bagasse Fibers Using Enzymatic Hydrolysis Followed by Sonication. *Cellulose* **2013**, *20* (3), 1491–1500. https://doi.org/10.1007/s10570-013-9909-3.

164. Chen, H.; Fu, X. Industrial Technologies for Bioethanol Production from Lignocellulosic Biomass. *Renew. Sustain. Energy Rev.* **2016**, *57*, 468–478. https://doi.org/10.1016/J.RSER.2015.12.069.

165. Sindhu, R.; Binod, P.; Pandey, A. Biological Pretreatment of Lignocellulosic Biomass – An Overview. *Bioresour. Technol.* **2016**, *199*, 76–82. https://doi.org/http://dx.doi.org/10.1016/j.biortech.2015.08.030.

166. Gregg, J. S.; Bolwig, S.; Hansen, T.; Solér, O.; Amer-Allam, S. Ben; Viladecans, J. P.; Klitkou, A.; Fevolden, A. Value Chain Structures That Define European Cellulosic Ethanol Production. *Sustain.* **2017**, *9* (1), 1–17. https://doi.org/10.3390/su9010118.

167. Sánchez, O. J.; Cardona, C. A. Trends in Biotechnological Production of Fuel Ethanol from Different Feedstocks. *Bioresour. Technol.* **2008**, *99* (13), 5270–5295. https://doi.org/10.1016/j.biortech.2007.11.013.

168. POET-DSM. Project Liberty - POET-DSM Advanced Biofuels http://www.poetdsm.com/liberty (accessed Apr 9, 2019).

169. Iogen Corporation. Iogen Corporation https://iogen.ca/cellulosic_ethanol/index.html (accessed Apr 9, 2019).

170. Rocha-Meneses, L.; Raud, M.; Orupõld, K.; Kikas, T. Second-Generation Bioethanol Production: A Review of Strategies for Waste Valorisation. *Agron. Res.* **2017**, *15* (3), 830–847.

171. Ernsting, A.; Smolker, R. Dead End Road: The false promises of cellulosic biofuels http://www.biofuelwatch.org.uk/wp-content/uploads/Cellulosic-biofuels-report-low-

resolution.pdf (accessed Aug 15, 2019).

172. Behrens, S. H.; Breedveld, V.; Mujica, M.; Filler, M. A. Pretreatment Processes of Biomass for Biorefineries: Current Status and Prospects. *Annu. Rev. Chem. Biomol. Eng.* **2017**, *8* (1), 1–26. https://doi.org/10.1146/annurev-chembioeng.

173. Chandel, A. K.; Garlapati, V. K.; Singh, A. K.; Antunes, F. A. F.; da Silva, S. S. The Path Forward for Lignocellulose Biorefineries: Bottlenecks, Solutions, and Perspective on Commercialization. *Bioresour. Technol.* **2018**, *264*, 370–381. https://doi.org/10.1016/j.biortech.2018.06.004.

174. Julio, R.; Albet, J.; Vialle, C.; Vaca-Garcia, C.; Sablayrolles, C. Sustainable Design of Biorefinery Processes: Existing Practices and New Methodology. *Biofuels, Bioprod. Biorefining* **2017**, *11* (2). https://doi.org/10.1002/bbb.1749.

175. Camargo, L. A.; Pereira, S. C.; Correa, A. C.; Farinas, C. S.; Marconcini, J. M.; Mattoso, L. H. C. Feasibility of Manufacturing Cellulose Nanocrystals from the Solid Residues of Second-Generation Ethanol Production from Sugarcane Bagasse. *Bioenergy Res.* **2016**, *9* (3), 894–906. https://doi.org/10.1007/s12155-016-9744-0.

176. Beltramino, F.; Roncero, M. B.; Vidal, T.; Torres, A. L.; Valls, C. Increasing Yield of Nanocrystalline Cellulose Preparation Process by a Cellulase Pretreatment. *Bioresour. Technol.* **2015**, *192*, 574–581. https://doi.org/10.1016/j.biortech.2015.06.007.

177. Oksman, K.; Etang, J. A.; Mathew, A. P.; Jonoobi, M. Cellulose Nanowhiskers Separated from a Bio-Residue from Wood Bioethanol Production. *Biomass and Bioenergy* **2011**, *35* (1), 146–152. https://doi.org/10.1016/j.biombioe.2010.08.021.

178. Pirani, S.; Hashaikeh, R. Nanocrystalline Cellulose Extraction Process and Utilization of the Byproduct for Biofuels Production. *Carbohydr. Polym.* **2013**, *93* (1), 357–363. https://doi.org/10.1016/j.carbpol.2012.06.063.

179. Elliot, D. Hydrothermal Processing. In *Thermochemical Processing of Biomass: Conversion into Fuels, Chemicals and Power*; Brown, R. C., Ed.; John Wiley & Sons, Ltd: Chichester,

2011; p 347.

180. Tekin, K.; Karagöz, S.; Bektaş, S. A Review of Hydrothermal Biomass Processing. *Renew. Sustain. Energy Rev.* **2014**, *40*, 673–687. https://doi.org/10.1016/j.rser.2014.07.216.

181. Okajima, I.; Sako, T. Energy Conversion of Biomass with Supercritical and Subcritical Water Using Large-Scale Plants. *J. Biosci. Bioeng.* **2014**, *117* (1), 1–9. https://doi.org/10.1016/j.jbiosc.2013.06.010.

182. Savage, P. E.; Levine, R. B.; Huelsman, C. M. Thermochemical Conversion of Biomass to Liquid Fuels and Chemicals. In *Thermochemical Conversion of Biomass to Liquid Fuels and Chemicals*; Crocker, M., Ed.; Royal Society of Chemistry: Cambridge, 2010; pp 192–221. https://doi.org/10.1039/9781849732260-00192.

183. Tjeerdsma, B. F.; Militz, A. H. Chemical Changes in Hydrothermal Treated Wood: FTIR Analysis of Combined Hydrothermal and Dry Heat-Treated Wood. **2005**, *63*, 102–111. https://doi.org/10.1007/s00107-004-0532-8.

184. Militz, H. Heat Treatment Technologies in Europe: Scientific Background and Technological State-of-Art. In *Enhancing the durability of lumber and engineered wood products*; Orlando, 2002.

185. Inagaki, T.; Siesler, H. W.; Mitsui, K.; Tsuchikawa, S. Difference of the Crystal Structure of Cellulose in Wood after Hydrothermal and Aging Degradation: A NIR Spectroscopy and XRD Study. *Biomacromolecules* **2010**, *11* (9), 2300–2305. https://doi.org/10.1021/bm100403y.

186. Isogai, A.; Akishima, Y.; Onabe, F.; Usuda, M. Structural Changes of Amorphous Cellulose by Thermal and Hydrothermal Treatments. *Transaction* **1991**, *47* (11), 573–579. https://doi.org/https://doi.org/10.2115/fiber.47.11_573.

187. Bhuiyan, M. T. R.; Hirai, N.; Sobue, N. Changes of Crystallinity in Wood Cellulose by Heat Treatment under Dried and Moist Conditions. *J. Wood Sci.* **2000**, *46* (6), 431–436. https://doi.org/10.1007/BF00765800.

188. Kirschner, K. N.; Woods, R. J. Solvent Interactions Determine Carbohydrate Conformation. *Proc. Natl. Acad. Sci.* **2001**, *98* (19), 10541–10545. https://doi.org/10.1073/pnas.191362798.

189. Dwianto, W.; Tanaka, F.; Inoue, M.; Norimoto, M. Crystallinity Changes of Wood by Heat or Steam Treatment. *Wood research: bulletin of the Wood Research Institute Kyoto University*. Kyoto 1996, pp 47–49.

190. Biziks, V.; Andersons, B.; Andersone, I.; Grinins, J.; Irbe, I.; Kurnosova, N.; Militz, H. Hydrothermal Modification of Soft Deciduous Wood: Bending Strength Properties. In *The Fifth European Conference on Wood Modification ECWM5*; Hill, C. A. S., Militz, H., Andersons, B., Eds.; Agentura Radars Ltd: Riga, 2010; pp 99–106.

191. Eifert, T.; Liauw, M. A. Process Analytical Technology (PAT) Applied to Biomass Valorisation: A Kinetic Study on the Multiphase Dehydration of Xylose to Furfural. *React. Chem. Eng.* **2016**, *1* (5), 521–532. https://doi.org/10.1039/c6re00082g.

192. Brownlee, H. J. Furfural Manufacture from Oat Hulls I-A Study of the LIquid-Solid Ratio. *Ind. Eng. Chem.* **1927**, *19*, 422–424. https://doi.org/doi.org/10.1021/ie50207a031.

193. Cai, C. M.; Zhang, T.; Kumar, R.; Wyman, C. E. Integrated Furfural Production as a Renewable Fuel and Chemical Platform from Lignocellulosic Biomass. *J. Chem. Technol. Biotechnol.* **2014**, *89* (1), 2–10. https://doi.org/10.1002/jctb.4168.

194. Sluiter, J. B.; Ruiz, R. O.; Scarlata, C. J.; Sluiter, A. D.; Templeton, D. W. Compositional Analysis of Lignocellulosic Feedstocks. 1. Review and Description of Methods. *J. Agric. Food Chem.* **2010**, *58* (16), 9043–9053. https://doi.org/10.1021/jf1008023.

195. Ghose, T. K. Measurement of Cellulase Activites. *Pure Appl. Chem.* **1987**, *59* (2), 257–268. https://doi.org/10.1351/pac198759020257.

196. Zhang, H.; Ping, Q.; Zhang, J.; Li, N. Determination of Furfural and Hydroxymethyl Furfural by UV Spectroscopy in Ethanol-Water Hydrolysate of Reed. *J. Bioresour. Bioprod.* **2017**, *2* (4), 170–174. https://doi.org/10.21967/JBB.V2I4.84.

197. Nordin, J.; Jackson, M.; Skold, H.; Larose, J.-P. Continuous On-Line Measurement of Pulp Quality. *Pulp Pap. Canada* **1993**, *94*.

198. Segal, L.; Creely, J. J.; Martin, A. E.; Conrad, C. M. An Empirical Method for Estimating the Degree of Crystallinity of Native Cellulose Using the X-Ray Diffractometer. *Text. Res. J.* **1959**, *29* (10), 786–794. https://doi.org/10.1177/004051755902901003.

199. Wang, Y.; Zhao, Y.; Deng, Y. Effect of Enzymatic Treatment on Cotton Fiber Dissolution in NaOH/Urea Solution at Cold Temperature. *Carbohydr. Polym.* **2008**, *72* (1), 178–184. https://doi.org/10.1016/j.carbpol.2007.08.003.

200. Boluk, Y.; Danumah, C. Analysis of Cellulose Nanocrystal Rod Lengths by Dynamic Light Scattering and Electron Microscopy. *J. Nanoparticle Res.* **2014**, *16* (1). https://doi.org/10.1007/s11051-013-2174-4.

201. Malvern instruments. Zetasizer Nano Series User Manual http://www.biophysics.bioc.cam.ac.uk/files/Zetasizer_Nano_user_manual_Man0317-1.1.pdf (accessed Dec 3, 2014).

202. Bhattacharjee, S. DLS and Zeta Potential - What They Are and What They Are Not? *J. Control. Release* **2016**, *235*, 337–351. https://doi.org/10.1016/j.jconrel.2016.06.017.

203. Abitbol, T.; Kloser, E.; Gray, D. G. Estimation of the Surface Sulfur Content of Cellulose Nanocrystals Prepared by Sulfuric Acid Hydrolysis. *Cellulose* **2013**, *20* (2), 785–794. https://doi.org/10.1007/s10570-013-9871-0.

204. Lee, S. B.; Shin, H. S.; Ryu, D. D. Y.; Mandels, M. Adsorption of Cellulase on Cellulose: Effect of Physicochemical Properties of Cellulose on Adsorption and Rate of Hydrolysis. *Biotechnol. Bioeng.* **1982**, *24* (10), 2137–2153. https://doi.org/10.1002/bit.260241003.

205. Rosenberg, S. L. Cellulose and Lignocellulose Degradation by Thermophilic and Thermotolerant Fungi. *Mycol. Soc. Am.* **1978**, *70* (1), 1–13. https://doi.org/DOI: 10.2307/3758681.

206. Reese, E. T.; Segal, L.; Tripp, V. W. The Effect of Cellulase on the Degree of Polymerization

of Cellulose and Hydrocellulose. *Text. Res. J.* **1957**, *27* (8), 626–632. https://doi.org/10.1177/004051755702700806.

207. Song, Q.; Winter, W. T.; Bujanovic, B. M.; Amidon, T. E. Nanofibrillated Cellulose (NFC): A High-Value Co-Product That Improves the Economics of Cellulosic Ethanol Production. *Energies* **2014**, *7* (2), 607–618. https://doi.org/10.3390/en7020607.

208. Ramos, L. P.; Nazhad, M. M.; Saddler, J. N. Effect of Enzymatic Hydrolysis on the Morphology and Fine Structure of Pretreated Cellulosic Residues. *Enzyme Microb. Technol.* **1993**, *15* (10), 821–831. https://doi.org/10.1016/0141-0229(93)90093-H.

209. Zhu, J. Y.; Sabo, R.; Luo, X. Integrated Production of Nano-Fibrillated Cellulose and Cellulosic Biofuel (Ethanol) by Enzymatic Fractionation of Wood Fibers. *Green Chem.* **2011**, *13* (5), 1339. https://doi.org/10.1039/c1gc15103g.

210. Chen, Y.; Stipanovic, A. J.; Winter, W. T.; Wilson, D. B.; Kim, Y. J. Effect of Digestion by Pure Cellulases on Crystallinity and Average Chain Length for Bacterial and Microcrystalline Celluloses. *Cellulose* **2007**, *14* (4), 283–293. https://doi.org/10.1007/s10570-007-9115-2.

211. Mansfield, S. D.; De Jong ', E.; Stephens, R. S.; Saddler, J. N. Physical Characterization of Enzymatically Modified Kraft Pulp Fibers. *J. Biotechnol.* **1997**, *57*, 205–216.

212. Dai, J.; Chae, M.; Beyene, D.; Danumah, C.; Tosto, F.; Bressler, D. C. Co-Production of Cellulose Nanocrystals and Fermentable Sugars Assisted by Endoglucanase Treatment of Wood Pulp. *Materials (Basel).* **2018**. https://doi.org/10.3390/ma11091645.

213. United States Department of Agriculture. USDA ERS - Sugar and Sweeteners Yearbook Tables https://www.ers.usda.gov/data-products/sugar-and-sweeteners-yearbook-tables/sugar-and-sweeteners-yearbook-tables/#World and U.S. Sugar and Corn Sweetener Prices (accessed Jul 20, 2005).

214. Blue Goose Biorefineries Inc. Purchase Nanocellulose Buy Nanocellulose Nanocrystalline Cellulose Blue Goose Biorefineries http://bluegoosebiorefineries.com/purchase/ (accessed May 1, 2017).

215. Shaw, R. Dynamic Light Scattering Training Achieving reliable nano particle sizing http://149.171.168.221/partcat/wp-content/uploads/Malvern-Zetasizer-LS.pdf (accessed Mar 27, 2018).

216. Dong, X. M.; Kimura, T.; Gray, D. G. Effects of Ionic Strength on the Isotropic - Chiral Nematic Phase Transition of Suspensions of Cellulose Crystallites. *Langmuir* **1996**, *12* (8), 2076–2082. https://doi.org/0743-7463/96/2412-2076$12.00.

217. Heux, L.; Chauve, G.; Bonini, C. Nonflocculating and Chiral-Nematic Self-Ordering of Cellulose Microcrystals Suspensions in Nonpolar Solvents. *Langmuir* **2000**, *16* (21), 8210–8212. https://doi.org/10.1021/la9913957.

218. Kvien, I.; Tanem, B. S.; Oksman, K. Characterization of Cellulose Whiskers and Their Nanocomposites by Atomic Force and Electron Microscopy. *Biomacromolecules* **2005**, *6* (6), 3160–3165. https://doi.org/10.1021/bm050479t.

219. Jacobs, C.; Müller, R. H. Production and Characterization of a Budesonide Nanosuspension for Pulmonary Administration. *Pharm. Res.* **2002**, *19* (2), 189–194. https://doi.org/10.1023/A:1014276917363.

220. Satyamurthy, P.; Jain, P.; Balasubramanya, R. H.; Vigneshwaran, N. Preparation and Characterization of Cellulose Nanowhiskers from Cotton Fibres by Controlled Microbial Hydrolysis. *Carbohydr. Polym.* **2011**, *83* (1), 122–129. https://doi.org/10.1016/j.carbpol.2010.07.029.

221. Hamad, W. Y.; Hu, T. Q. Structure-Process-Yield Interrelations in Nanocrystalline Cellulose Extraction. *Can. J. Chem. Eng.* **2010**, *88* (3), 392–402. https://doi.org/10.1002/cjce.20298.

222. Yildirim, N.; Shaler, S. A Study on Thermal and Nanomechanical Performance of Cellulose Nanomaterials (CNs). *Materials (Basel).* **2017**, *10* (7), 1–12. https://doi.org/10.3390/ma10070718.

223. Cengel, Y. A.; Boles, M. A. *Thermodynamics An Engineering Approach*, 5th ed.; McGraw-Hill Science: Boston, 2004.

224. Boonstra, M. J.; Tjeerdsma, B. Chemical Analysis of Heat Treated SoftwoodsChemische Analyse von Wärmebehandeltem Holz. *Holz als Roh- und Werkst.* **2006**, *64* (3), 204–211. https://doi.org/10.1007/s00107-005-0078-4.

225. Jing, Q.; Lin, X. Y. Kinetics of Non-Catalyzed Decomposition of D-Xylose in High Temperature Liquid Water. **2007**, *15* (20476089), 666–669. https://doi.org/10.1016/S1004-9541(07)60143-8.

226. Boonstra, M. J.; van Acker, J.; Kegel, E.; Stevens, M. Optimisation of a Two-Stage Heat Treatment Process: Durability Aspects. *Wood Sci Technol* **2007**, *41*, 31–57. https://doi.org/10.1007/s00226-006-0087-4.

227. Huerta, R. R.; Saldaña, M. D. A. Pressurized Fluid Treatment of Barley and Canola Straws to Obtain Carbohydrates and Phenolics. *J. Supercrit. Fluids* **2018**, *141* (November 2017), 12–20. https://doi.org/10.1016/j.supflu.2017.11.029.

228. Paksung, N.; Matsumura, Y. Decomposition of Xylose in Sub- and Supercritical Water. *Ind. Eng. Chem. Res.* **2015**, *54* (31), 7604–7613. https://doi.org/10.1021/acs.iecr.5b01623.

229. Pińkowska, H.; Wolak, P.; Złocińska, A. Hydrothermal Decomposition of Xylan as a Model Substance for Plant Biomass Waste - Hydrothermolysis in Subcritical Water. *Biomass and Bioenergy* **2011**, *35* (9), 3902–3912. https://doi.org/10.1016/j.biombioe.2011.06.015.

230. Bhuiyan, T. R.; Hirai, N. Study of Crystalline Behavior of Heat-Treated Wood Cellulose during Treatments in Water. *J. Wood Sci.* **2005**, *51* (1), 42–47. https://doi.org/10.1007/s10086-003-0615-x.

231. Agarwal, U. P.; Ralph, S. A.; Reiner, R. S.; Hunt, C. G.; Baez, C.; Ibach, R.; Hirth, K. C. Production of High Lignin-Containing and Lignin-Free Cellulose Nanocrystals from Wood. *Cellulose* **2018**, *25* (10), 5791–5805. https://doi.org/10.1007/s10570-018-1984-z.